CONTRACT NO. 94-336
FINAL REPORT
NOVEMBER 1998

Measurement and Modeling of PM10 and PM2.5 Emissions from Paved Roads in California

CALIFORNIA ENVIRONMENTAL PROTECTION AGENCY

AIR RESOURCES BOARD
Research Division

MEASUREMENT AND MODELING OF PM_{10} AND $PM_{2.5}$ EMISSIONS FROM PAVED ROADS IN CALIFORNIA

Final Report
Contract No. 94-336

Prepared for:

California Air Resources Board
Research Division
2020 L Street
Sacramento, CA 95814

Prepared by:

Akula Venkatram, Principal Investigator
Dennis R. Fitz, Co-Investigator
College of Engineering
Center for Environmental Research and Technology
University of California
Riverside, CA 92521-0434

November, 1998

For more information about the ARB's Research Division, its research and activities, please visit our Web site:

http://www.arb.ca.gov/rd/rd.htm

Table of Contents

Appendices

Appendix A: PM_{10} Sampling from Roadways Data Set

Appendix B: Silt Sampling Data Set

Appendix C: SF_6 Tracer Gas Experiment Data Set

Appendix D: An Analysis of the Asymptotic Behavior of Cross-wind Integrated Ground-level Concentrations using Lagrangian Stochastic Simulation
Atmospheric Environment 34(10):1467-1476

Appendix E: The Effect of Streamwise Diffusion on Ground-level Concentrations
Atmospheric Environment 32(11):1955-1961

Appendix F: A Parameterization of Vertical Dispersion of Ground-level Releases
J. Appl. Met. (36)-1004-1015

1. Executive Summary

Motivation

This report describes the results from a two-year study to develop and evaluate a reliable method to estimate PM_{10} (particulate matter with an aerodynamic diameter of less than 10 μm) and $PM_{2.5}$ emissions from paved roads. The study was motivated by two observations:

- Calculations made by the California Air Resources Board (Gaffney et al., 1996) suggest that PM_{10} emissions from paved roads constitute a major fraction of total *primary* emissions from urban areas in California. For example, in the Los Angeles South Coast Air Basin, automobile traffic on paved roads generates about 170 tons/day or 30% of the total of 640 tons/day of PM_{10} emissions.

- Currently used methods, described in AP-42, to estimate particulate emissions from paved roads are uncertain (Claiborn et. al., 1995; Kantameni et al., 1996; Zimmer et al., 1992). Furthermore, because the emissions model is a purely statistical relationship between measured emission rates and silt loading, its has limited applicability to situations different from those used in its derivation.

Objectives

The study described in this report is designed to reduce the uncertainties associated with estimating particulate emissions from paved roads. This report pertains to results from the following tasks:

1. Examine in detail the studies conducted to date to characterize fugitive emissions from paved roads.
2. Design and implement field experiments to evaluate improved emission measurement methods.
3. Collect input data to run the AP-42 model at different roadways in southern California.
4. Evaluate the AP-42 model with data collected at selected sites.

Technical Approach

From January 1996 to June 1997, we carried out a series of measurements of emissions of $PM_{2.5}$ and PM_{10} from paved roads in Riverside County, California. The program involved the measurement of upwind and downwind vertical profiles of particulate mass concentrations in addition to meteorological variables such as wind speed and vertical turbulent intensity. We took several steps to make sure that these data were interpreted correctly:

1. We developed a new dispersion model to infer emissions from measured concentration differences. The new model (Du and Venkatram, 1997; Venkatram and Du, 1997) overcomes problems with currently available Gaussian dispersion models by incorporating current understanding of dispersion and micrometeorology. The model was evaluated with data collected in a study that used SF_6 as a tracer.

2. We used several collocated monitors to estimate the precision of the measurement. Concentration measurements at different heights upwind of the source were used to estimate the inherent fluctuations in the ambient PM_{10} concentrations. These estimates were used to judge the significance of the concentration differences between upwind and downwind monitors.

Results and Conclusions

The literature survey indicates that the current AP-42 model for estimating PM_{10} emissions does reflect the general correlation between emission factor and measured silt loading. However, the scatter between estimates from the AP-42 model and corresponding observations limits our ability to make estimates of emission factor from measured silt loading. Our analysis of the data shows that close to 60% of the emission observations are expected to lie outside a factor of two of a model estimate. To see what this means, assume that the model predicts an emission factor of 1 g/VKT (vehicle kilometer traveled) for 100 roads with the same silt loading. Then, the actual emission factor for about 60 of these roads is going to be greater than 2 g/VKT or less than 0.5 g/VKT. For 5 of these roads (95% confidence interval), the actual emission factor is likely to be 14 times less or greater than the model prediction.

A detailed reanalysis of the data (EPA, 1993) used to derive the latest version of the model showed that it was possible to obtain different but equally plausible empirical models for different subsets of the data set. These models differed in their predictions of emissions by as much as a factor of two.

These results on the link between silt loading and emission factor suggest that making spot measurements of emission factor might be the most reliable method of constructing emission inventories for PM_{10}. Our examination of available measurement methods indicated that use of a dispersion model to interpret upwind-downwind concentration differences represents the best compromise between reliability and operational convenience.

The major results of the measurement program to estimate PM emission factors are:

1. The upwind-downwind PM_{10} concentration differences were comparable to the expected fluctuations in ambient concentrations. For $PM_{2.5}$, the concentrations were either too small (or even negative) to allow meaningful estimates of emission factor.
2. In most cases, the concentration profiles did not show the expected monotonic decrease with height; they sometimes increased and then decreased with height. Under these circumstances, it was not possible to estimate the vertical extent of the plume.
3. Out of the 35 studies conducted, 8 (~23%) were associated with negative or zero PM_{10} concentration differences. These negative differences were not used to calculate emissions, so the emission estimates may be biased high. Because most of the $PM_{2.5}$ concentration differences were negative, we did not estimate the corresponding emissions.
4. The emission estimates were sensitive to the initial value of plume spread caused by vehicle motion. Because the initial spread cannot be measured directly, the emission calculations depend on an estimate of the plume spread.

The interpretation of concentration measurements indicates that the standard deviation of the emission estimates is comparable to the mean. This means that there is a 16% probability that the emissions are zero; this is consistent with the empirical estimate of 23% from the study. Using shorter averaging times, such as a few minutes, is not likely to lead to better results because concentration fluctuations increase as averaging times decrease. The study conducted by Harding Lawson Associates (1996) supports this. In a program to measure PM_{10} emissions from paved roads in Arizona, they found that close to 50% of the 15-minute averaged (measured using TEOMs) upwind-downwind concentration differences were negative or zero.

For the experimental conditions of this study, the upwind-downwind technique, even in combination with the best available dispersion model, does not have the sensitivity to provide accurate estimates of PM_{10} emissions. There is no reason to believe that other studies based on upwind-downwind concentration differences to infer emissions are any more accurate.

The emission factors presented in Table 1-1 should be qualified with the preceding caveats. It is seen that emission factors for paved roads range from 0.1 to 10 g/VKT. There is some indication that well maintained freeways have values at the lower end of the range, while older roads have values between 1 to 10 g/VKT. We find that silt loading, used in the AP-42 model, is a poor predictor of the emission factor.

Table 1-1. Emission Factors and Silt Loadings at Selected Roads in Riverside County

Site	Date	EF(g/VKT)	Silt content (g/m^2)	EF (g/VKT) by AP-42	Comments
Canyon Crest Dr.	3/18/97	0.4	0.065	0.3	
Canyon Crest Dr.	11/20/96	0.89			After sweeping
Canyon Crest Dr.	6/5/97	0.74	0.085	0.36	After sweeping
Main Street	6/17/96	3.58	5.93E-03	0.063	
Main Street	6/19/96	2.61	5.93E-03	0.063	
Main Street	9/3/96	2.72			
Main Street	9/5/96	3.51			
Main Street	9/24/96	2.6			After sweeping
Main Street	11/19/96	3.01			After sweeping
Riverside Dr.	3/17/97	0.8	0.2	0.62	
Riverside Dr.	5/29/97	0.67	0.17	0.56	
Riverside Dr.	3/19/97	1.76	0.19	0.6	After sweeping
Riverside Dr.	6/4/97	1.1	0.085	0.36	After sweeping
Fogg Street	5/27/97	8.57	0.38	0.94	
Fogg Street	3/26/97	31.3	0.13	0.47	After sweeping
Fogg Street	6/3/97	5.27	0.14	0.5	After sweeping

Recommendations

The results of this study suggest that it is necessary to measure emissions using a technique that does not rely on the small upwind-downwind concentration differences (relative to fluctuations in measured concentrations) associated with paved road emissions. We believe that better emission estimates can be obtained only by collecting particulate material continuously as it is

ejected by the action of the wheel against the road. This suggests an on-board PM_{10} filter with its inlet close to the contact between the wheel and the road. It is only after we have obtained reliable estimates of emissions that we can proceed to understanding the mechanisms for particulate generation.

Structure of Report

The second chapter of this report provides a detailed examination of past studies on particulate emissions from paved roads. It pays particular attention to the derivation of the paved road emissions model in AP-42, and the performance of the model in explaining observations. This chapter is followed by a chapter discussing the estimation of emission rates of particulate matter from paved roads. Following this is the Field Measurement Report for the project, describing measurement methodology, results, and analysis. The appendices consist of three papers and details of the experimental program:

An Analysis of the Asymptotic Behavior of Cross-wind Integrated Ground-level Concentrations using Lagrangian Stochastic Simulation

Atmospheric Environment 34(10):1467-1476. This paper describes the theoretical aspects of the dispersion model used in the analysis.

The Effect of Streamwise Diffusion on Ground-level Concentrations

Atmospheric Environment 32(11):1955-1961. This paper describes the theoretical aspects of the dispersion model used in the analysis.

A Parameterization of Vertical Dispersion of Ground-level Releases

J. Appl. Met. (36)-1004-1015. This paper describes the model used to estimate PM_{10} emissions.

2. Critique of the AP-42 Model for Estimating PM_{10} Emissions from Paved Roads

Motivation

Current estimates of PM_{10} (particulate matter with an aerodynamic diameter of less than 10 μm) emissions from paved roads are based on the model included in the AP-42 document (AP-42, fifth edition). This model suggests that large fractions of PM_{10} emissions in urban areas originate from paved roads. For example, Gaffney et al. (1995) estimated that about 30% of primary PM_{10} emissions in California are associated with traffic activity on paved roads. Zimmer et al. (1992) estimated that PM_{10} emissions from paved roads accounted for about 40-70% of the total PM_{10} impacts at model receptors in the Denver metropolitan area. Such results, by themselves, would point to a careful re-examination of the AP-42 model. This need is made more urgent by recent studies (Claiborn et al., 1995; Kantamaneni et al., 1996) that show that PM_{10} emission estimates from the model compare poorly with measurements.

In the following sections, we first review the formulation of the model to understand the governing variables. We next critically examine the performance of the model in explaining observations and the experimental methods used to measure emissions.

AP-42 Model for Paved Road Emissions

The AP-42 model for estimating PM_{10} emissions from paved roads was developed by the Midwest Research Institute (MRI) under contract with the USEPA (Cowherd and Englehart, 1984; EPA, 1993). The first version of the model (Cowherd and Englehart, 1984) expressed the emission factor, E, from a paved road in terms of the silt loading, sL, as follows:

$$E = k(sL)^p, \qquad (1)$$

where E is the mass emitted per unit distance traveled by the motor vehicle expressed as grams per vehicle kilometer, L is the surface mass loading of the paved road expressed as mass per unit area, and s corresponds to the fraction of the surface loading that passes through a 75 μm sieve. In the equation, k and p are empirical constants. The value of k depends on the units used to express the emission factor and silt loading, and p has been empirically determined to be 0.8.

The latest version of the AP-42 model for PM_{10} emissions includes the average weight of the motor vehicle *in tons*, W, as an explanatory variable (EPA, 1993):

$$E = k(sL)^p W^b, \qquad (2)$$

where p is now 0.65 and the exponent b=1.5.

In the following sections, we will examine the AP-42 model in detail. Our discussion is organized around the following subjects:

1. How the model was formulated.
2. Its performance in explaining observations.
3. Limitations of the model.

In discussing these limitations, we will examine:

1. The theoretical basis of the model.
2. The statistical derivation of model parameters.
3. The methods used to measure the variables incorporated in the model.

The final section of this chapter summarizes the critique, and provides suggestions on how to improve the model.

Formulation of the Paved Road Emissions Model

The paved road emissions model in AP-42 is based on the intuitively appealing idea that PM_{10} emissions from paved roads are primarily caused by resuspension of material deposited on the road. If this is true, a motor vehicle is likely to resuspend more PM from a dusty road than from a clean road. The most straightforward method of characterizing dustiness is the mass per unit area of loose material on the road surface. This surface loading can be measured by vacuuming the traveled portion of the road. Because only a fraction of the surface material contributes to PM_{10} emissions, it reasonable to assume that only a certain size fraction is relevant. Silt loading refers to the mass of the surface material that passes through a 75 μm mesh. A second factor that is believed to be important in the resuspension process is the weight of the vehicle; this also makes intuitive sense.

The first version of the model, Equation (1) (Cowherd and Englehart, 1984), used silt loading, (measured by vacuuming test roadways and sieving the collected material) as the primary explanatory variable. The emission factor for PM_{15} was determined using an upwind-downwind mass balance technique, which is described in more detail later. The PM_{10} emission factor was obtained by scaling the PM_{15} factor by the measured particle mass distribution. The emission factor was directly correlated with silt loading, and inversely correlated with vehicle speed. But because silt loading and vehicle speed were inversely correlated, silt loading was chosen to be the primary explanatory variable.

The data were collected at commercial/industrial roads, an expressway, and a rural road. As expected the silt loading was highest on the rural road and lowest on the expressway. Equation (1) resulted from regression analysis of 10 data points that met the quality control criteria. The equation was developed by assuming that it is of the form,

$$E = a(sL)^b, \qquad (3)$$

where the unknown constants "a" and "b" are obtained by fitting the data with the following linear equation obtained by taking logarithms of both sides of Equation (3):

$$\ln(E) = \ln(a) + b\ln(sL). \qquad (4)$$

The fitting is designed to minimize the sum of the squares of the residuals between the logarithms of the predicted (left side of Equation (3)) and observed emission factors. This procedure also ensures that the average of the logarithmic residuals is zero.

The latest version of the PM_{10} emissions model was developed using a larger data set consisting of about 60 data points for a variety of roads ranging from public paved roads to uncontrolled industrial roads. The data indicated that the average weight of the vehicle explained some of the variance of the observed emission factor. Equation (2) resulted from a regression analysis of the data. The next section examines the performance of the model in explaining observations.

Performance of Model

Figure 2-1 plots the predicted against the observed emission factor for the data set used to derive Equation (2) (EPA, 1993). We see that the model explains 75% of the variance. The magnitude of the unexplained scatter is seen more clearly in the residual plot of Figure 2-2, which shows the ratio of the observed to the predicted emission factor as a function of the corresponding predicted emission factor. The ratio varies over two orders of magnitude. This means that when the predicted EF is 1 g/VKT, the observed EF varies from 0.1 to 10 g/VKT. The consequences of such scatter are discussed later.

Figure 2-1: Predicted versus Observed Emission Factors for Complete MRI Data Set

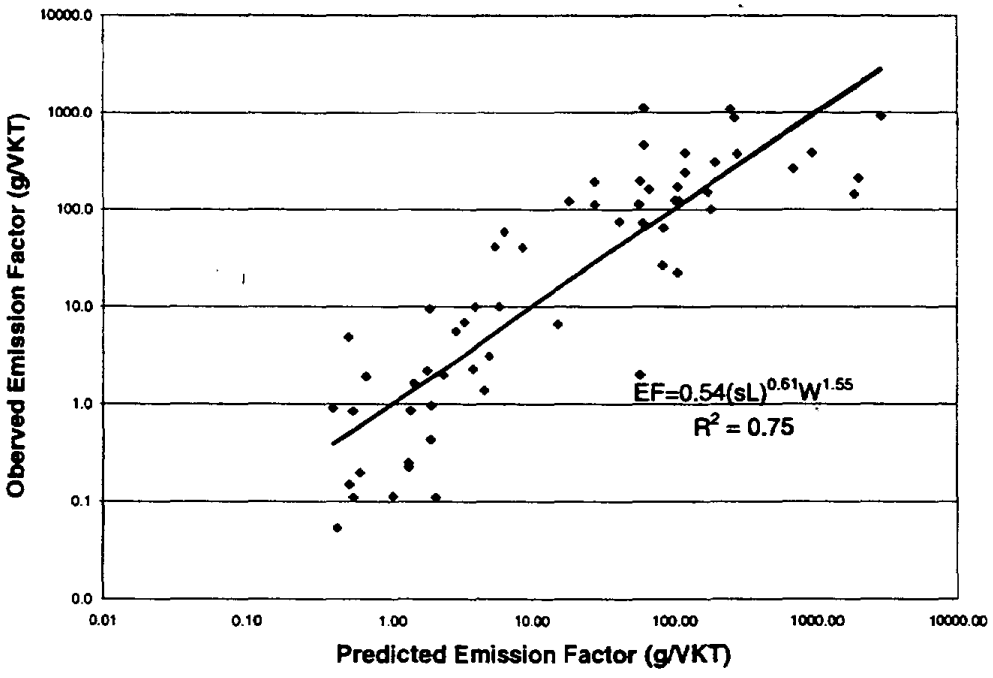

Zimmer et al. (1992) were among the first to evaluate the AP-42 model using a data set that was independent of that used to derive it. In a study performed in the Denver metropolitan area, they measured emission factors with associated silt loadings at several different types of roads. Figure

2-3 plots the emission factors against these silt loadings. As noted by Zimmer at al. (1992), the silt loading explains only 20% of the variance of the observations. Furthermore, the implied relationship between EF and silt loading is very different from that of Equation (1) or (2).

Figure 2-2: Ratio of Observed to Predicted Emission Factor versus Silt Loading for MRI Data Set

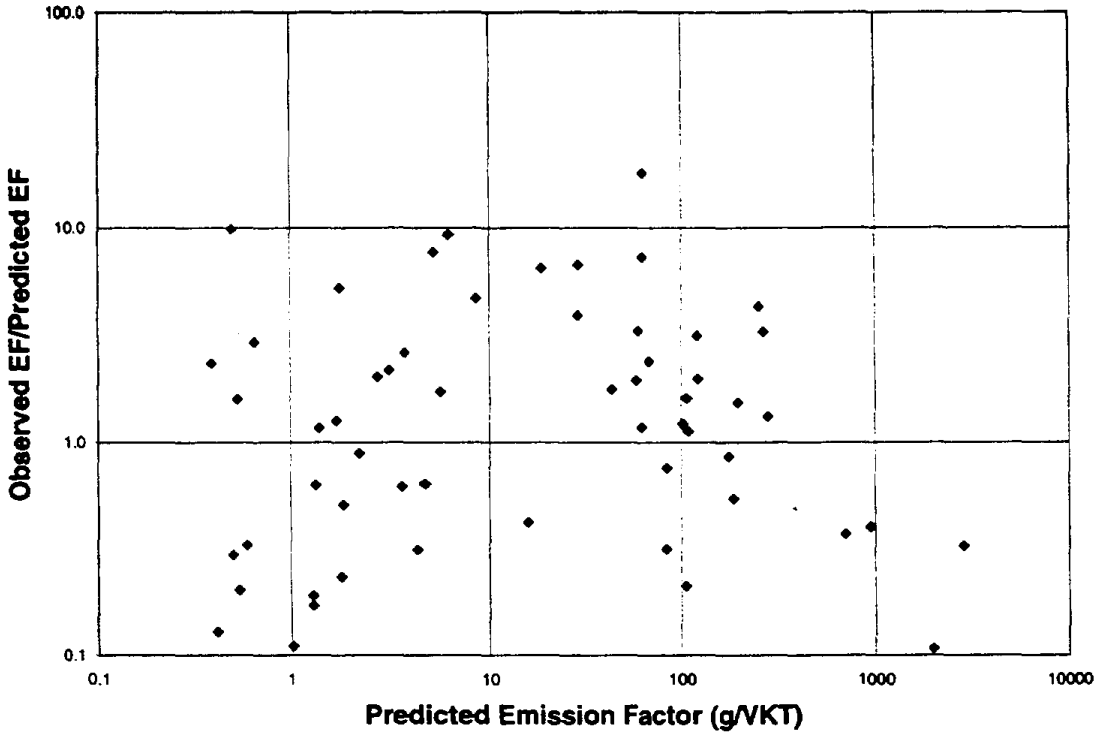

Similar results were obtained by Kantamaneni et al. (1996), who compared measurements of PM_{10} emissions made at paved roads in Spokane, Washington, to estimates from the AP-42 model. The measured silt loadings showed very little variation, about 3.25 g/m^2 over the period of 2 months in 1994 of the experimental study. While Equation (1) predicts a constant value of about 10.5 g/VKT corresponding to the measured silt loading, the measured emission factors range from 0.47 to 1.71 g/VKT. These results led the authors to conclude that "no correlation was found between experimentally determined emission factors and silt loading observations."

Figure 2-3: Emission Factor versus Silt Loading for data from Zimmer et al. (1992)

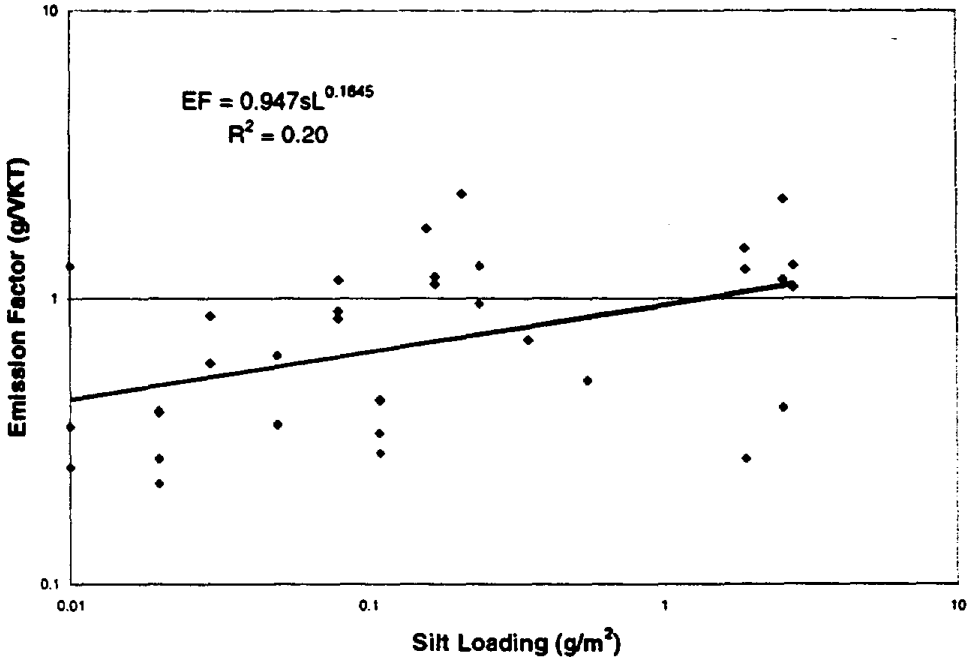

This difficulty in using silt loadings to estimate emission factors is illustrated in another study conducted by Ashbaugh et al. (1996) at an intersection in Sacramento, California, over a period of 4 days in August 1995. The measured emission factor averaged over this period was about 0.1 g/VKT. The silt loadings on the four roads leading to the intersection varied substantially: 0.0543, 0.0034, 0.0016, and 0.0020 g/m^2. Notice that the first value is about 10 times the remaining three values, which suggests one of two things: The number is an outlier or silt loadings are inherently unstable. Both possibilities cannot be ruled out. If we assume that the largest silt loading is an outlier, we find that the emission factor calculated using Equation (2) using an average of the remaining three values is 0.03 g/VKT, which is three times lower than the measured emission factor. On the other hand, if we assume that the largest silt loading is valid, we have to conclude that silt loading is an unreliable indicator of PM_{10} emissions. That is, although the observed emission rate is relatively steady, the predicted emission rate can vary from 0.03 g/VKT to 0.3 g/VKT depending on where silt loading is measured.

These results from independent evaluations of the AP-42 model for paved road emissions highlight the problem of basing a model on a particular data set. This and other limitations will be discussed in the following sections.

Limitations of the Paved Road Emissions Model

The formulation of the AP-42 model assumes that the balance between production and removal of particulate matter gives rise to a layer of PM that acts as a reservoir. The sources of particulate matter include vehicular carry-out from unpaved roads, water and wind erosion from adjacent exposed areas, motor vehicle exhaust, brake dust, pavement wear, cargo spills, winter sanding

and salting, and atmospheric deposition. The removal mechanisms include resuspension by direct contact with vehicle wheels, aerodynamic effects induced by moving vehicles, wind shear, and rain.

The assumed reservoir of PM has to be reduced continuously through resuspension by moving vehicles. In other words, silt loading has to decrease with time unless the silt is replenished at the same rate that it is removed. If this were true, silt loading cannot explain the vehicle-induced resuspension rate because, by assumption, it is unaffected by emissions. The actual depth of this permanent reservoir of silt cannot affect the rate at which material is removed from its surface. To see the difficulty, consider the analogous problem of estimating evaporation from the surface of a lake. The actual depth of the lake (read silt loading) has little to do with evaporation rate (read particulate emissions) from the surface.

Thus, using silt loading as an explanatory variable in the emission factor model poses a logical dilemma. If it affects emissions, it cannot be a stable parameter that characterizes the road surface — it has to change with time. If it is a stable variable, it cannot affect the emission factor. It is possible that silt loading at a particular instant might provide an estimate of the emission factor for that particular slice of time. For example, the silt loading of a road used by a construction site might provide information on paved road emissions during the construction activity on a particular day. But, it would be unreasonable to use the silt loading to estimate emissions after the construction activity has ceased.

Another problem with the AP-42 model is that the so-called constant, k, in Equations (1) or (2) has physical dimensions, which implies that it contains hidden physical variables that should not vary from road to road. Because we do not know what these variables are, we are not in a position to examine the validity of the assumption. We can suspect that the equations are missing something because they do not reduce to the model for *unpaved* roads in the limit of infinite silt loading. After all, a very dirty paved road should behave like an unpaved road.

One can argue that the theoretical foundation of the emissions model is irrelevant as long as it produces useful estimates of emissions. We will address this issue by first discussing the impact of the deviations between model estimates and corresponding observations of EF.

The Framework

A model prediction will always differ from the corresponding observation because the model cannot include all the variables that affect the observation. So we have to assume that the best that the model can do is to provide an estimate of the average over the ensemble of all possible observations corresponding to the model inputs, α. Because observations respond to a set β not included in the model, we will have an infinite ensemble of observations associated with a given model input set α. Then, we can write

$$E_o(\alpha,\beta) = E_p(\alpha) + \varepsilon(\alpha,\beta), \qquad (5)$$

where E refers to the variable of interest, such as emission factor, the subscript o refers to an observation, and p refers to the model prediction. The residual between model prediction and observation is $\varepsilon(\alpha,\beta)$. For a given value of the model input set α, we will have an infinite number

of observations corresponding to different values of the unknown set β. By definition, the average of these observations for a given α is the model prediction,

$$\langle E_o(\alpha,\beta)\rangle^{\beta} = E_p(\alpha), \quad (6)$$

which implies that

$$\langle \varepsilon(\alpha,\beta)\rangle^{\beta} = 0. \quad (7)$$

These concepts are illustrated in Figure 2-4. Notice that Equation (7) states that for an ideal model, the average of residuals for a given set of model inputs should be as small as possible. Such an average cannot be taken in practice because we cannot keep the model inputs fixed as we make observations. Therefore, we need to make sure that the statistics of the residuals do not vary with model inputs. This enables us to compute these statistics from the residuals between model estimates (for different α) and corresponding observations. Before we can analyze the residuals between model estimates and observations, it is necessary to convert them into a white noise sequence, which is unrelated to the model input variables. In principle, this can be done through appropriate choice of the model and/or transformation of the model inputs. A plot of residuals against model inputs, such as that in Figure 2-2, provides a visual indication of the success of this procedure. A quantitative estimate is provided by the correlation coefficient between model estimates/inputs and corresponding residuals.

Figure 2-4: Ensemble of Observed Emission Factors Corresponding to Predicted Emission Factor

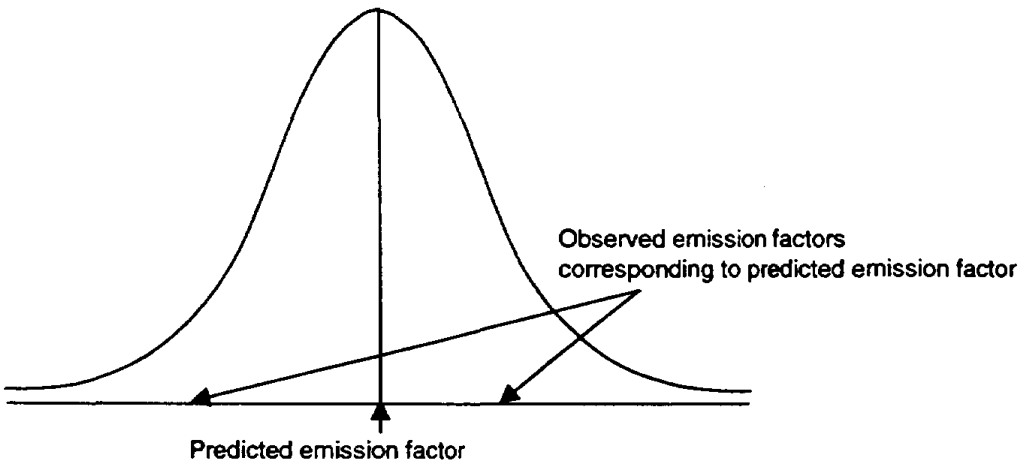

The statistics of residuals obviously contain important information on model performance, which needs to be incorporated explicitly in the use of the model prediction. Before we illustrate this idea, it is useful to transform the residuals so they are normally distributed about the mean. The required transformation is based on the observation that concentrations are lognormally distributed about the model prediction (Csanady, 1973). Then, the residuals are defined by the equation:

$$\ln(E_o) = \ln(E_p) + \varepsilon \quad . \qquad (8)$$

Notice that this also ensures that the observation is always positive even when the residual, ε, is a large negative number.

To avoid interpreting residual statistics in terms of logarithms, it is convenient to define the geometric mean and standard deviation as follows:

$$m_g = \exp(\bar{\varepsilon})$$
$$\textit{and} \qquad . \qquad (9)$$
$$s_g = \exp(\sigma_\varepsilon)$$

We see that that the deviation of m_g from unity tells us whether the model is underpredicting or overpredicting; it is a measure of bias of the model estimate. Note that a model developed by regressing the logarithm of the observed emission factor on data will, by design, have an m_g close to unity for residuals corresponding to the data used to derive the model. The geometric standard deviation, s_g, is a measure of the uncertainty in the model prediction.

Interpretation of Residual Statistics

We will illustrate the application of the model evaluation framework to the data presented in Figure 2-1. For the data in Figure 2-1, m_g is close to unity as expected, but s_g is 3.9. This implies that close to 60% of the observations are expected to lie outside a factor of two of a model estimate. To see what this means, assume that the model predicts an emission factor of 1 g/VKT for 100 roads with the same silt loading. Then, the actual emission factor for about 60 of these roads is going to be greater than 2 g/VKT or less than 0.5 g/VKT. For 5 of these roads (95% confidence interval), the actual emission factor is likely to be 14 times less or greater than the model prediction.

These statistics clearly indicate that even the improved emission factor model, Equation (2), has a large degree of uncertainty that needs to be accounted for in an emission inventory calculation. Uncertainty can be incorporated into an emission inventory calculation by simulating observations of emission factor using Equation (9). We first estimate an emission factor for a given road using the measured silt loading. We then simulate an observed emission factor by adding a residual ε selected at random from a normal distribution with a mean of $\ln(m_g)$ and a standard deviation of $\ln(s_g)$ to ln(model estimate).

$$\ln(E_{simulated}) = \ln(E_{predicted}) + \varepsilon(\ln(m_g), \ln(s_g)) \, . \qquad (10)$$

The synthetic observed emission factor is $\exp(E_{simulated})$. This simulation will lead to sets of emission inventories rather than a single set, which can be analyzed further to obtain statistics.

One can argue that if we have a large number of roads, we will overpredict at roughly half of them, and underpredict at the remaining roads, so that total emissions will be roughly correct when observations are averaged over all these roads. This result is comforting only if we are interested in emissions summed over an area that includes a large number of roads with the same silt loading. We also have to be convinced that the model provides a reasonable estimate of the

mean EF. This, as we will see in the next section, is debatable because the model is purely statistical.

Problems with Statistical Models

Equation (2) is a purely statistical model based on the observed correlation between measured emission factor and possible explanatory variables, such as silt loading and vehicle weight. We call the model statistical because the parameters, k, p, and b in Equation (2) are entirely based on the data used to derive them. To illustrate this, we fitted Equation (2) to different subsets of the data set used by MRI to develop Equation (2). Table 2-1 shows the values of model parameters corresponding to data sets divided according to different ranges of silt loading. The parameter values for the complete data set are slightly different from those recommended by MRI (EPA, 1993); but this difference does not change our conclusions.

Table 2-1: Variation of Model Constants with Data Set

$$EF=k(sL)^{p}W^{b}$$

No of Data Points	Range of sL (g/m^2)	k	p	b	r^2
60	0 to 400	0.54	0.61	1.55	0.75
37	0 to 4	0.18	0.52	2.14	0.66
23	1 to 20	1.02	0.93	1.1	0.6
23	5 to 400	33.7	0.22	0.43	0.12

When we used data for silt loadings in the range 0 to 4 g/m^2, which corresponds to most urban roads and freeways, the resulting model parameters are substantially different from those for the complete data set, even though the r^2 is still a respectable 0.66. Note that the parameter k is a factor of three smaller than the recommended value of 0.54. For silt loading in the range 1 to 20 g/m^2, the parameters are substantially different from the base case values, but the model still explains 60% of the variance of the emission factor observations. Figures 2-5 and 2-6 show that the models corresponding to these data ranges provide plausible descriptions of the data. It is clear that there is no rationale for choosing one of these models over another. In fact, because most measured silt loadings fall in the range 0 to 4 g/m^2, the fit for this data range ought to be preferred over that recommended in AP-42.

There is no reason to believe that the purely empirical AP-42 model for paved road emissions provides credible estimates of the "mean" emission factor. Models derived from different data ranges can provide different but equally plausible estimates. To illustrate this, we have plotted the ratio of the AP-42 model to the "small sL" model (0 to 4 g/m^2) as a function of silt loading in Figure 2-7. We see that when the average vehicle weight is 1.5 tons, the ratio is over 2 for most of the range of silt loading encountered in practice. When the vehicle weight is 3 tons, the ratio is about 1.25 for sL=0.5 g/m^2, and exceeds 1.5 when silt loading is greater than 1 g/m^2. These

results indicate that the AP-42 paved road emissions model has the potential of overstating even the mean emission factor by as much as 100%. Note that this overestimate does not refer to an individual road. It refers to the average over a large number of roads, which means that emission factor estimates for area wide averages can be in error by large factors.

Figure 2-5: Predicted versus Observed Emission Factors for Silt Loadings less than 4 g/m²

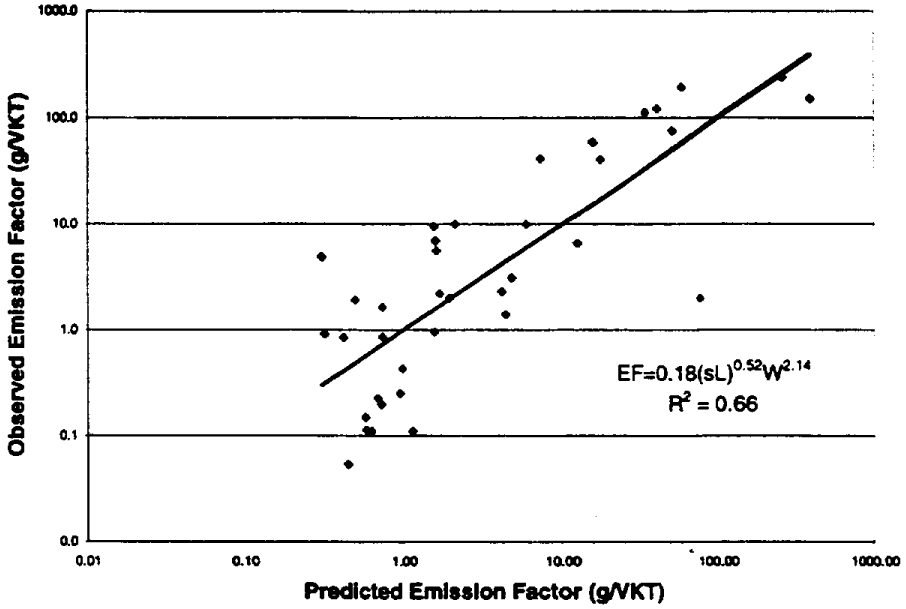

Figure 2-6: Predicted versus Observed Emission Factor for Silt Loadings between 1 and 20 g/m²

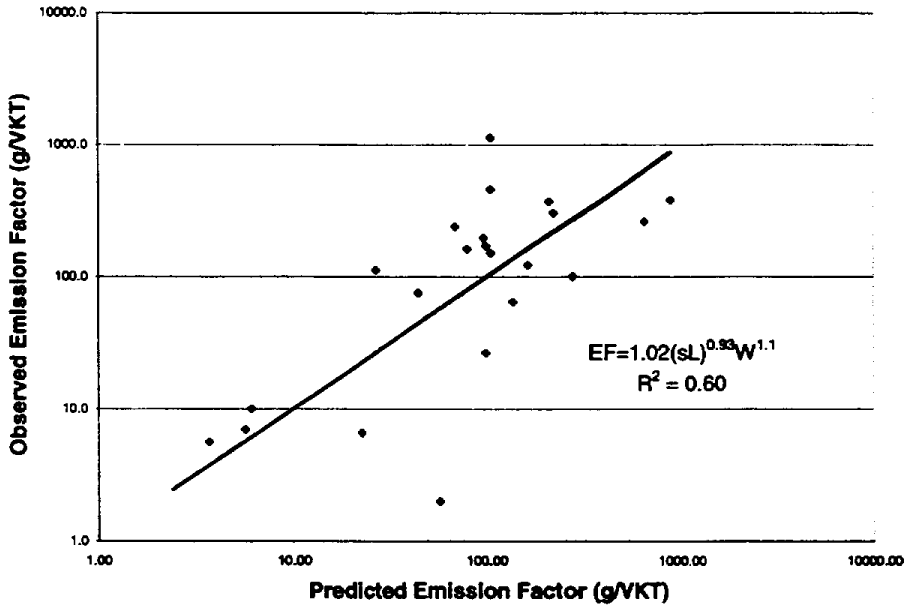

Figure 2-7: Ratio of Emission Factors Predicted by Two Different Empirical Formulas.

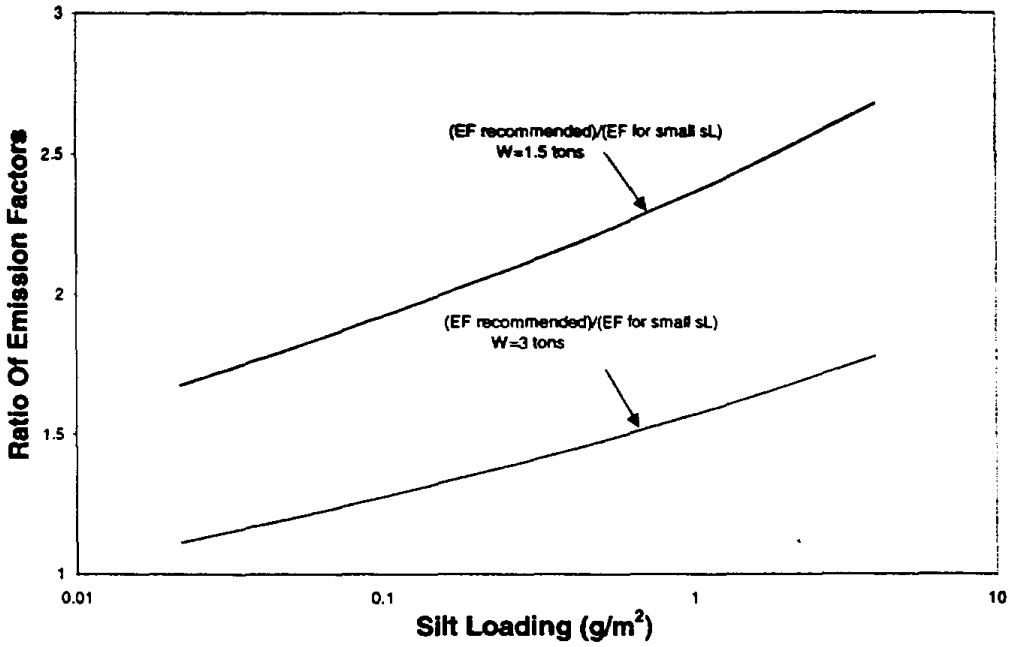

The primary message of this discussion is that emission factor estimates for paved roads from the AP-42 model are likely to be highly uncertain. This uncertainty is the result of several factors, some of which have been examined earlier. But the most important source of uncertainty could well be the measurement of the emission factor itself. We need to remind ourselves that measurements are the foundation of the AP-42 model. In the next section, we examine the accuracy of some of the methods that have been used to measure PM_{10} emissions from paved roads.

Emission Factor Measurements

Several methods have been used to infer emissions from paved roads. These include:

1. Mass balance calculations using profiles of PM_{10} concentrations (Cowherd and Englehart, 1984).
2. Dispersion models to fit concentration measurements (Dyck and Stukel 1976; Cahill et al., 1995).
3. Tracer methods (Claiborn et al., 1995).

All these methods rely on measuring PM_{10} concentration differences associated with emissions from the road. Figure 2-8 shows the typical experimental setup used to measure emissions. In the ideal experiment, the wind blows across the road. PM concentrations are measured both upwind

and downwind of the road. These measurements are made at several heights to obtain information on concentration profiles. Meteorological towers are used to measure temperature, wind and turbulence at several heights. On the downwind side, there can be PM monitors at several downwind distances.

The following sections describe the specifics of different measurement techniques.

Mass Balance Method

The mass balance method is based on measuring the difference between the upwind and downwind horizontal mass fluxes. The difference is the emission from the road. The horizontal flux per unit length across a plane parallel to an infinitely long road can be written as

$$Horizontal\ Flux = \int_0^{\infty} \langle uC \rangle dz\,, \qquad (11)$$

where the angle brackets refer to an average over the sampling period, u is the instantaneous velocity normal to the plane, and the C is the simultaneously measured PM_{10} concentration.

Figure 2-8: Ideal Experimental Setup to Measure PM_{10} Emissions from Paved Roads

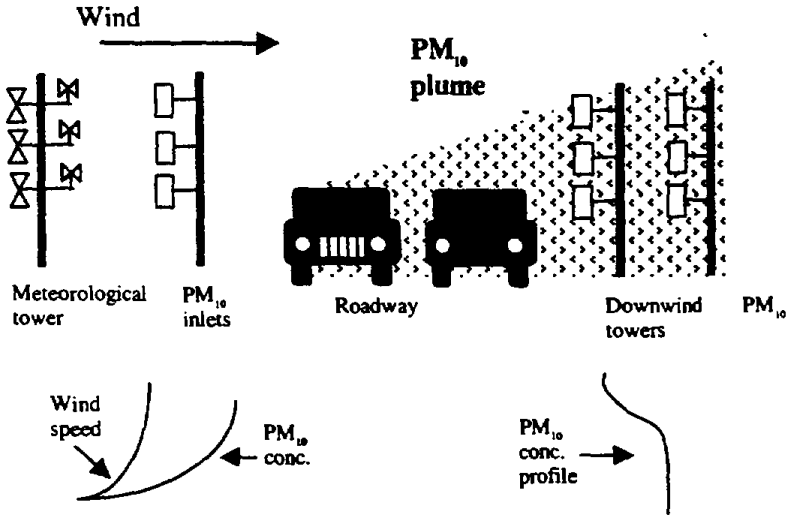

The first thing we notice about this expression is that the calculation of horizontal flux requires simultaneous measurements of concentration and velocity normal to the road. The flux is *not* equal to the product of the mean velocity and the mean concentration, as can be seen by expressing the concentration and velocity in terms of time means and deviations:

$$u = \bar{u} + u'$$
$$\text{and} \quad , \qquad (12)$$
$$C = \bar{C} + C'$$

so that

$$\langle uC \rangle = \bar{u}\bar{C} + \langle u'C' \rangle . \qquad (13)$$

The second term on the right is the turbulent flux, which is related to the variations in wind speed and concentration during the sampling period of interest. Because PM_{10} sampling typically occurs over several hours, the second term can be as large as the first.

The second aspect of horizontal flux calculation is that it requires information at several heights to allow accurate interpolation of point fluxes and identification of the edge of the plume from the road. In practice, this is a difficult assignment.

Cowherd and Englehart (1984) measure horizontal fluxes using a technique called isokinetic sampling, in which airflow into a sampler is adjusted to match the local wind speed. Four samplers are attached to a mobile tower placed downwind of the road. Usually, only two samplers are used to measure upwind concentrations, which are then averaged to produce a so-called background value that is subtracted from the downwind mean concentrations. This procedure assumes that the upwind concentration does not vary significantly with height. The flow rate into the samplers and the direction of the head are controlled by the wind speed measured by a warm wire anemometer.

In principle, this method can measure fluxes without measuring concentration and velocity separately and multiplying them out. There are several errors than can affect this point flux measurement. The first is introduced by the fact that the inertia of the blower motor will inevitably filter out short-term mass fluxes. Thus, it is not clear that the sampling heads actually measure total mass fluxes. It is also necessary for the airflow to correspond to the velocity normal to the road. This cannot be done with a sampler design (Cowherd and Englehart, 1984) that uses a warm wire anemometer to measure the velocity. Furthermore, the sampler head should point along the normal to the road to measure the correct horizontal flux. The description in the report indicates that the head is designed to point into the wind, which is likely to overestimate the required flux. Because upwind fluxes are not measured accurately, emission estimates based on the differences between upwind and downwind fluxes cannot be reliable.

Another difficulty with the isokinetic exposure method is that it does not account for the wind reversals that are likely to occur over a sampling period of a few hours. The fluxes into the road are not measured during these periods. The net flux calculation might be in error if these negative fluxes are not included.

The horizontal flux calculation depends on accurate interpolation and extrapolation of a limited set of measurements. Unlike the concentration, the flux does not decrease steadily with height because large mass fluxes can occur in the upper part of the plume where low concentrations are accompanied by large winds. Under these circumstances, it is difficult to identify the height at which the vertical integration can be terminated.

To show that the errors that we have discussed can be minimized, it is necessary to demonstrate that the flux measured by the system is equal to the product of the instantaneous concentrations and velocities. Because this equivalency has not been established, it is impossible to quantify the errors in the isokinetic sampling technique.

Dispersion Model Method

Emissions also can be calculated using dispersion models. Here, the measured profiles of upwind-downwind concentration differences are fitted to a dispersion model by treating emission rate as the unknown parameter. The major advantage of the method is that it is not necessary to identify the top of the plume, as long as we can fit part of the predicted concentration profile to the observed profile. The second advantage is that it is not necessary to make simultaneous (space and time) measurements of concentration and velocity. In principle, we can manage with time averaged quantities. The accuracy of this technique depends on the accuracy of the dispersion model and the significance of the concentration contribution of the road relative to the inherent fluctuations of the background concentration. Let us discuss each of these factors in turn.

The geometric standard deviation of deviations between model estimates of concentrations and corresponding observations is close to 2 even when the meteorology is well known (Venkatram, 1984,1988). The cross-wind integrated concentration might be estimated with less uncertainty but the 95% confidence interval is no better than a factor of 2. This suggests that if we should be able to derive emission factors with this degree of uncertainty if we can use an adequate dispersion model with the required input data.

Using a dispersion model to estimate PM emissions is complicated by the fact that vehicular motion can eject particles vertically and can also induce turbulence that might affect dispersion in the near field. The conventional method of accounting for these effects is to ascribe an initial plume spread associated with vehicle motion. The problem is that there is no consensus on how this plume spread is specified. Because this spread can dominate that associated with atmospheric turbulence, this lack of knowledge can become critical in the application of a dispersion model to infer emissions.

In principle, we can infer initial plume dimensions by fitting model estimates to observations of tracer releases designed to mimic emissions from paved roads. This was done by Kantamaneni et al. (1996) in a study to estimate PM_{10} emissions from paved roads in Spokane, Washington. They were able to adjust the vertical dimensions of the vertical plume to fit estimates from a Gaussian model to observations of SF_6 concentrations associated with a release upwind of the road. Although the calibration appeared to be successful, it was clear that there was no systematic method of specifying the vertical spread. The vertical spread was varied between 0 to the unrealistic value of 45 m to obtain agreement between model estimates and observations of cross-wind integrated concentrations. This suggests that the vertical spread was no more than an arbitrary calibrating factor, which cannot be related to any of the governing physical variables. It is clear that our ability to use a dispersion model to estimate emissions is limited by our lack of understanding of dispersion induced by vehicular motion.

Another problem that can affect both the mass balance as well as the dispersion model methods is that the PM incremental concentration contributed by the road can be comparable to the

inherent fluctuations in the background concentrations; emission factor estimates become suspect under these conditions. The measured upwind concentrations can be larger than the downwind concentrations. For example, in a study conducted by Harding Lawson Associates (1996) to measure paved road emissions in Arizona, close to 50% of the 15-minute averaged downwind-upwind PM_{10} concentration differences were negative. This suggests that errors in emission factors can be introduced by fluctuations in background concentrations.

Tracer Methods

To avoid using a dispersion model to measure emissions, Claiborn et al. (1995) used a tracer to provide the dispersion function, which is essentially the ratio of the concentration of the tracer and the known emission rate of the tracer. This method is clearly superior to a dispersion model if the tracer release mimics that of the fugitive emissions. For example, if the road behaves as an area source of emissions, the tracer release should be distributed over the road. Because this is not possible in practice, Claiborn et al. (1995) and Kantamaneni (1996) have used either line sources or point sources located just upwind or downwind of the road being studied. Because these studies did not compare vertical profiles of SF_6 and PM_{10}, it is not apparent that these approximations are justified.

We have shown that methods currently used to measure PM_{10} emissions from paved roads are prone to error for various reasons. At present, we have little information on the magnitudes of these errors.

Conclusions

Our examination of the data used to derive the AP-42 paved road emissions model indicates that there is significant correlation between emission factor and silt loading. The analysis also shows that we can develop different but equally plausible empirical models by using different subsets of the data set. These models provide EF estimates that can differ by a factor of two.

The correlation between emission factor and silt loading is not reproduced by other studies (Zimmer et al., 1992; Kantamaneni et al. 1996), which supports the earlier observation that the form of the emission factor model is a strong function of the data used to derive it. This is to be expected of a purely empirical model, which lacks a mechanistic foundation.

Even though the AP-42 model explains over 70% of the variance of the observations used to derive it, the scatter between model estimates and corresponding observations has a significant impact on our ability to make emission estimates. For example, EF estimates from the latest version of the model (Equation 2) are likely to deviate by more than a factor of two from the corresponding observation as much as 60% of the time.

Until we learn more about the mechanisms of PM emissions from paved roads, it is prudent to rely on spot measurements to obtain reliable estimates of emission factors. We have surveyed current methods to infer emissions, and have concluded that the use of a dispersion model to interpret upwind-downwind concentration measurements represents the best compromise between accuracy and ease of implementation. The next chapter describes results obtained using a dispersion model.

3. Estimating Emission Rates of Particulate Matter from Paved Roads

The following section describes the approach and results to measurements of particulate matter from paved roads in Riverside County, California. This text has been accepted for publication in *Atmospheric Environment.*

Technical Approach

In the last chapter, we examined currently available methods for measuring PM emissions from paved roads. In choosing one of them for this project, we were guided by the following criteria:

- It is reliable, in the sense that one can estimate the error involved in using it. Using this criterion, we eliminated the mass balance technique because its accuracy depends on the vertical extent of the plume, which is difficult to determine experimentally.

- It uses instruments that were commonly available, and can be used routinely. This criterion is based on the observation that existing models of PM_{10} emissions are uncertain; thus, until better models become available, it might be necessary to make measurements to obtain reliable estimates of emissions in new situations. It is clear that, while tracer techniques might be accurate under certain conditions, they cannot be used routinely. We chose to use the dispersion model technique with the realization that it was necessary to first improve upon current modeling techniques for surface releases.

- It was based on a measure of PM_{10} equivalent to the Federal Reference Method.

Thus, our approach to estimating emissions consisted of the following steps:

1. Select state-of-the-art dispersion model applicable to surface releases.

2. Evaluate the model using tracer experiments.

3. Measure PM_{10} concentration concentrations and associated meteorology at a number of representative roadways.

4. Apply the model to estimating PM_{10} emissions from paved roads.

5. Evaluate the applicability of the AP-42 model to measured emissions.

6. Develop improved model for PM_{10} and $PM_{2.5}$ emissions from paved roads.

The Dispersion Model and Its Use in Estimating Emissions

Most existing dispersion models, such as the Industrial Source Complex model, are based on empirical dispersion curves derived from the Prairie Grass experiment conducted in 1956 (See

Venkatram, 1996 for discussion). Other models (Nieuwstadt and van Ulden, 1978; van Ulden, 1978; Gryning et al., 1983) are based on either K-theory or Lagrangian Similarity theory, which can be justified only posteriori by comparing model estimates with observations. Because the accuracy of the PM_{10} emission estimates depends on the dispersion model, we developed a new dispersion model using a method that represents current understanding of dispersion. This method is based on conducting simulations of particle motion with a Lagrangian Stochastic model formulated by Thomson (1987) and others (Wilson, 1982). The simulations generated data, which were then used to develop a parameterized model. The model was evaluated with observations from the Prairie Grass experiment (Barad, 1958). The development of the model as well as its evaluation is described elsewhere (Venkatram and Du, 1997; Du and Venkatram, 1997). In this paper, we describe the evaluation of the accuracy of this new model in estimating emissions from a distributed source representative of a road.

The results described in Du and Venkatram (1997) can be summarized in terms of the cross-wind integrated concentration, $C^y(z)$, as

$$C^y(z)/C^y(0) = \exp\left[-b(z/\bar{z})^s\right] \qquad (1)$$

where the values of parameters, s and b, are given later. The ground-level concentration $C^y(0)$ can be expressed as

$$C^y(0) = \frac{Q}{u_e \bar{z}}, \qquad (2)$$

where the plume height, $\bar{z}$, is parameterized as

$$\bar{z} = 0.04 x g(x_*), \qquad (3)$$

where $x_* = x/|L|$, and the Monin-Obukhov length, L, is defined by

$$L = -\frac{T_s}{g}\frac{u_*^3}{kQ_s}, \qquad (4)$$

where Q_s is the surface kinematic heat flux, and T_s is the near surface temperature.
The function $g(x_*)$ is given by

$$g(x_*) = \begin{cases} (1+0.35x_*)^{1/2}, & (L<0) \\ (1+0.24x_*)^{-1/2} & (L>0) \end{cases} \qquad (5)$$

The effective transport velocity, u_e, is a function of distance from release, x, the plume height $\bar{z}$, and the friction velocity, u_*,

$$u_e = m(x_*)u_* x/\bar{z}, \qquad (6)$$

where the function m(x.) is given by

$$m(x_*) = \begin{cases} (1+0.525x_*^2)^{1/4} & (L<0) \\ (1+0.26x_*)^{-1/3} & (L>0) \end{cases} \qquad (7)$$

We find that s = 1.3 for unstable stratification and s = 2.0 for stable stratification. For near neutral conditions, in the narrow range 1 / L = (-0.01, 0.01) m^{-1}, we propose linear interpolations for *s* and the corresponding value of *b*

$$\begin{aligned} &s = 1.3 + 70(x + 0.01). \qquad (-0.01m^{-1} < x < 0.01m) \\ &b = 0.68 - 18(x + 0.01) \\ &where \\ &x = 1/L \end{aligned} \qquad (8)$$

The model is used to calculate the emission rate by fitting model estimates to corresponding observations as follows. At any downwind distance, the observed concentration can be written as:

$$C_o^r(z) = C^r(0) f(z/\bar{z}) + \varepsilon, \qquad (9)$$

where ε is a random deviation. The dispersion model is used to estimate the mean plume height, $\bar{z}$. We estimate the surface concentration, $C^r(0)$, by minimizing the sum of the squares of these deviations over the heights of measurement. The resulting least squares estimate is

$$C_{est}^r(0) = \frac{\sum_i C_o^r(z_i) f(z_i/\bar{z})}{\sum_i f^2(z_i/\bar{z})}, \qquad (10)$$

where z_i is the height of measurement. Then, the estimate of the emission rate follows from Equation (2),

$$Q_{est} = C_{est}^r(0) u_* \bar{z}. \qquad (11)$$

The next section describes experiments conducted to estimate the error involved in this estimation technique.

Evaluation of Dispersion Model Using Tracers

The theory described in the previous section was evaluated using three experiments conducted in the parking lot of the College of Engineering-Center for Environmental Research and Technology (CE-CERT), University of California, Riverside. These experiments were designed to simulate emissions from roads/freeways by releasing SF_6 from a grid of tubes with the width of a typical paved road. The grid consisted of five columns and six rows. The width of the five columns was 20 m, corresponding to the width of a typical four-lane road. The rows were evenly

spaced along a distance of 30 m. The tracer was released at a measured flow rate from nozzles at the nodes of the tube grid. SF_6 was collected in bags over a time period of 30 minutes at 1, 3, 5, and 10 m on a tower located 5 m downwind of the artificial area source. A 5 m tower measured wind speed and temperature at three levels (1, 3, and 5 m). This information was used to estimate the micrometeorological variables, the surface friction velocity and the Monin-Obukhov length, required by the dispersion model; this estimation involved fitting similarity profiles to the measured values at the three heights (Nieuwstadt and an Ulden, 1978).

Emissions from the area sources were estimated by modeling them as an equivalent line source placed in the middle of the grid. Because the accuracy of this approximation depends on our ability to estimate emissions from a line source, we conducted a fourth experiment in which SF_6 was released from a line source 15 m long containing seven evenly spaced nozzles. The emission estimates from the four tracer experiments are presented in Table 3-1. We see that the mean error involved in estimating emissions from the simulated area source is about 60%. In the only experiment with the line source, the error is almost negligible. This set of tracer experiments suggests that the error associated with using a dispersion model to estimate emissions is well within a factor of 2.

Table 3-1: Results from SF_6 Experiments to Examine Effect of Traffic on Dispersion

Site	Measured Q (g/s)	Predicted Q (g/s)	Error (%)
CE-CERT (line)	0.043	0.043	0
CE-CERT (area)	0.067	0.039	72
CE-CERT (area)	0.022	0.022	0
CE-CERT (area)	0.046	0.022	113
Iowa Avenue	0.044	0.053	20

We also conducted a tracer experiment to estimate the impact of automobile generated turbulence on dispersion. We located a line source of SF_6 at a prescribed emission rate upwind of Iowa Avenue, which has a traffic volume of about 1,200 vehicles per hour. The release line was 30 m long and located 1 m away from the curb. Nozzles were evenly spaced at 3 m intervals. The emissions were sampled 20m at the opposite curb at heights of 1, 2, 5 and 10 m by filling bags. The concentrations of these samples were used to estimate the emission rate assuming that traffic generated turbulence was absent. We found that the resulting emission rate was within 20% of the actual value. This suggests that for this particular situation, the effect of traffic is within the expected error in estimating emissions. We tentatively assumed that we could neglect the direct effect of traffic on dispersion. However, as we will show later, automobiles can affect dispersion indirectly by ejecting particles upwards.

Measurement of PM_{10} Emission Rates from Paved Roads

We then proceeded to estimate emission rates of PM_{10} from roads by carrying out concentration and meteorological measurements at 6 sites in the vicinity of Riverside, California. These sites

included one at a freeway, Highway 215/60, one at a local unpaved road crossing an agriculture field, and three at major streets: Iowa Avenue, Canyon Crest Drive, Riverside Drive, and one at a local street, Fogg street.

At each site, PM_{10} concentrations were measured upwind and downwind of the road using low-volume samplers at heights of 1 m, 3 m and 5 m. The sampling time at each site was determined by the steadiness of the wind flow; it ranged from 1.5 hours (unpaved road) to 32 hours of multi-day collection, with a mean value of 9.4 hours. Table 3-2 summarizes the data collected.

Separate collections with 5 collocated low-volume samplers indicated that at these sampling durations, the measurement uncertainty was about 10% of the mean concentration. Because the upwind-downwind concentration differences were of the same order as this uncertainty, it is necessary to use the fitting procedure described earlier to obtain useful information on the emission rate.

At each measurement site, the following meteorological variables were measured at a height of 3 m: mean wind speed (U), wind direction (θ), temperature (T), humidity (q) and standard deviation of vertical fluctuating velocity (σ_w). This information was used to calculate the variables required to estimate dispersion, the friction velocity u_* and the Monin-Obukhov length L (Venkatram, 1992), through the iterative solution of the following coupled equations for σ_w and U (Panofsky and Dutton, 1984):

$$\sigma_w = \begin{cases} 1.25u_*(1-3\frac{z}{L})^{1/3} & (1/L<0) \\ 1.25u_* & (1/L \geq 0) \end{cases}, \qquad (12)$$

$$U = \frac{u_*}{\kappa}[\ln(\frac{z}{z_0}) - \Psi_m(\frac{z}{L})], \qquad (13)$$

where

$$\Psi_m = \begin{cases} \ln\left[\left(\frac{1+\phi_m^{-2}}{2}\right)\left(\frac{1+\phi_m^{-1}}{2}\right)^2\right] - 2arc\tan\phi_m^{-1} + \frac{\pi}{2}, & (1/L<0) \\ -5\frac{z}{L}; & (1/L \geq 0) \end{cases}$$

and

$$\phi_m = \begin{cases} (1-16z/L)^{-1/4} & (L<0) \\ 1+5z/L & (L>0) \end{cases} \qquad (14)$$

Table 3-2: Summary of PM_{10} sampling (3 samplers for upwind, 3-6 samplers for downwind)

Date	Location	Sampling Duration (hours)	Average Upwind Concentration µg/m3	Average Downwind Concentration µg/m3	Average Concentration Difference µg/m3	Average Wind Speed m/s
5/2/96	Hwy 215&60	9.5	77.5	84.5	7.0	1.5
5/6/96	Hwy 215&60	9.4	58.5	66.5	8.0	1.5
5/9 - 5/10/96	Hwy 215&60	13.0	73.0	74.9	1.9	1.5
5/13 - 5/16/96	Hwy 215&60	31.0	66.4	62.9	-3.6	1.8
5/31 - 6/3/96	Hwy 215&60	32.3	57.0	56.0	-1.0	1.6
6/4 - 6/7/96	Hwy 215&60	32.0	86.0	83.0	-3.0	1.5
1/8/96	Iowa Ave.	3.3	65.4	81.2	15.8	1.8
1/9/96	Iowa Ave.	3.3	70.6	81.1	10.5	1.2
1/18/96	Iowa Ave.	7.1	38.5	46.4	7.9	1.6
4/26/96	Iowa Ave.	10.0	102.0	96.5	-5.5	1.8
5/20 - 5/23/96	Canyon Crest	28.0	57.0	57.0	0.0	2.3
11/12/96	Canyon Crest	5.0	56.5	59.2	2.7	1.1
11/20/96	Canyon Crest	6.8	122.8	128.5	5.7	1.3
3/18/97	Canyon Crest	4.0	56.1	61.2	5.1	1.5
3/27/97	Canyon Crest	5.5	83.0	78.0	-5.0	1.8
5/28/97	Canyon Crest	7.0	64.1	60.1	-4.0	2.1
6/5/97	Canyon Crest	7.0	40.1	45.7	5.6	2.4
6/17 - 6/18/96	Riverside Drive	14.0	96.7	110.9	14.2	2.5
6/19 - 9/20/96	Riverside Drive	6.3	116.0	133.2	17.2	3.4
6/25 - 6/26/96	Riverside Drive	14.8	77.4	79.6	2.2	3.7
8/6/96	Riverside Drive	5.0	76.8	81.9	5.1	0.7
9/3/96	Riverside Drive	8.0	87.4	91.6	4.2	2.3
9/5/96	Riverside Drive	9.0	77.0	98.0	21.0	2.5
9/24/96	Riverside Drive	8.0	154.8	167.3	12.5	2.3
10/2/96	Riverside Drive	6.0	126.8	135.2	8.4	1.2
11/19/96	Riverside Drive	6.0	162.8	178.7	15.9	2.1
3/17/97	Riverside Drive	6.0	83.1	78.0	-5.1	1.8
3/19/97	Riverside Drive	5.0	40.6	61.6	21.0	2.4
5/29/97	Riverside Drive	6.3	67.2	71.9	4.6	2.6
6/4/97	Riverside Drive	5.8	65.0	75.2	10.2	2.9
3/21/97	Fogg St.	5.0	65.0	66.7	1.7	2.2
3/26/97	Fogg St.	5.5	81.6	92.4	10.9	3.2

Continued next page

Table 3-2 (continued)

Date	Location	Sampling Duration (hours)	Average Upwind Concentration µg/m3	Average Downwind Concentration µg/m3	Average Concentration Difference µg/m3	Average Wind Speed m/s
5/27/97	Fogg St.	7.0	59.7	63.4	3.7	2.5
6/3/97	Fogg St.	7.0	85.6	87.7	2.1	2.0
7/9/96	Agric. Field*	1.5	156.7	431.5	274.7	2.5
7/9/96	Agric. Field*	2.5	88.1	416.8	328.7	2.5
9/12/96	Agric. Field*	2.5	93.2	436.1	342.8	2.5
9/12/96	Agric. Field*	2.5	107.0	379.4	272.4	2.5

* Unpaved road on the UC Riverside campus where experimental agricultural crops are grown.

In solving these equations, we assumed two widely different values for surface roughness length z_0, 0.01 m and 0.1 m, which can be considered as lower and upper limits for the present measurement sites. While these different values of z_0 do result in substantial changes in L, the variation in the associated values of the emission rate is less than 30% because, as we will see later, the initial dispersion height makes a major contribution to dispersion at the sampling distances of concern. The next section describes results from the experiments conducted near roads and freeways.

Results from Road Sampling

Figures 3-1 and 3-2 illustrate the typical locations of the different instruments used in the sampling program. In most experiments, there were 2 or 3 PM_{10} samplers located at different heights up to a maximum height of 5 m. The upwind samplers were located at distances ranging from 1 to 50 m from the curb; in most experiments the distance was over 10 m to minimize the effect of emissions from the road. The downwind PM_{10} samplers were located at 3 heights if possible, and at distances ranging 1 to 15 m from the curb. Whenever possible, we located two samplers at each height to obtain a measure of the variation in PM_{10} concentrations at each height. Meteorological variables were measured at height of 3 m on a tower usually located near the upwind sampler.

The contribution of the road was calculated by subtracting the average of the upwind concentrations from each of the downwind concentrations. Figures 3-3 and 3-4 show examples of the measured contributions. The figures also show profiles estimated by the model through the fitting procedure described earlier. More details on how these were produced are described later.

An examination of the measured PM_{10} concentrations indicated several qualitative features:

1. The upwind-downwind PM_{10} concentration differences were around 10 μ g/m^3.
2. PM_{10} concentrations rarely followed the ideal profile, which is a maximum at the surface, and then decreasing with height.
3. PM_{10} concentrations at 5 m were comparable to those at 1 m, suggesting that particles were being ejected upwards by automobile motion.

Figure 3-1: PM_{10} and $PM_{2.5}$ sampling on Iowa Avenue on 1/8-1/9, 1/18/96

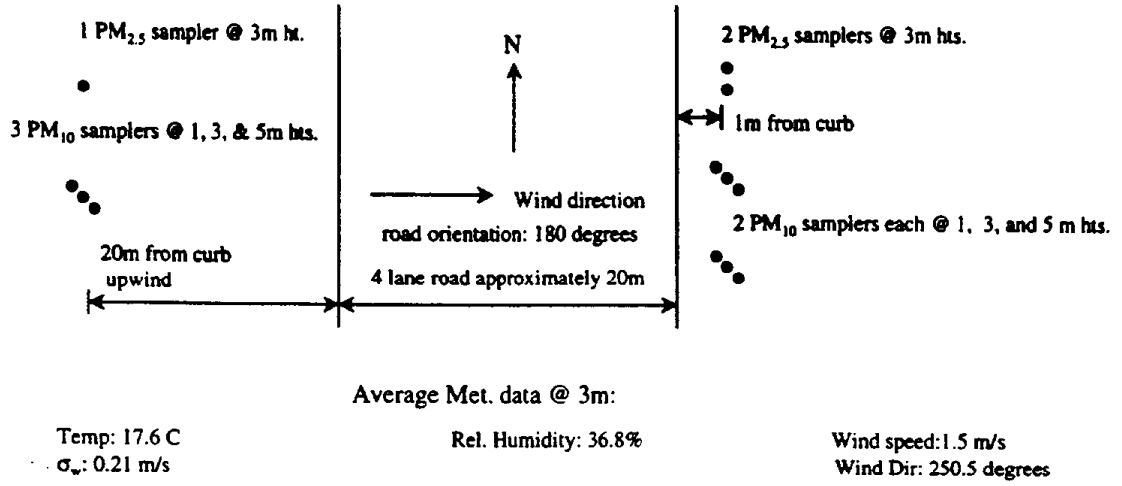

Figure 3-2: PM_{10} sampling on Canyon Crest on 11/20/96 (after sweeping)

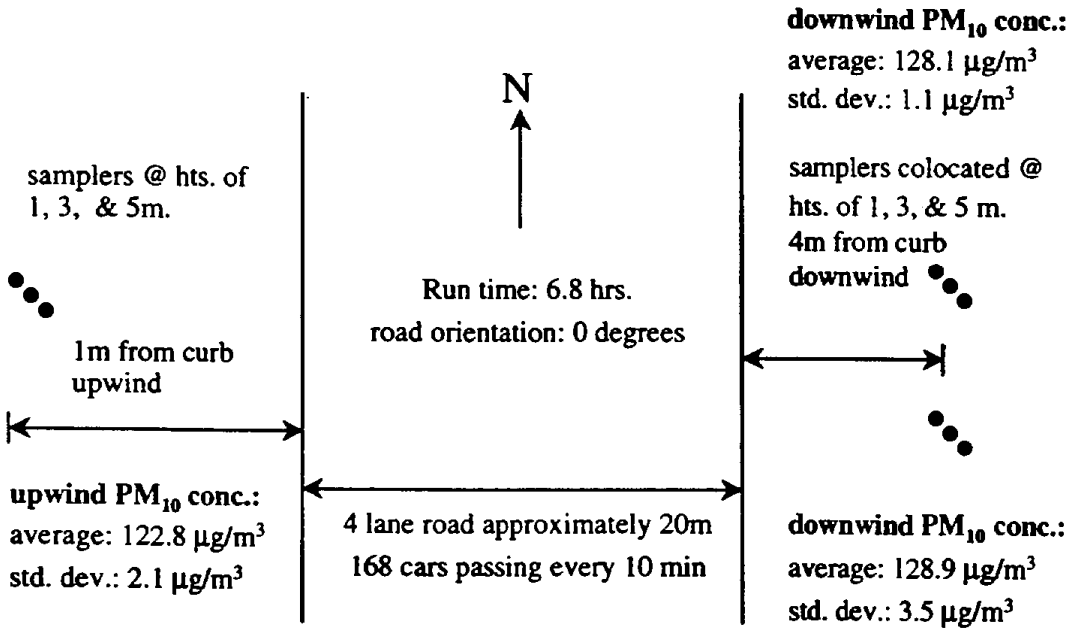

Figure 3-3: Predicted versus Measured Concentrations at Riverside Drive on 6/17/96

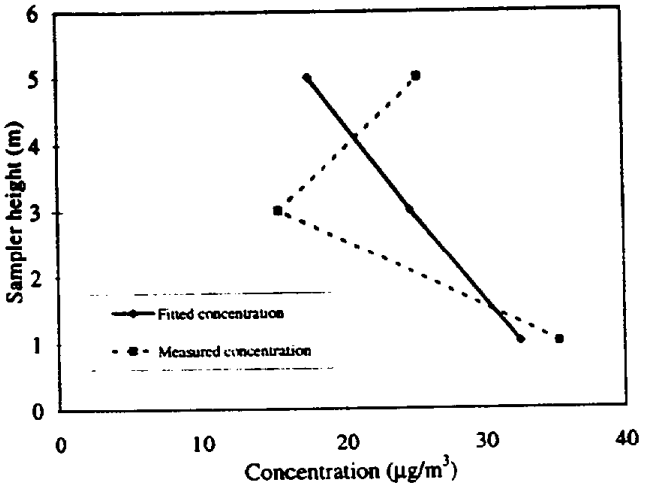

Figure 3-4: Predicted versus Measured Concentrations at Canyon Crest Drive on 11/20/96

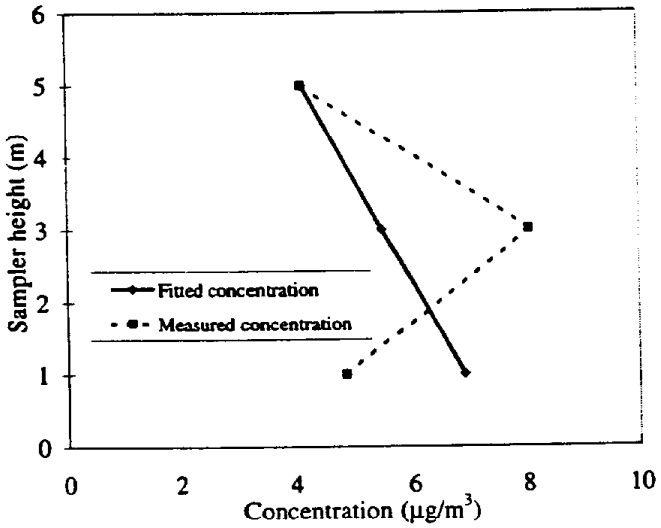

Because the PM_{10} concentration profiles measured near the roads were associated with uncertainty comparable to the mean values, we estimated the initial plume height using measurements made near the unpaved road. At the unpaved road, the upwind-downwind concentration differences were of the order of 100 $\mu g/m^3$, as seen in Figure 3-5. Notice that the concentration shows the expected decrease with height. This profile was used to infer initial dispersion height by fitting the dispersion model to the data using least squares; the fitted profile, seen in Figure 3-5, is within 10% of the observed profile. The initial dispersion height turned out to be 3.5m, which is comparable to the 3.2 observed by McCaldin (1978). While this height is likely to depend on average automobile speed and other factors, in the absence of more information, we assumed that this initial height applied to other sites near roads and freeways.

Figure 3-5: Predicted versus Measured Concentrations at an Unpaved Road on 7/9/96

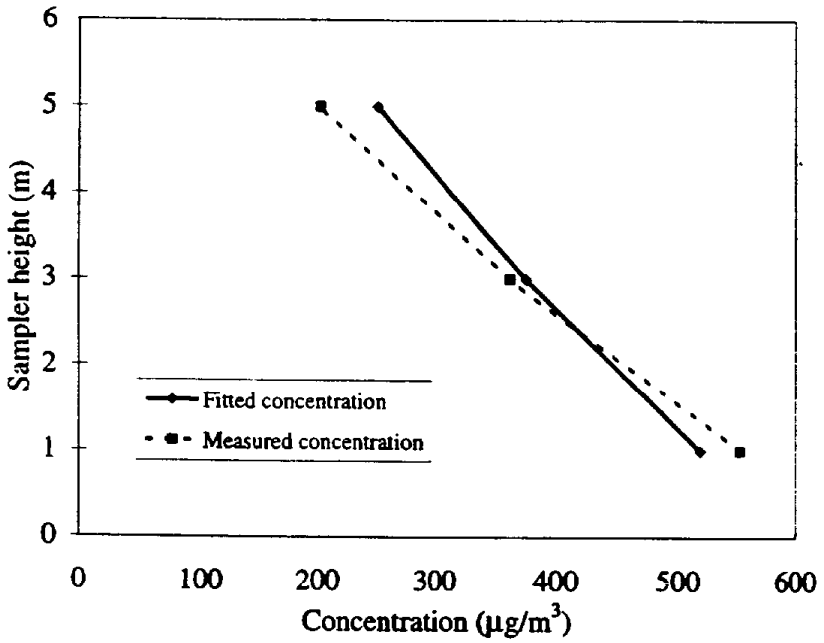

Table 3-3 presents PM_{10} emission estimates at the seven sites considered in this study. The estimates represent averages over several sampling periods at each site. The emission rates vary from about 180 to 730 $\mu g/(m.s)$, and the corresponding emission factors vary from 0.1 to 3 g VKT^{-1}. The emission rate and emission factor for the unpaved road is about two orders of magnitude higher. Where possible, we have used the measured silt loading to compute the emission factor predicted by the AP-42 model. We see that there is little correlation between the measured emission factors and those from AP-42. This observation is consistent with those of other studies (Claiborn et. al, 1995 Zimmer et al., 1992). Kantamaneni et al. (1996) found that

emission factors estimated with the AP-42 model, using silt loading as input, differed from measured emissions by as much as an order of magnitude.

Table 3-3: Measured Emission Factors and Comparison with Estimates from the AP-42 Model.

Site	Silt Content (g/m^2)	Emission Rate ($\mu g/m.s$)	Traffic Flow (vehicles/hr)	Emission Factor (g/VKT)	Emission Factor (AP-42)
Highway 215/60	-	372	8000	0. 17	-
Canyon Crest Dr.	7.50E-02	184	990	0. 68	0.33
Iowa Avenue	1.60E-04	215	1200	0.65	0.006
Main Street	6.00E-03	734	875	3.01	0.063
Riverside Dr.	1.60E-01	278	892	1.08	0.54
Fogg Street	2.20E-01	173	42	0.22	0.64
Unpaved Road	-	14000	66	790	-

Table 3-4 compares the results of this study with those of similar studies. The range of emission factors from this study lies within that of other measured values. In general, the emission factors calculated using measured silt loadings are unrelated to measured emission factors.

Table 3-4: Comparison with Other Studies

Study	Road type	Emission factor (g/VKT)	Silt loading (g/m^2)
This Study	Freeway-local	0.1 to 3	1.6E-4 to 2.2E-1
Cahill et al. (1995)	Intersection	< 0.3	1.6E-3 to 5E-2
Claiborn et al. (1995)	Freeway-local	0.5 to 34	N/A
Harding Lawson (1996)	Freeway-local	0.03 to 180	N/A

Conclusions

The results of this study show that measuring emissions of PM_{10} from paved roads is not a straightforward analysis of concentrations measured upwind and downwind of road. We found that the contribution of the road to PM_{10} concentrations is often comparable to the uncertainty in the mean measured concentrations. Furthermore, the profiles of the difference in upwind-

downwind concentrations did not show monotonic decreases or increases with height. The profiles also suggested that emissions were being mixed over an initial height by automobile motion. Because this initial dispersion height is a major fraction of the total dispersion at the distances of concern, its reliability determines the accuracy of the derived emission rates of PM_{10}; the measured concentration profiles did not allow us to make accurate estimates of automobile induced dispersion. These features of the upwind-downwind concentration differences suggest that the associated emission rates are uncertain to a degree that we cannot quantify at this stage.

Our experience with interpreting PM_{10} concentration differences is similar to those of other investigators (For example, Claiborn et al., 1995; Kantamaneni et al., 1996), who also found that measured concentrations did not follow expected behavior, such as monotonic decreases with distance from the road. Their data, like some of ours, indicated negative upwind-downwind concentration differences in a number of cases. In view of uncertainties, the best we can say about emission factors is that they range from 0.1 to 10 g VKT^{-1}. There is some suggestion that well maintained freeways have values at the lower end of the range, while older roads, such as Main Street in Riverside, might have values between 1 to 10 g VKT^{-1}. Our experience suggests that silt loading is a poor predictor of emission factor.

Freeways and roads can make a major contribution to total PM_{10} emissions. Calculations made by the California Air Resources Board (using default silt loadings) indicate that in the Los Angeles South Coast Air Basin, automobile traffic on paved roads contributes about 170 tons day^{-1} or 30% of the total of 640 tons day^{-1}. This calculation is consistent with the emission factors found in this study. There are roughly 12×10^6 cars in the LA basin. Taking an average of 40 km day^{-1} per vehicle, we arrive at roughly 500×10^6 VKT day^{-1}. Now assuming that the emission factor is between 0.1 for freeways and 1 g VKT^{-1} for local roads, the emission rate works out to be 0.5 g VKT^{-1} times 500×10^6 VKT day^{-1} = 250 tons day^{-1}.

These calculations suggest that it is necessary to obtain better understanding of the mechanism for the generation of paved road emissions; silt loading is clearly not a component of this understanding. This study shows that using the best possible dispersion model does not address the uncertainty introduced by the fact that measured concentration differences are comparable to the inherent fluctuations in the measurements. One way of solving this problem is to measure PM_{10} emissions directly by on-board sampling of material that is ejected through contact of the automobile wheel with the road surface. On-board sampling avoids the problem of using uncertain dispersion models or meteorological data. All we have to do is to measure the concentration and the approximate extent of the particulate "bubble" created by the moving vehicle. The excess PM_{10} concentration in the bubble is likely to be much higher than the time averaged excess measured on the side of the road. To illustrate the technique, assume that the excess concentration is 100 $\mu g / m^3$, and the cross-sectional area of the bubble is 10 m^2. If we assume that the particulate matter in the bubble does not settle immediately, the effective emission factor is the product of the excess concentration and the cross-sectional area, which works out to be 1 gm/VKT. This type of estimate is likely to be more reliable than those based on upwind-downwind concentration differences.

Experimental Methods

- **Tracer**

Sulfur hexafluoride (SF_6) was used as a tracer gas based on its inertness and the ability to analyze low concentrations using gas chromatography with electron capture detection. Release lines were constructed consisting of ¼-inch OD polyethylene tubing with T's. A stainless steel capillary (0.007 in ID x 10 cm long) was attached to the arm of each T. The pressure on the tubing was adjusted to achieve a flow rate of 20-30 ml/min per capillary. A rotameter was used to determine the total SF_6 flow rate.

Sampling equipment was set up such that the midpoint of the source was directly downwind of the prevailing on-shore flow. The mean measured wind directions were all within 10 degrees of that expected, while the variability of the wind ranged from 15-20 degrees. Samples were collected in 30 L Tedlar bags by means of a diaphragm pump. The fill rate was controlled with a needle valve and monitored with a rotameter. Sampling durations varied from 10 to 30 minutes. Samples were analyzed with a Hewlett Packard 5890 gas chromatograph equipped with a gas injection valve (0. 25 ml loop), a column (1/8 inch by 2 m) packed with mole sieve 5a, and an electron capture detector. The chromatograph was calibrated by diluting SF_6 in nitrogen with a ±2% certification (Scott-Marrin) with ultra zero grade air using a mass flow-controlled diluter (Columbia Scientific model 1700).

- **PM_{10} Measurements**

PM_{10} samples were collected using a Graseby Andersen model 246B low volume size selective inlet. The inlet was modified to adapt directly to an open face 47 mm PFA Teflon filter holder (Savillex Corp) using a viton o-ring to make the seal. Flow was controlled to 16.7 L / min using a rotameter and needle valve assembly (Dwyer) attached to a carbon vane pump (Gast model 1022). Flow rates were verified with a transfer rotameter calibrated with a certified dry test meter (Singer model DTM-115)). Gelman 2 µm pore Teflon filters were used for all collections. They were equilibrated at 25 •C and 50% RH for 24 hours prior to weighing to the nearest µg using a Cahn model 40 electrobalance. The calibration of the balance was checked before and after each set of filters were weighed using a class M 200 mg weight. All filters were weighed three times prior to and after sampling.

- **Meteorological Measurements**

RM Young AQ wind speed/direction, temperature, and humidity sensors were used. These sensors were placed on either a 5- or 10-m tower. The 10 m tower was equipped with wind sensors at either the top or at every 3 m depending on the experiment performed. The data from the meteorological sensors were collected using a Campbell CR-10 data logger using either a 5 or 15 minute averaging time. Anemometers were calibrated by attaching a synchronous motor to the cup shaft as described in the manual. Factory conversion factors to convert rpm to speed were used to generate a calibration curve by comparison with the readout of the data logger. The temperature sensor was calibrated by immersing the sensing element in water in close proximity to a thermometer traceable to the NIST. The relative humidity sensor response was verified by comparison with a sling psychrometer.

4. Field Measurement Report

4.1 Introduction

The objective of this study was to develop a more accurate method of estimating particulate matter (PM) emissions from paved roads. PM_{10} (particles less than 10 μm aerodynamic diameter) mass concentrations were determined using samplers upwind and downwind of roadways. Meteorological parameters were concurrently measured. Particulate matter was collected using cyclone or impactor size-selective inlets followed by 47 mm Teflon membrane filters. Sampling periods were approximately six hours during afternoons, when the prevailing wind direction was westerly and perpendicular to the freeway. Filters were weighed with a microbalance to determine the mass loading. Silt samples were collected from either representative roadways or from the actual roadways during testing. In addition tracer releases were made upwind of roadways or surrogate roadways and concentrations of tracer gas measured downwind in order to provide data for model validation.

4.2 Approach

4.2.1 Measurement Methodology

This section describes the equipment used for the field measurements. The quality control measures such as calibration are included with each method. More generic quality assurance is described at the end of this section.

4.2.1.1 Meteorological Sensors

RM Young AQ wind speed/direction, temperature, and humidity sensors were used. These sensors were placed on either a 5- or 10-meter tower. The 10-meter tower was equipped with wind sensors at either the top or at every 3 m depending on the experiment performed. Three component measurements were obtained at each level.

The wind anemometers were calibrated by attaching a synchronous motor to the cup shaft as described in the manual. Factory conversion factors to convert rpm to speed were used to generate a calibration curve by comparison with the readout of the data logger. Application of this calibration was applied, if necessary, during data post-processing. The wind direction sensor was aligned with true north using a compass mounted on a tripod. Responses were verified by comparing the data logger output with compass measurements while the sensor was held at the four cardinal directions. The temperature sensor was calibrated by immersing the sensing element in water in close proximity to a thermometer traceable to the NIST. Three nominal temperatures were used, 0, 20, and 40 °C. The relative humidity sensor was not calibrated, but the response was verified by comparison with a sling psychrometer.

4.2.1.2 PM

Two different types of PM samplers were used, one for PM_{10} and the other for $PM_{2.5}$. For PM_{10} a Graseby-Andersen model 246B was used, but modified such that a single filter could be directly attached to the inlet. The filter sampler was operated at 16.7 L/min using tubing, needle valves, and rotameters to direct, control and measure the flow through each filter. For $PM_{2.5}$, Sensidyne model 240 cyclones sampling at 113 L/min were used to provide the cutpoint. Filters used for both were Gelman Teflo, chosen for their low tare weight and mass stability. Samplers were operated on batteries, generators or commercial electricity depending on the site location.

Each sampler used a rotameter in-line to measure flow stability. A single rotameter was used to check the flow. Rotameters were calibrated against a dry test meter (Singer model DTM-115) that has a primary calibration traceable to the NIST. The dry test meter was installed at the inlet to the filter holder with a filter in place. Five nominal flow rates were used (1, 2,14,16,18,20 L/min). The flows were determined over a 1-minute nominal period timed with a hand held digital stopwatch. Flow rates were converted to standard conditions of temperature and pressure and a calibration equation obtained from a linear regression of the data. Temperature was determined on-site with a thermometer traceable to the NIST. Site pressure was calculated from the altimeter setting obtained at the Riverside airport and adjusted for differences in elevation (using a topographic map). The rotameter flow rate corresponding to 16.7 avg. L/min was determined and used as the set point. The bypass flow of the cyclone sampler were measured with a Dwyer model RMA rotameter calibrated against an American Meter model Al-175 dry gas meter.

Filter sampling forms were used to tabulate pertinent sampling data. This includes filter number, sampler ID and location, beginning and end indicated flow rates, date, time, and identification of technician performing the filter loading and unloading. Unusual conditions and handling were noted in a comments area. After sampling, the filters were transferred from the holder to a Petri dish for storage. A copy of the sampling form accompanied the sample and each movement and change in custody were noted on this form. Figure 4-1 shows the filter sampling form.

Figure 4-1. Filter sampling form.

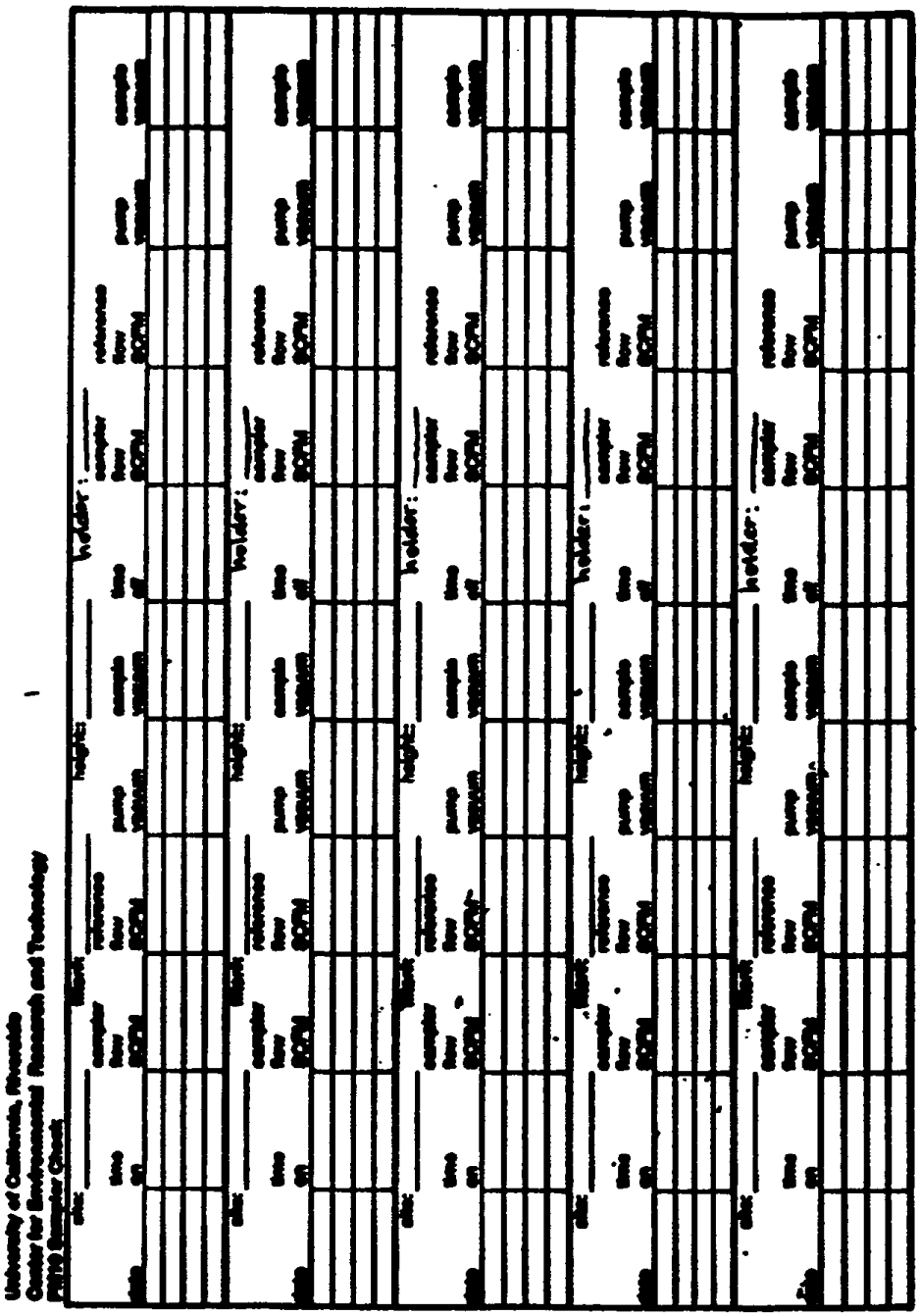

Integrating nephelometers have been traditionally calibrated by purging them with Freon 12 to obtain a standard response. As a stratospheric ozone depleter, the release of this gas into the atmosphere is no longer acceptable. We therefore performed the calibration by purging with Freon 134a, one of the acceptable replacements. The response of this gas is approximately half that of Freon 12. The calibration was otherwise conducted as described in the operator's manual.

While the responses of both gases are far below the expected measurements in the field, suitable and consistent response factors may be obtained. For these experiments, the relationship between B_{scat} and measured PM_{10} were used to estimate short-term particulate concentrations.

4.2.1.4 SF_6 Tracer

Samples for tracer analysis were analyzed by either a flame photometric sulfur analyzer for high concentrations (above 100 ppb) and a gas chromatograph equipped with an electron capture detector (below 100 ppb).

These instruments were calibrated with a commercial gas blend with a concentration of tracer gas traceable to NIST. A Columbia model 1800 calibrator was used to blend the calibration gas to the concentration range needed. The model 1800 was calibrated quarterly with a certified dry test meter using a CE-CERT SOP.

4.2.1.5 Silt Loading

Samples taken from vacuumed roadways were sifted and weighed into three categories:

- Particles > 425µm in diameter (#40 mesh screen).
- Fines < 425µm in diameter but > 75µm in diameter (#200 mesh screen).
- Silt ≤ 75µm in diameter (bottom tray).

After sampling, the opening of each bag was covered by a small piece of duct tape so as to keep in airborne particles. The duct tape was removed before performing the sieving and weighing. Non-powder gloves were worn throughout the sieving process for quality assurance. The CSC Scientific Meinzer Sieve Shaker, model #18480-033, was used in the silt loading analysis.

Bags were tared before they were used for vacuuming a sample. After vacuuming, bags and their contents were weighed before and after sieving. They were opened at the top by unfolding the manufacturer's glued-down seam. Contents were emptied into the top sieve tray, which had a 425 µm diameter opening sieve. The bottom portion of the bag was also opened in the same manner as the top and the contents were removed. The cover was fastened over the top tray and placed on the sieving shaker, where it was bolted down securely. Sieving was achieved after 5 minutes of shaking. The emptied bag was weighed and recorded. Each individual tray was dusted and weighed for fines sticking to the wire mesh or adhering to the sides. The top two trays were weighed to ±0.01g using a Denver Instruments Model XL-1810 balance while the bottom tray was weighed at ±0.0001g with a Denver Instruments Model A-1600 balance. All samples were equilibrated to 50% RH and 70°F prior to weighing. Each sample and original bag that contained

the fines was sealed and labeled describing the site location, date, time, and collecting technician for storage.

Roadway vacuuming was performed using the Sears Kenmore vacuum cleaner model #1162501290 equipped with a "Micron Filtration Bag," #[20] 50558. These bags were used so as to retain those fines less than 75μm in diameter within the bag. Filter bags were weighed before and after each run to the nearest milligram. This was to assure that silt trapped inside the filter medium would also be accounted for in a mass balance.

Due to variables such as freeway access, car count, and the terrain of each road, two different procedures were fabricated when vacuuming freeways as opposed to arterial, collector, and local roads. The roadways were defined as the following:

- Freeways: Four or more lanes with a car count of at least 150,000 cars per day.
- Arterial: Four or more lanes with a car count of 10,000 to 150,000 cars per day.
- Collector: Two lanes with 500 to 10,000 cars per day.
- Local: Two lanes with 500 cars or fewer in a day.

Because active freeway lanes had significantly less material on them than the other three roadway types, a longer section of lane was vacuumed in order to obtain a significant amount of silt to weigh. Two 10-foot long, 4-inch by 4-inch beams were placed 50 feet. apart, connected by rope. The rope was tied to each beam at 9 equal sections 13 inches apart. This rope acted as a guide that the vacuum head would run along. The width of the vacuum head was 14.5 inches with an exposed rotating brush that was 13 inches in length. Therefore, there was 3/4 of an inch overlap from the top of the vacuum to the side of the rope. Ultimately, the area vacuumed was 500 ft^2 for one bag. This was a reproducible area if more sample needed to be collected per bag. The vacuuming speed, performed by one operator, was on the order of 12 ft/min. The manufacturers' vacuum speed was set to "XLOW."

Non-freeway roads were individually measured and marked depending on the estimated sample that lay on the surface. Prior to 11/13/96, the active traffic lanes of non-freeway roads were vacuumed parallel with the traffic lines. After this date, due to safety reasons, the marked area was vacuumed perpendicular to the traffic lines. In which case, duct tape was laid down every 2 ft. within the marked area as a guide for the vacuum head.

4.2.1.5.1 Resuspension Chamber

The resuspension chamber was a mobile device that collected and fractionated fines directly from a paved road. The chamber's base was a two shelved utility cart. Figure 4-2 is a diagram of the layout.

The top shelf was equipped with a pair of Sensidyne model 240 cyclones to collect $PM_{2.5}$ and a pair of Graseby-Andersen model 245B inlets to collect PM_{10}. Two 2-inch diameter PVC pipes

were installed to act as a sampler collecting total suspended particulate (TSP). A 3-foot-high, 25-inch diameter cylinder of 16 gauge sheet metal was used to hermetically seal the sampler inlets. Each of the six samplers used a 47mm Teflo filter, which was weighed before and after each run. Sampler inlets were located equidistant from the sides and the center. Tubing connected each sampler/filter to a corresponding rotameter (fastened to the side of the cart) that measured the flow rates. On the bottom shelf were two 3/4 Hp Gast pumps, model #1023-V1310-G608X, that supplied the flow rates for the $PM_{2.5}$, PM_{10}, and TSP samplers, which operated at 240, 35, and 7 scfh respectively. In the center of the chamber was an inlet pump assembly from a high volume PM_{10} sampler providing a 1600 L/min flow to the system. A type A/E, 8-inch x 10-inch glass fiber filter was fastened above the high-volume sampler to protect the motor and to collect a third TSP sample.

Along the outside of the chamber was a 4-foot-long impactor made from a 4.5-inch inside diameter ABS pipe. It was designed to remove particles of greater than 75mm in diameter, which were trapped at the bottom. These particles would then be removed and weighed by use of a removable cap on the bottom of the impactor. Fines less than 75mm in diameter were carried by the vacuum's air stream into the chamber. The Sears Kenmore vacuum cleaner head was fitted to the inlet of the impactor.

The length of the collection period was the amount of time required for the blower pressure from the high-volume TSP sampler to go from 3.5-inches to 2 inches of H_2O. Below this pressure, the 8 x 10-inch glass fiber filter above the blower would rapidly become plugged, thereby, hindering the flow of air. The area vacuumed was directly proportional to the blower pressure and air flow. The more fines that were vacuumed, the faster the blower would have a decrease in pressure. The vacuumed area was recorded in the logbook along with the start and end time and flow rates for each run. The weight of sample in the cap (located on the bottom of the impactor) and the 8 x 10-inch filter media were also recorded.

4.2.1.6 Dustfall

Dustfall was collected in open-mouth polypropylene jars with an inside diameter of 11.0 cm and a height of 13.0 cm. Jars were tared before collection to the nearest 0.1 μg and weighed after collection. Due to the small amount of material and high tare weights, the collected material was also weighed by washing into a tared weighing jar with deionized water and evaporating to dryness at 100 °C prior to reweighing.

Figure 2-2. Resuspension Chamber.

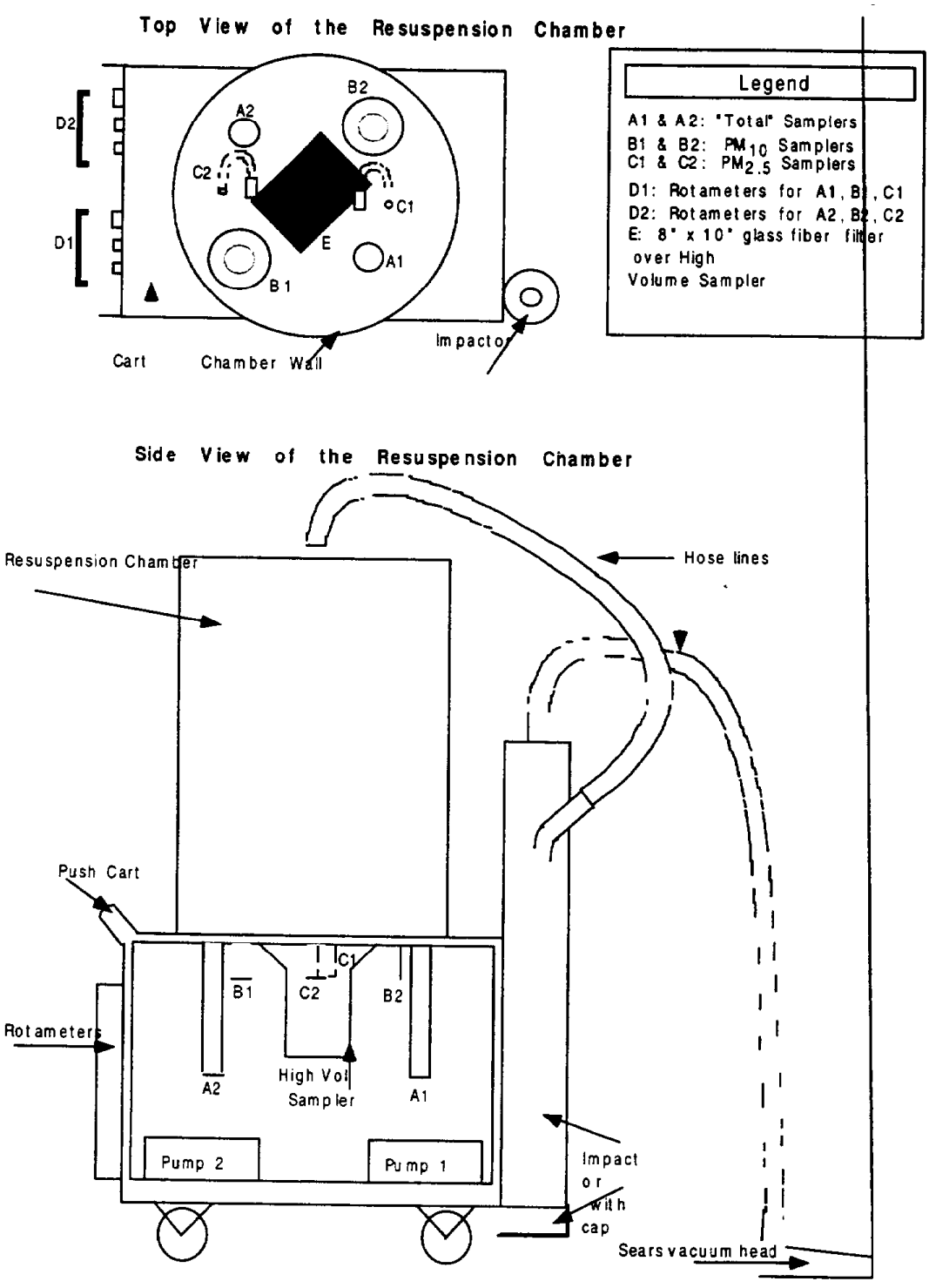

4.2.1.7 Data Collection

The data from the meteorological sensors and one of the nephelometers were collected using a Campbell CR-10 data logger. A Telog single channel data logger was used to record nephelometer data from the instrument on the other side of the road. This was programmed to collect data every second and store data as 5-minute averages. Data were downloaded in the field with a laptop personal computer and stored on a floppy disk. The data on the floppy disk were then transferred to the hard drive of a PC for storage prior to validation and analysis.

4.2.1.8 Quality Assurance

A daily checklist form was completed before each sampling day. Responses found to be out of the acceptable range would require instrument recalibration and/or repair. The following quality control checks were conducted and recorded:

- PM_{10} Samplers
  The flow at the inlets was verified while sampling with a test filter using a single transfer rotameter. The acceptable range is 16.7 +/- 1 L/min.

- Integrating Nephelometer
  The nephelometers were purged with particle-free air and the response at the data logger to this and an internal calibration source noted. The acceptable ranges are $0.2 +/- 0.1 \times 10^{-4}$ m^{-1} for the particle-free air and +/- 10% of the response of the internal source observed immediately after the last calibration.

- Wind Speed Sensor
  The reading of a rotameter-type (Dwyer Portable Wind Meter) anemometer held next to the site anemometer was noted along with the instantaneous response of the instrument. An acceptable comparison is agreement within 2m sec^{-1}.

- Wind Direction Sensor
  The direction of the wind vane was determined with a compass and compared with the instantaneous response of the data logger. An acceptable comparison was in agreement within 20 degrees.

- Relative Humidity Sensor
  The relative humidity was determined with a Psychro-Dyne electric sling psychrometer and compared with the data logger response. An acceptable comparison is agreement within 10% RH.

- Temperature Sensor
  The temperature of the sling psychrometer dry bulb is compared with the instantaneous reading from the data logger. An acceptable comparison is +/- 2°C.

A logbook was maintained at the site and all relevant calibrations, experimental procedures and observations were recorded. Separate data sheets, described previously, were maintained for

entering filter sampling data and instrument QC checks. Calibration factors were applied to continuous data after transferal to a spreadsheet maintained in a PC. PM_{10} concentrations were calculated from the completed filter sampling form and also entered into the spreadsheet.

The validity of the data was checked as follows: Data were not be removed unless there was a good reason or the measurement was physically impossible. All data were screened for outliers that are not within the normal ranges physically reasonable. The following control limits were used:

PM_{10}	0-1000 $\mu g\ m^{-1}$
B_{scat}	0-100 x $10^{-4}\ m^{-1}$
Temperature	0- 40û C
RH	0-100%
Wind Speed	0- 50 m sec^{-1}
Wind Direction	0-360û

Meteorological data were reviewed as time series plots. Rapidly changing, anomalous or otherwise suspect data were examined with respect to other data at this and nearby meteorological monitoring stations to determine validity. B_{scat} data were compared with PM_{10} measurements at the same site by averaging the B_{scat} over the sampling interval. Time series plots and linear regressions were reviewed to determine consistency. The original data and logbook entries were examined to determine the cause of inconsistent data.

4.3 Field Study Designs

4.3.1 Upwind-Downwind PM

The intensive monitoring approach involves setting up sampling equipment upwind and downwind of highway activities, and intensively measuring concentration and micro-meteorological parameters. AP 42 identifies particulate emission to be occurring from paved roads as a result of the silt loading on the road and the mean vehicle weight, speed and the number of wheels. Rather than using default silt loadings, these were measured, when possible, by vacuuming a section of the road, as described previously.

The traffic flow was characterized by counting cars for 10-minute intervals each hour of sampling. Measurement of meteorological data (e.g. temperature, velocity profile) and particulate concentrations were also be performed. Figure 3-1 (in Section 3 of this report) shows the typical experimental layout. Sampling equipment was set up both upwind and downwind of the road to be characterized. A 10-meter tower was located on each side at a distance of 5 m from the edge of the road. PM_{10} and $PM_{2.5}$ sample inlets were placed at three elevations (1, 3 and 5m) on each tower. These instruments were operated following EPA procedures (U.S. Environmental Protection Agency 1977, 1989) as closely as practical for this application. Two additional samplers were occasionally located at 10 and 20 m downwind at a height of 1 m. A Graseby model SA 246B (16.7 L/min) inlet was used for PM_{10} and a Sensidyne model 240 cyclone (113 L/min) for $PM_{2.5}$ size cuts, each coupled to a sampling plenum with 47 mm filter holders and a

Gelman Teflo Filter. The PM_{10} inlet has been accepted by the EPA as equivalent to the PM_{10} reference method. Sensors to measure wind speed, direction, and temperature were also located at three elevations on the upwind tower; a three component anemometer was placed at the top of the tower. Met data was collected using a data logger and was stored either as five or fifteen-minute averages. .

As a means of supplementing the filter sampler data, integrating nephelometers with PM_{10} inlets were placed at the middle level of each of the towers during the initial tests. The response of the nephelometers was much faster than even the "continuous" PM_{10} devices. While these devices are not EPA-approved and do not directly measure mass loading, they provide a scattering coefficient measurement, which can be related to mass concentration through the filter samples. For selected experiments, a tracer gas (sulfur hexafluoride, SF_6) was released at a predetermined rate in the field experiments as a line source along the paved road. The line source consisted of 200 feet of 0.25-inch OD polyethylene tubing with union "T"s inserted every 6 feet. A section of 2-inch-long capillary tubing, 0.0625 inch OD x 0.0.050 inch ID, was attached to the arm of each "T." A gas regulator was used to maintain a constant pressure to the polyethylene tubing while flows of SF_6 through the capillaries were measured with a bubble flow meter and found to have a standard deviation of 10%. Samples for SF_6 analyses were collected in 30 L Teflon bags by using a diaphragm pump.

These intensive experiments were performed on six roads in Southern California (one freeway, three arterial, one collector, and one local) during three seasons. Each short-term test was conducted over one to four day periods with one sample set collected per day during the time when the wind was from the west, the prevailing on-shore flow in the Riverside area.

4.3.2 Dustfall

Dustfall collection jars were placed on the sites of Canyon Crest and Riverside Drive. The plastic jars were tared prior to exposure to atmospheric conditions and again weighed after sampling.

4.3.3 Silt Loading

Silt loading experiments were performed on freeway sites while accompanied by the California Department of Transportation (Caltrans) employees. Access was gained by permission of Caltrans superintendents in the event of a planned lane closure. During the lane closure, technicians were placed within the Caltrans convoy and blocked by a safety vehicle. This and other safety provisions, such as wearing hard hats and orange vests, were stated by Caltrans in the permits (#08-96-N-SV-0783 and #08-96-N-SV-1140) granted for sampling. As in the case of freeway sampling, cones, flags, blocking trucks, and other safety equipment were arranged by Caltrans and not by the technicians performing the silt loading. A generator supplied power for the vacuum and was left in the back of the technicians' vehicle. Extension lines were run from the generator to the vacuum. Heavy equipment was intentionally left in the vehicle in case Caltrans unexpectedly moved to another site.

Shoulders, active lanes, exit and entrance ramps were sampled for silt loading. The type of area and extent was usually dependent upon the work that Caltrans needed to accomplish. To ensure complete vacuuming, two wooden 4 x 4-inch beams were connected with guide ropes were

placed over the area to be sampled. The vacuum cleaner was moved parallel with the traffic lines. Due to Caltrans' traffic control system for lane closures, cones hindered access to some entire active traffic lanes. In this case, the shoulder was vacuumed. Shoulders of most freeways contained an excess of particles along the curb. The 4 x 4-inch beams were not included in this portion. Instead, a small sample area adequate for sieving was vacuumed. This area was relative to the amount on material deposited. This allowed the 500 ft^2 of shoulder to be vacuumed without the bag becoming overloaded and the silt loading of the fines closest to the curb. In some instances, a second 500 ft^2 area was vacuumed with the same bag when an amount of fines less than 100g was observed.

Two technicians were present while vacuuming for silt loading samples along any roadway. While one operated the vacuum, the other assisted in changing the rope guides along the beams and moving the extension cord while acting as a spotter for cars. Each vacuum bag was labeled and sealed. Documentation of the labeled bag and area vacuumed was noted in the logbook. Any peculiarities in texture of the asphalt or concrete, change of vacuum speed, and particle distribution along the road were also noted. Pictures of each site were taken before and after sampling to show the appearance of any distribution.

Sampling along non-freeway sites took a similar approach. Orange cones were set up 100 feet beyond the area that would be sampled. Power was supplied to the vacuum from a generator also supplying power to the pumps for the PM_{10} sampling.

Shoulders of streets were treated similarly to those of freeways where much of the particles and fines were located adjacent to the curb. Shoulders on non-freeway sites were usually smaller than those on freeways, and depending on the amount of deposit, a larger area was generally vacuumed. The area sampled on arterial and collector roads was dependent on size of the deposit estimated visually. Sampling the active traffic lane of these streets was different since the safety equipment that Caltrans utilized was not available. The roads were individually measured and marked and the area sketched in the logbook. The width of the area marked was at least 12 inches from the lane striping (in cases of arterial roadways that have at least 4 lanes.) In situations such as the collector roadways, the traffic lane was visibly determined by the pattern of debris deposition, but it was not feasible to close the entire lane. In this case, duct tape was laid down every 2 feet perpendicular to the road to serve as a guide for the vacuum head. A technician vacuumed the area when the road remained clear of cars as another spotted for hazards.

4.3.4 Tracer

The SF_6 line source was 200 feet long and was laid out parallel with the road on the upwind side. It was made with ¼-inch inside diameter polyethylene tubing. At every 6 feet there was a Teflon tee fitting with a 3-inch-long, 10/1000 inch outside diameter capillary tubing that released the gas. A total of 30 capillaries comprised the release mechanism. Each capillary opening was tested for adequate flow and leaks. Each capillary was held upright by use of a small clamp drilled on top of a 12-inch long, 2 x 6-inch block of wood. Two sets of 100 foot line were connected to a diaphragm pump that diluted the flow of SF_6 from the cylinder with ambient air. The cylinder was equipped with a regulator and rotameter for a desired pressure and flow rate.

The SF_6 flow rate, regulator pressure, and individual release capillary flow rates were noted in the logbook.

The receptor site was located downwind of the roadway. It consisted of a 40-foot tower placed on a car trailer. The trailer allowed the receptor site to be mobile so the tower could be centered within the SF_6 plume. Along the tower, individual pieces of ¼-inch polyethylene tubing were attached at various heights. Tubing ends were individually connected to the inlet of a 1/20 Hp diaphragm pump. The pumps contained rotameters and needle valves allowing the receiving flow rate to be altered. The outlet of each pump was connected to a Tedlar bag equipped with a shut-off valve. Each bag was numbered and recorded into the logbook. The heights sampled for SF_6 analysis also were recorded.

4.3.4.1 Parking Lot

A SF_6 experiment was performed on CE-CERT's parking lot as a trial run for the roadway tracer experiment. The meteorological tower was assembled first so as to find the wind direction and consequently the placement of the receptor tower and release line.

The tower was raised at the far east side of the parking lot. Individual pieces of tubing were attached with tape at heights of 40, 33, 23, 18, 9, and 5 feet. Each end of the tubing was connected to the diaphragm pumps, whose flow rates were set at 3 cc/min. Bags attached to the pumps were labeled and recorded into the logbook.

The 200-foot release line was placed so that the center of the line was 300 feet from the tower. This distance was used because it was the same as the distance used for previous freeway measurements. A pump connecting the two 100-foot. lines was set at 18 psi, delivering a flow rate of 21 scfh. The SF_6 cylinder regulator was set for 10 psi with a flow rate of 200 cc/min. Each of the 30 capillaries was checked and compared for flow rates with a rotameter. Nozzles with inadequate flows were repaired on site.

A 1/20 Hp pump was placed 116 ft. upwind from the release line at a flow rate of 1 cc/min. The SF_6 sample was collected from a height of 9 feet. This point was the blank in which to measure any background SF_6. Pumps used for the release line and the two receptor locations were powered by two generators. Duplicate runs were executed, both with a 45-minute run time.

4.3.4.2 Roadway

For evaluating the effect of traffic turbulence along the freeway, the following field situation was designed. The freeway site located was Interstate 15 in Ontario. Its estimated width was 300 feet. Figure 3-11 (in Section 3 of this report) shows the layout. The width was found by measuring the distance of the overpass bridge running perpendicular to the freeway near the proposed site. The distance between the upwind release system and downwind receptor tower was the same for the freeway and the non-freeway sites. The non-freeway site was a vacant field east of Interstate 15 running parallel with the freeway between Kettering Drive and Auto Center Drive. Due to the curvature of the street, the tower was arranged such that the distance from the center of the line to the receptor tower was 300 feet. Wind direction also was taken into account in order to have the

tower in the center of the plume. A meteorological tower was used to measure and observe the wind speed, temperature and humidity, and vertical wind speed. Since it was downwind of the actual freeway site, the non-freeway experiment was chosen first so SF_6 would not be exposed in the background for the next run. The SF_6 flow rate release was set for 600 cc/min and the regulator at 20 psi. The pump connecting the two release lines were set at 18 psi and a flow rate of 21 scfh. Receptor heights on the tower were 40, 33, 23, 18, 9, and 5 feet. Each pump was set for a flow rate of 300 cc/min. The run time for the non-freeway site was 45 minutes.

The second run of the pair of roadway/non roadway sampling was achieved by moving the source line and the tower to monitor the active freeway. The source line was set on Rochester Avenue (the upwind side of the freeway) and the tower on Kettering Drive. (the downwind side the freeway). The wind vane aided in the placement of the tower with respect to the line source when doing these runs. Flow rates on the cylinder and diaphragm pumps and the pressure gauges were not changed from the previous run, but were examined for consistency. The start and finish time for each run were recorded into the logbook. The freeway and non-freeway road orientations also were noted in the logbook.

4.3.5 Shoulder Resuspension

The AP-42 model explains that particulate emissions are a result of silt loading, the weight of vehicles, and the distance the vehicle travels. The shoulder and curb sites were found from our vacuuming to contain much higher loadings of silt than the road itself. An experiment was therefore performed to analyze the movement of silt along a block length.

The street outside of CE-CERT, Columbia Avenue (in Riverside), was chosen. This site was lightly traveled; therefore, the car count could be controlled using our own vehicles. Dirt was from a neighboring field was laid evenly with a lawn seeder 3 feet in width along a 255-foot. stretch of shoulder. A vacuum sample was collected before the experiment began at three points along the dirt strip: 1 foot, 126 feet, and 254 feet from the beginning of the strip. At each point, a section of 2-feet, 4 inches by 3 feet was vacuumed, which was equivalent to two passes of the vacuum cleaner head. This was to ensure that enough sample was taken for sieving. Cones were initially placed 9 feet from the curb as a marker for vehicles. Vehicles drove past this stretch of shoulder a designated number of times at a constant speed. After 24 passes with a Suburban truck, at 35 mph, the cones were placed on top of the dirt edge. Other vehicles, including a Toyota pickup truck, a Ford station wagon, and a Ford pickup truck, also were used. The combined vehicles made a total of 100 passes at an average speed of 35 mph. The next sections sampled were at 5 feet, 122.5 feet, and 250.5 feet from the beginning of the dirt so there was a 1-foot section between each sampling. Pictures were taken to document the differences in dirt height and any plumes that were created by vehicles as they passed the section. The following day, a total of 15 passes were made at 35 mph with the Suburban truck on top of the dirt stripe. Three sections were vacuumed at 8.5 feet, 119 feet, and 247 feet. It was noted in the logbook that moisture the night before had hardened the remaining dirt particles to the surface of the shoulder.

4.4 Measurement Sites

Streets were chosen on the basis of accessibility, safety, orientation and car count. The accessibility of roads was a factor because there was a need for vehicles to drop off sampling

equipment. Safety issues also became apparent if the vehicle would stop the flow of traffic. Only streets running north-south were used. This was to assure that the onshore winds coming from the west would be perpendicular to the street. The car count was a major factor in helping to define the type of street that would be sampled. There were four types of roadways measured for PM_{10}. They are defined by car count and the number of lanes on the road:

- Local: < 500 cars/day (2 lanes)
- Collector: 500 - 10,000 cars/day (2 lanes)
- Arterials: 10,000 - 150,000 cars/day (3–4 lanes)
- Freeway: More than 150,000 cars/day (>4 lanes)

Figure 2-3 shows the location of the streets selected. The site chosen to represent local roads was Fogg Street. Most of the traffic on this two-lane road is residential, although a few large trucks also were counted. Atlanta Avenue was determined to be a collector street. It is a two-lane road that runs through an industrial area, and most of the traffic was from workers whose jobs are in the area. Riverside Drive (formerly named Main Street in previous progress reports), Canyon Crest Drive, and Iowa Avenue were used as arterial streets. These streets each have four lanes and car counts of about 1,000 vehicles per hour. They either are at the entrance or exit of a freeway or are major streets. The 6-lane freeway used was the Interstate 215/Highway 60, which runs through Riverside toward San Diego. A one-lane dirt road with a zero car count located in the Agricultural Operations Field on the University of California, Riverside, property was used as a comparison for the previously mentioned roads as the maximum amount of silt loading obtainable on a road.

4.5 Results and Discussion

The results of the roads sampled for PM_{10} can be found in Appendix A to this Field Data Report. This table presents each road with an upwind and downwind concentration of PM_{10} along with average meteorological data for that sampling day. The meteorological data includes temperature, relative humidity, wind speed, wind direction, and ΣW, which is the standard deviation of the vertical wind speed. In addition to PM_{10} field measurements, silt loading field measurements can be seen in Appendix B to this Field Data Report. This table shows the street name, the area vacuumed, the total mass collected, and the silt content in g/m^2.

Figure 4-3. Map of the Riverside/Colton Area, showing sampling locations.

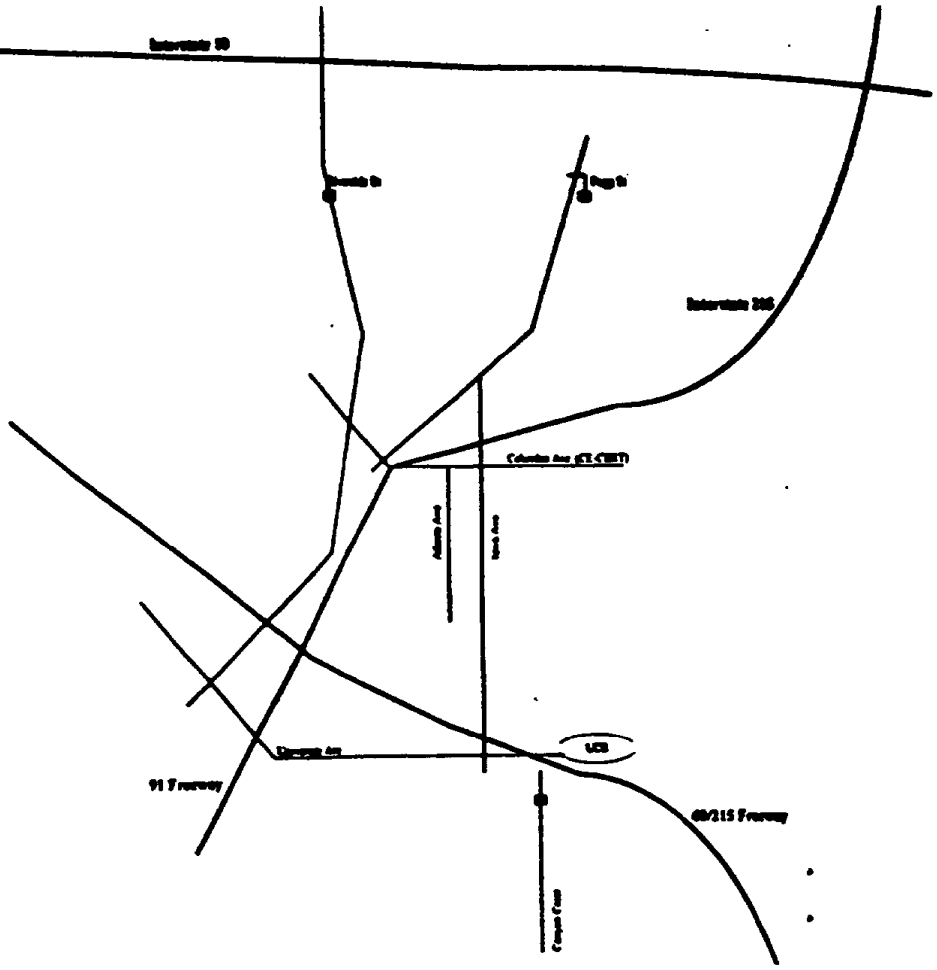

4.5.1 Measurement Precision

Teflon filters used to collect PM_{10} were equilibrated inside a LaminAir flow hood at 25•C and 40% RH for a 24 hour period both before and after sampling. Filters were weighed on a Cahn 40 balance adhering to the CE-CERT SOP. Filters were weighed to the nearest micorgram. Calibrations were performed at the start and end of weighing and at every 20th filter weighed. They were weighed within 200.000 +/- 0.003 mg. Zero checks were performed at the beginning and end of every weighing and at every 5th filter weighed. Zero checks had to be within tolerances of +/- 0.003mg in order to have a non-failed filter.

Filters were labeled sequentially, corresponding to a logbook. Each filter was weighed three times before and after sampling. An average of these three weighings was calculated to be the weight of the filter.

To evaluate the overall sampling precision, five collocated PM_{10} samplers were operated for five collection periods averaging 13 hours. The average concentration was 68 $\mu g/m^3$ with an average

standard deviation of 12%. We conclude that measurement uncertainty under these conditions was ± 8 $\mu g/m^3$.

4.5.2 Upwind-Downwind PM

As seen from the data sets of paved roadways in Appendix A, the concentration differences from downwind PM_{10} to upwind PM_{10} varied from 21 $\mu g/m^3$ (Riverside Drive, 9/5/96) to no difference at all (Canyon Crest, 5/20 - 5/23/96). A large concentration difference was seen for the unpaved roadway in the Agricultural Operations Field (Ag Ops). The differences were as high as 328.7 $\mu g/m^3$ (7/9/96) and 272.4 $\mu g/m^3$ (9/12/96). A summary of the location, setup, and sampling of each site is below. The months between November and March were found to be non-conclusive of sampling due to the irregular wind patterns or rain.

4.5.2.1 Iowa Avenue

Iowa Avenue is a four-lane road in Riverside. It is an arterial street with a traffic count of 1,000 vehicles per hour. The street runs from the Interstate 215 through industrial buildings to the University of California, Riverside. The upwind PM_{10} samplers were at Hunt's Park, 20 meters from the curb. The downwind samplers were on the front yard of the Bourns building, 1 meter from the curb. Samplers on both ends were set at heights of 1, 3, and 5 m. A diagram of the sampling set up can be seen in Figure 4-4. Having sampled Iowa Avenue for three days, average concentration differences of 15.8, 10.5, and 7.9 $\mu g/m^3$ were calculated as seen in Table 4-1.

Table 4-1. The upwind and downwind concentrations, standard deviations, and concentration difference on Iowa Avenue for four days.

Date	Avg. Upwind Conc. ($\mu g/m^3$)	Standard Deviation of Upwind Conc. ($\mu g/m^3$)	Avg. Downwind Conc. ($\mu g/m^3$)	Standard Deviation of Downwind Conc. ($\mu g/m^3$)	Conc. Difference ($\mu g/m^3$)
1/18/96	65.4	6.9	81.2	11.3	15.8
1/9/96	70.6	4.2	81.1	1.7	10.5
1/18/96	38.5	2.8	46.4	4.3	7.9
4/26/96	102	11.3	96.5	13	-5.5

Figure 4-4. Site set up on Iowa Avenue for the dates of 1/8, 1/9, 1/18, and 4/26/96.

PM_{10} and $PM_{2.5}$ Sampling on Iowa Avenue

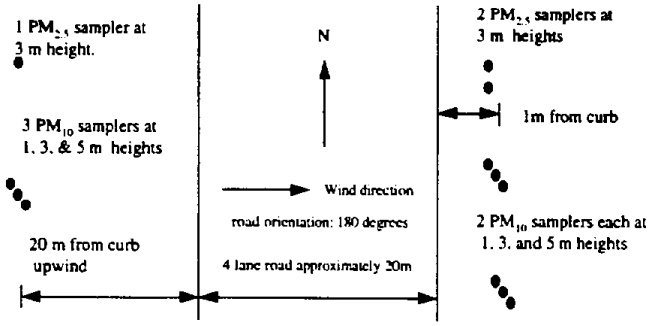

4.5.2.2 Riverside Drive (Main St.)

Riverside Drive (formerly called Main Street in progress reports) runs through downtown Riverside and into the city of Rialto. It is an arterial road that passes through industrial and commercial buildings and farmland. The site where sampling took place was on the county portion of Riverside Drive near the corner of Agua Mansa. Both upwind and downwind samplers were set up on dirt lots. The nearest building was within 100feet of the downwind samplers. The downwind and upwind sites were accessible by either the road's shoulder or by driving onto the dirt lots. The upwind samplers were 85 feet from the curb and downwind samplers were 3 feet from the curb. Generators supplying power to the pumps were set at a minimum of 100 feet away and out of direct contact from the samplers. The heights of the samplers varied from 1, 3, and 5 m to collocated sampling at 2 m. A diagram of the sampling set up can be seen in Figures 4-5 and 4-6. Car counts, taken every 10 minutes, were calculated to be 900 to 1,000 vehicles per hour. From June through September, average PM_{10} differences ranged from 2.2 to 21.0 $\mu g/m^3$. The differences during October and November ranged from 8.4 to 15.9 $\mu g/m^3$. Differences during March through June were 4.6 $\mu g/m^3$ to 21 $\mu g/m^3$. Table 4-2 shows the sampling dates for Riverside Drive and the concentrations for each. A more detailed table including meteorological conditions can be found in Appendix A.

Table 4-2. The upwind and downwind sampling of Riverside Drive with the standard deviations and concentration differences.

Date	Avg. Upwind Conc. ($\mu g/m^3$)	St. Dev. of Upwind Conc. ($\mu g/m^3$)	Avg. Downwind Conc. ($\mu g/m^3$)	St. Dev. of Downwind Conc. ($\mu g/m^3$)	Avg. Downwind Conc. ($\mu g/m^3$)	St. Dev. of Downwind Conc. ($\mu g/m^3$)	Avg.Conc. Difference ($\mu g/m^3$)
6/17-6/18/97	96.7	7.9	110.9	8.8	N/A	N/A	14.2
6/19-6/20/96	116	34.6	133.2	14.9	N/A	N/A	17.2
6/25-6/26/97	77.4	2.7	79.6	N/A	N/A	N/A	2.2
8/6/96	76.8	2.4	83.5	6.1	80.37	4.1	5.1
9/3/96	87.4	1.7	89.6	4.8	93.6	2.6	4.2
9/5/96	77	2.3	107.6	33	88.4	3.8	21.0
9/24/96	154.8	2.2	168.5	4.5	166.1	2.3	12.5
10/2/96	126.8	4.2	133.63	2.25	136.81	0.6	8.4
11/19/96	162.8	3.13	179.8	0.4	177.5	1.6	15.9
3/17/97	83.13	5.34	74.81	4.77	81.25	3.15	-5.1
3/19/97	40.6	2.45	59.3	0.4	63.9	1.6	21.0
5/29/97	67.2	3.5	69.5	1.4	74.2	2.5	4.6
6/4/97	65	8.3	75.7	6.8	74.7	2.1	10.2

Figure 4-5. Site setup on Riverside Drive on the Following dates: 6/17-6/18/96, 6/19-6/20/96, 8/6/96, 9/6/96, 9/5/96, 9/24/96, 11/19/96, 3/17/97, 3/19/97, 5/29/97, 6/4/97.

PM_{10} Sampling on Riverside Drive

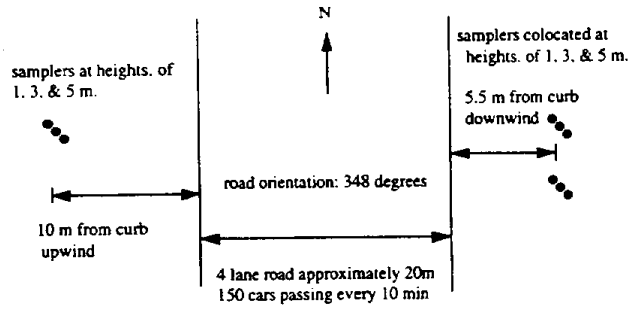

Figure 4-6: Alternate Sampling Setup for Riverside Dr. on 6/25-6/26/96.

PM_{10} Sampling on Riverside Dr. (alternate sampling)

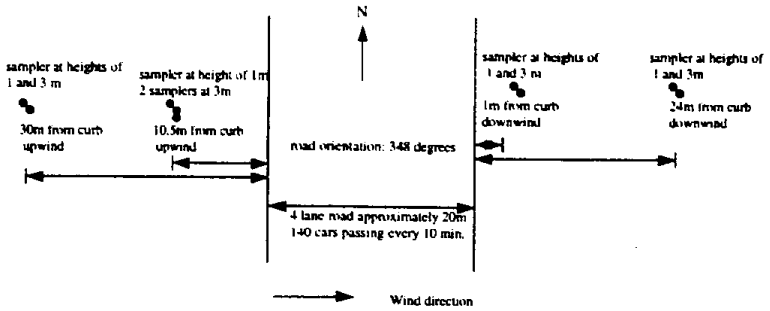

4.5.2.3 Canyon Crest Drive

Canyon Crest Drive is an arterial roadway located in Riverside near the University of California, Riverside campus. It is a four lane roadway with a car count of 1000 vehicles per hour. The site is less than a quarter of a mile near the intersection of Martin Luther King Blvd. and Canyon Crest. Beyond the sidewalks on each side of the sampling site were two citrus fields. A one lane dirt road separated the fence line of the citrus fields from the sidewalk and roadway. The speed limit on the dirt roads were kept to a minimum of 15 mph due to the Agricultural Operation's experiments on these trees. This speed on each side of Canyon Crest limited the contamination of any road dust from the field from a University vehicle. The upwind samplers were set 4 ft. from the curb and the downwind samplers were 15 ft. from the curb. This was to allow access of the sidewalk for pedestrians. Generators were set 100 ft. away from the samplers and in a non-direct wind path to the downwind samplers. Samplers were set at heights of 1, 3, and 5 m or collocated at 2 m. A diagram of the sampling set up can be found in Figure 4-7.

Table 4-3 summarizes the experimental results. Canyon Crest had generally low concentration differences. No differences were accounted for on 5/20-5/23/96. During November, two sampling days showed low values of 2.7 (11/12/96) and 5.7 $\mu g/m^3$ (11/20/96). In the months of March through June, the value stayed at 5 $\mu g/m^3$ (3/18/97 & 6/5/97) or negative differences were found (3/27/97 & 5/28/97). A more detailed table for Canyon Crest is provided in Appendix A.

Table 4-3. Upwind and downwind concentrations with standard deviations and concentration differences for sampling Canyon Crest for the given dates.

Date	Avg. Upwind Conc. ($\mu g/m^3$)	St. Dev. of Upwind Conc. ($\mu g/m^3$)	Avg. Downwind Conc. ($\mu g/m^3$)	St. Dev. of Downwind Conc. ($\mu g/m^3$)	Avg. Downwind Conc. ($\mu g/m^3$)	St. Dev. of Downwind Conc. ($\mu g/m^3$)	Avg.Conc. Difference ($\mu g/m^3$)
5/20-5/23/96	57	3	57	3	N/A	N/A	0
11/12/96	56.5	0.5	57.1	1.4	61.2	1.4	2.7
11/20/96	122.8	2.1	128.1	1.1	128.9	3.5	5.7
3/18/97	56.1	1.8	60.8	5.2	61.5	1.0	5.1
3/27/97	83	5.3	74.8	4.8	81.3	3.2	-5
5/28/97	64.1	11.3	56.8	1.7	63.3	2.8	-4
6/5/97	40.1	2.9	42.2	3.3	49.2	0.3	5.6

Figure 4-7: Site Setup on Canyon Crest on 5/20-5/23/96, 11/12/96, 11/20/96, 3/18/96, 3/27/96, 5/28/96, and 6/5/97.

PM_{10} Sampling on Canyon Crest

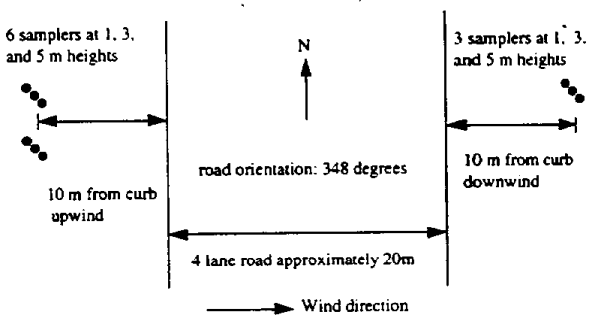

4.5.2.4 Highway 60/ Interstate 215

The portion of Highway 60/Interstate 215 sampled was near the Martin Luther King Boulevard off-ramp. The highway has six lanes with a traffic count in excess of 150,000 cars per day. Northbound and southbound traffic lanes are separated by a 3-foot concrete divider. Both the upwind and downwind samplers were located on the University's property, which was fenced. Power was supplied on site. The samplers were at 1, 3, and 5 m high or collocated at 3 m. The upwind sampler was 50 m from the shoulder, and the downwind sampler was 15 m from the shoulder. Figure 4-8 is a sampling diagram for this site. The freeway was not accessible to be vacuumed for silt content. However, other freeways were vacuumed to obtain a data set for silt content along freeways. Table 4-4 summarizes the results. The differences in concentration varied from -3 $\mu g/m^3$ (6/4/96) to 8 $\mu g/m^3$ (5/6/96). The sampling time also varied from these two dates from 32 to 10 hours of run time respectively.

Table 4-4. Upwind and Downwind Concentrations with Standard Deviations and Concentration Differences for Sampling Hwy 60 & 215.

Date	Avg. Upwind Conc. ($\mu g/m^3$)	St. Dev. of Upwind Conc. ($\mu g/m^3$)	Avg. Downwind Conc. ($\mu g/m^3$)	St. Dev. of Downwind Conc. ($\mu g/m^3$)	Avg. Downwind Conc. ($\mu g/m^3$)	St. Dev. of Downwind Conc. ($\mu g/m^3$)	Avg.Conc. Difference ($\mu g/m^3$)
5/2/96	77.5	2.1	84.5	6.2	N/A	N/A	7
5/6/96	58.5	2.2	66.5	4.2	N/A	N/A	8
5/9-5/10/96	73	5	74.3	2.1	75.5	1.7	1.9
5/13-5/16/96	66.4	10.1	61	3.4	64.7	2	-3.6
5/31-6/3/96	57	1	56	1	N/A	N/A	-1
6/4-6/7/96	86	4	83	N/A	N/A	N/A	-3

Figure 4-8: Site Setup on Highway 215/Highway 60 on 5/2, 5/6, 5/9-5/10, 5/13-6/3, 6/4-6/7/96.

PM_{10} and $PM_{2.5}$ Sampling on Hwy 215 & 60

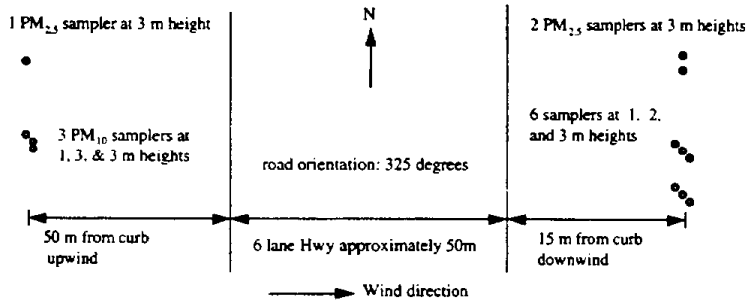

4.5.2.5 Atlanta Avenue

Atlanta Avenue is a two-lane collector road with an average traffic count of 200 cars per hour near downtown Riverside. This street is primarily used for access into small commercial buildings; consequently, most travel occurs at rush hours and noontime. Train tracks run diagonally across Atlanta. Sampling was restrained during train passage for a period of 10 minutes. Figure 4-9 shows the experimental layout. Upwind samplers were set up 30 feet from the curb in a vacant parking lot at heights of 1, 3, and 5 m. The downwind samplers were collocated at 3 feet from the curb and 10 feet from the train tracks at heights of 1, 3, and 5 m. Table 4-5 summarizes the results. The concentration difference was 13.6 $\mu g/m^3$ when sampled on 11/13/96.

Table 4-5. The upwind and downwind concentration with the standard deviation and concentration difference for sampling Atlanta Ave. on 11/13/96.

Date	Avg. Upwind Conc. ($\mu g/m^3$)	St. Dev. of Upwind Conc. ($\mu g/m^3$)	Avg. Downwind Conc. ($\mu g/m^3$)	St. Dev. of Downwind Conc. ($\mu g/m^3$)	Avg. Downwind Conc. ($\mu g/m^3$)	St. Dev. of Downwind Conc. ($\mu g/m^3$)	Avg.Conc. Difference ($\mu g/m^3$)
11/13/96	90.8	2.5	102.6	4.1	106.1	1.8	15.9

Figure 4-9: Site Setup on Atlanta Avenue on 11/13/96.

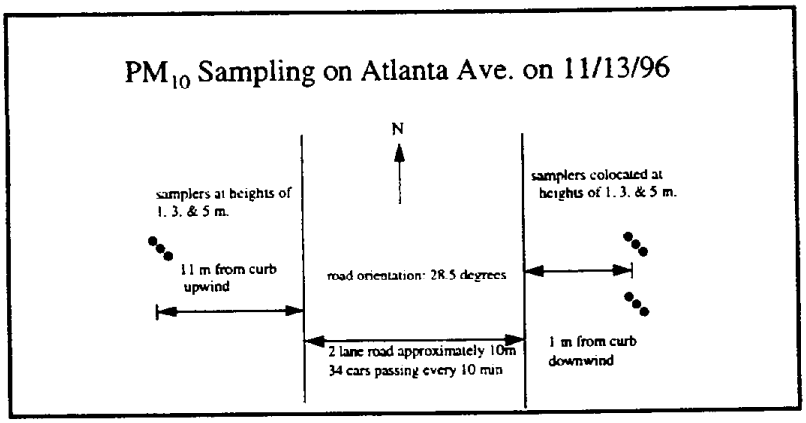

4.5.2.6 Fogg Street

Fogg Street is a two-lane local roadway in Colton a mile west of the Santa Ana River. It runs north-south in an undeveloped residential/industrial area consisting of vacant lots with a traffic count of 20 vehicles per hour. Upwind samplers were set at 1 m from the curb, 2 m high, and downwind samplers were set at 1 m from the curb at heights of 1 and 2 ms, as seen in Figure 4-10. Generators were placed 100 feet north of upwind and downwind samplers since wind direction came from the southwest during sampling. Measurement differences ranged from 10.9 $\mu g/m^3$ to 1.7 $\mu g/m^3$. Table 4-6 shows the results from four measurement days.

Table 4-6: Upwind and Downwind Concentrations with the Standard Deviations and Concentration Differences for Sampling Fogg Street.

Date	Avg. Upwind Conc. ($\mu g/m^3$)	St. Dev. of Upwind Conc. ($\mu g/m^3$)	Avg. Downwind Conc. ($\mu g/m^3$)	St. Dev. of Downwind Conc. ($\mu g/m^3$)	Avg. Downwind Conc. ($\mu g/m^3$)	St. Dev. of Downwind Conc. ($\mu g/m^3$)	Avg.Conc. Difference ($\mu g/m^3$)
3/21/97	65.0	3.45	66.3	5.3	37.1	7.14	1.7
3/26/97	81.6	7.9	91.0	5.4	93.8	1.8	10.9
5/27/97	59.7	2.2	63.1	2.4	63.7	3.7	3.7
6/3/97	85.6	1.9	85.2	3.2	90.2	1.7	2.1

Figure 4-10: Site Setup on Fogg Street on 3/21, 3/26, 5/27, 6/3/97.

PM_{10} Sampling on Fogg Street

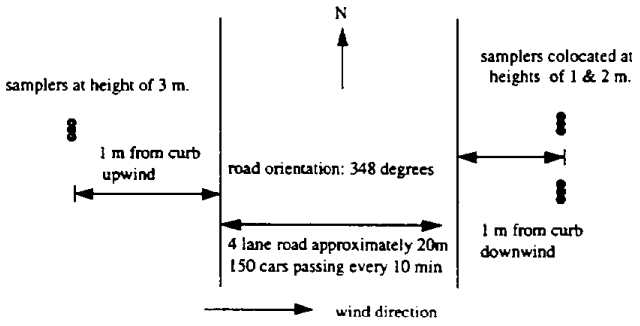

4.5.2.7 Unpaved Road (Riverside Campus Agricultural Operations)

The unpaved road within the University's agricultural field was used as an experiment to see the maximum concentration that could be obtained from a roadway. The site was an area that had no crops or other foliage to hinder the dust plumes. The collocated upwind samplers were placed 40

feet from the road at 3 m high. Downwind samplers were located at 12 feet and 80 feet from the road at 1, 3, and 5 m high. Figure 4-11 shows the sampling setup. The meteorological tower also was 12 feet from the road.

A different set of filters was used for each run. Each run consisted of two vehicles, a pickup truck and a Suburban traveling at an average speed of 15 mph. Each vehicle was timed to pass the sampling area individually since this was a one-lane road. For each day sampled, a different run time and number of passes were collected. These data are provided in Appendix A and summarized in Table 4-7. For 7/9/96 there was a run time of 1.5 hours and a total of 101 passes at 15 mph. The concentration difference for the first run was 274.7 $\mu g/m^3$. The second set had a run time of 2.5 hours and a total of 187 passes at 15 mph. The concentration difference for this run was 328.7 $\mu g/m^3$.

Table 4-7. Upwind and Downwind Concentrations with the Standard Deviations and Concentration Differences for Sampling on the Unpaved Road.

Date	Avg. Upwind Conc. ($\mu g/m^3$)	St. Dev. of Upwind Conc. ($\mu g/m^3$)	Avg. Downwind Conc. ($\mu g/m^3$)	St. Dev. of Downwind Conc. ($\mu g/m^3$)	Avg. Downwind Conc. ($\mu g/m^3$)	St. Dev. of Downwind Conc. ($\mu g/m^3$)	Avg. Conc. Difference ($\mu g/m^3$)
7/9/96	156.7	17.4	528.9	174.5	334	22.4	274.7
7/9/96	88.1	14.8	504.9	346.3	328.6	80.1	328.7
9/12/96	93.2	5.9	568.3	277.1	303.8	14.1	342.8
9/12/96	107	86.61	447.5	292.6	311.3	65.9	272.4

Figure 4-11: Site Setup on a Dirt Road in the University of California's Agricultural Operation Field on 7/9/96 and 9/12/96.

PM_{10} Sampling on an Unpaved Road

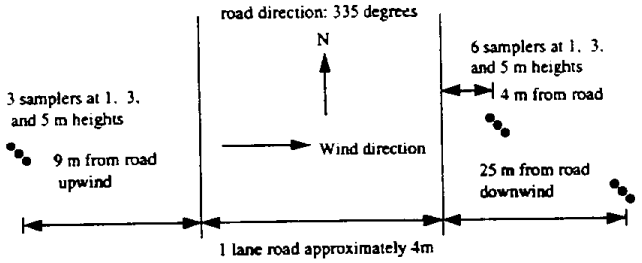

4.5.3 Dustfall

The average mass collected on the downwind side at Canyon Crest was 49.3 mg. Jars were placed on the upwind and downwind side at Riverside Drive. The average downwind and upwind depositions were 126.3 mg and 70.6 mg respectively, which gives a difference of 55.7 mg.

4.5.4 Silt Loading

Silt loadings were taken during each sampling day in order to obtain the silt content. Appendix B lists the accumulations. Loadings were taken with a vacuum cleaner on the side of the road where the generator was situated. Due to the non-uniformity of the roadway, the visible collection of dirt, and safety considerations, different areas of road were vacuumed. Larger amounts of silt were found to be closest to the curb than the shoulder or active lane. For example, on 6/27/96 the active lane and the curb on the east side of Riverside Drive had silt contents of 0.5 and 556.7 g/m^2 respectively. Silt content for the same date on the west side of the street for the shoulder and curb were 3.8 and 38.7 g/m^2. By law, the county is required to sweep streets such as Riverside Drive at least twice a year for drainage purposes. The measured silt content could have been deposition accumulated since the last sweeping. The silt content was significantly reduced almost a year later (6/4/97) on the active lane (0.12 g/m^2) and the curb on the east side (3.66 g/m^2).

Silt content on Canyon Crest was similar to that on Riverside Drive, showing that the active traffic lane had less silt than the shoulder or section closest to the curb. For example, vacuuming on 11/20/96 showed that the active lanes for the east and west side of the street had a silt content of 0.16 and 0.09 g/m^2, respectively. The bike lane closest to the curb had values of 3.16 and 1.12 g/m^2 for the east and west side respectively. This experiment was repeated again on 3/18/97, 3/27/97, 5/27/97, and 6/5/97 with similar results as seen in Appendix B.

Atlanta Avenue, a collector road, produced similar results. Silt loadings were taken from the shoulders on both sides of the road and the active lane on the west side. The shoulders on the east and west side were 15.7 and 3.3 g/m^2, respectively, and the active lane had a value of 0.49 g/m^2.

4.5.4.1 Vacuuming

Vacuuming was performed on each street sampled. The results from vacuum sampling are provided in Appendix B. The area vacuumed on the street was determined by the car flow, availability, and the amount of material that was visible on the roadway. A different procedure was used in vacuuming highways.

The entire active lane of highways, an average of 12 feet wide, was vacuumed in lengths of 50 to 100 feet at a time. This was necessary for obtaining a suitable amount of material that could be sieved, sorted, and weighed. A guide consisting of two 4-inch x 4-inch beams and rope was used for vacuuming small sections at a time, making sure vacuumed areas were equal in length and width. Although such a large area was vacuumed for silt, many fines were trapped inside the micro-lined filter bag. As part of the sieving procedure, the canister bag was weighed before and after vacuuming to account for those particles adhered to the sides of the bag. A device was built in order for particles to go directly from the road and onto filter substrates. These filters could then be weighed for concentration and/or sent for chemical analysis.

4.5.4.2 Resuspension

The portable resuspension chamber was designed to determine the concentrations of particulates directly from the roadway. A section of roadway would be vacuumed by the chamber's blower. Particles of all size diameters would be lofted through the vacuum hose and into an impactor.

Here, large particles would fall due to gravity and the rest would flow with the air stream into a chamber. Not more than 2% of the total mass collected in the impactor was silt (fines less than 75μm in diameter). The remaining fines that entered the chamber were then sorted by pairs of PM_{10} or $PM_{2.5}$ cyclones or "total mass" ports. A pair of each cyclone and port was connected in parallel to a pump. This configuration of air lines allowed for different flow rates of air through each cyclone and port. The reference flow rates for the $PM_{2.5}$, PM_{10}, and "total mass" ports were set for 350, 50, and 10 scfh, respectively. These reference flows were set in order to obtain the conventional sample flow rates of 240, 35, and 7 scfh, respectively. The area swept was determined by the pressure change of the blower. Total particulate matter accumulated onto the 8-inch x 10-inch filter paper that was placed directly above the blower to ensure that the blower would not be clogged with fines. Table 4-8 shows the results of the resuspension chamber on three roadways. In one of the three tests the $PM_{2.5}$ loading was significantly higher than PM_{10} indicating penetration of particles greater than 2.5μ diameter through the size-selective inlet.

Table 4-8: Average Concentrations of PM_{10}, $PM_{2.5}$, and Weight of the 8-inch x 10-inch filter Paper from the Resuspension Chamber.

Date	Street	Area Swept m^2	*Avg. PM_{10} mg/m^2	*Avg. $PM_{2.5}$ mg/m^2	Total PM mg/m^2
10/8/96	Columbia Ave	1.5	25.5	43.1	3082
10/9/96	Hwy 91 (off-ramp)	3	65.6	27.7	2161
10/10/96	Hwy 91 (on-ramp)	4	6.9	8.6	975

*Average of two collected samples.

4.5.5 Tracer

The tracer gas sulfur hexafluoride, SF_6, was released from an upwind line source to characterize the dispersion of PM_{10} and measure the turbulence caused by roadways. This approach to characterize dispersion with known SF_6 was used by Piccot et al. (1994). In the following experiments, the trace gas was released from a 200-foot line source from the upwind side of the roadway and was collected via Tedlar bags at different heights on the downwind side of the road.

4.5.5.1 Parking Lot

The Bourns parking lot was the first location for the tracer experiments. The downwind receptor tower was placed 300 feet from the release line to correspond to the measured width of Interstate 15. Figure 4-12 shows the dispersion of the gas from ground level (5 feet) to 40 feet for the first two runs on 12/6/96.

Other data concerning this can be found in Appendix C.

Figure 4-12: SF_6 Experiment Performed on the Parking Lot for the First Two Runs at a Source Flow Rate of 200 cc/min.

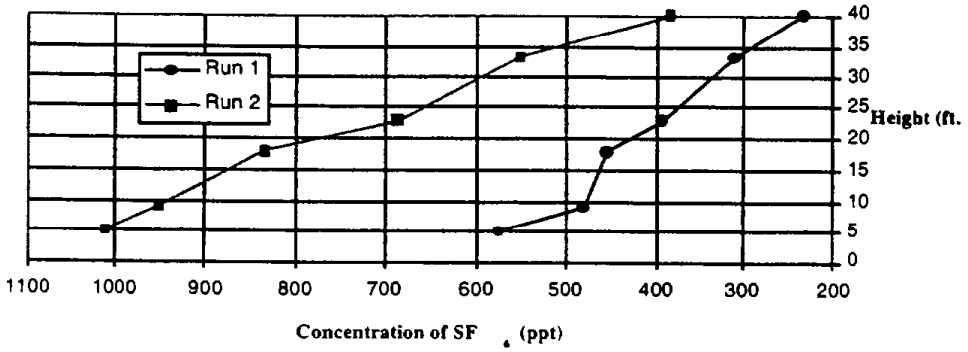

As seen from the graph, there is an even dispersion from 5 feet to 40 feet. The parking lot accounts for non-turbulence since no cars passed between the release line and the receptor tower.

4.5.5.2 Iowa Avenue

Figure 4-13 is a plot of three experiments where SF_6 was released along the upwind side of Iowa Avenue and measured at the heights on the down wind side of the street. The SF_6 decreases with height in the same manner as in the parking lot study where there was no traffic.

Figure 4-13: SF_6 Experiments on Iowa Avenue.

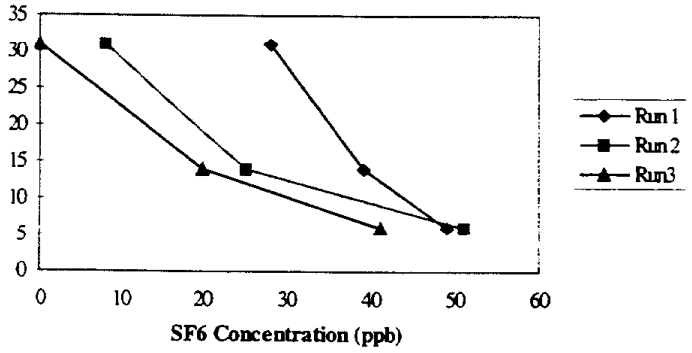

4.5.5.3 Interstate 15

After performing the pre-experiment in the parking lot to find the dispersion of a non-freeway site, the SF_6 apparatus was positioned along Interstate 15 for measurement of a freeway site and a non-freeway site. First, the release line and receptor tower were positioned along Kettering Drive. and Auto Center Drive 300 feet apart, separated by an open field adjacent to the freeway. The field was downwind of the freeway, representing the non-freeway site. The site was sampled first so the tracer would have time to be flushed out of the surrounding area before the next experiment began. However, since the site was on the downwind side of the freeway, the meteorological conditions would be similar to the actual freeway site. A meteorological tower was stationed along Kettering Drive in order for placement of the tower perpendicular to the wind and the release line.

After the non-freeway experiment, the equipment was moved to sample the freeway. The release line was placed 50 feet from the shoulder of the freeway on the upwind side. The tower was placed on Kettering Drive, also at 50 feet from the shoulder on the downwind side at an angle to the release line such that it was centered in the SF_6 plume. Figure 4-14 shows the setup of this experiment. The results from the 12/20/96 experiment are provided in Appendix C. Figure 4-15 shows the height vs. concentration of gas.

Figure 4-14: Site Setup of the SF_6 Tracer on Interstate 15 on 12/20/96 and 1/28/97.

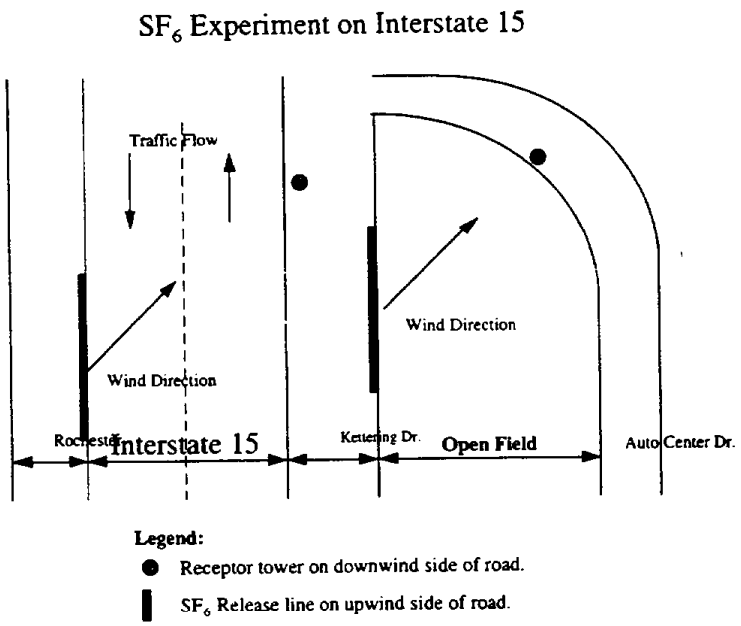

The tracer experiment was repeated for Interstate 15 on 1/31/97 with the addition of a collection bag for the 53-foot. height in order to find the maximum mixing height. Figure 4-16 shows the results for this experiment.

Figure 4-15: SF_6 Plume Concentrations at Heights of 5, 9, 18, 23, 33, and 40 Feet.

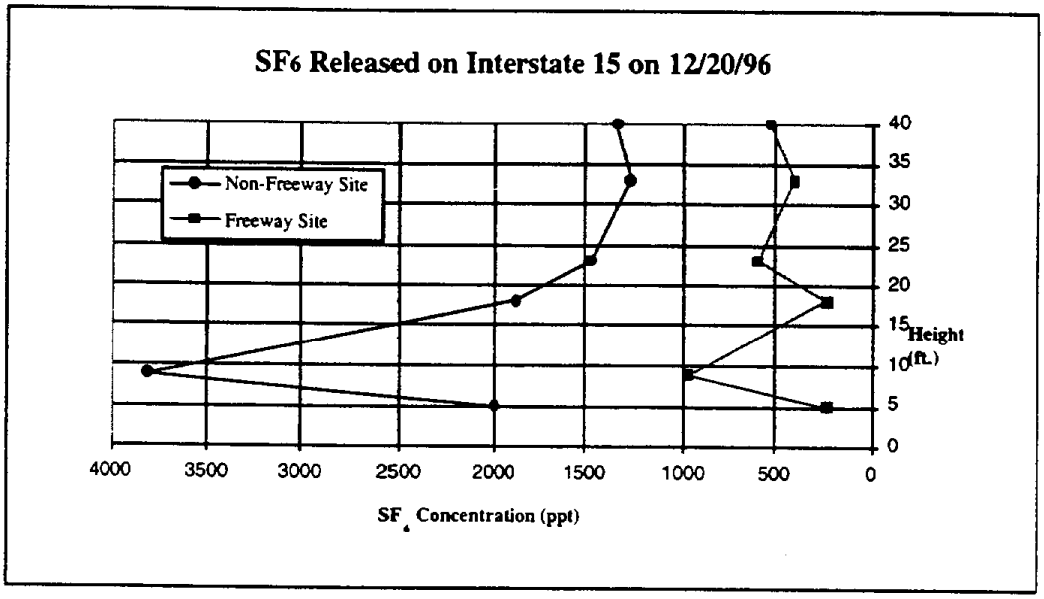

Figure 4-16: Height vs. Tracer Concentration for Heights of 5, 9, 18, 23, 33, 40, and 53 Feet.

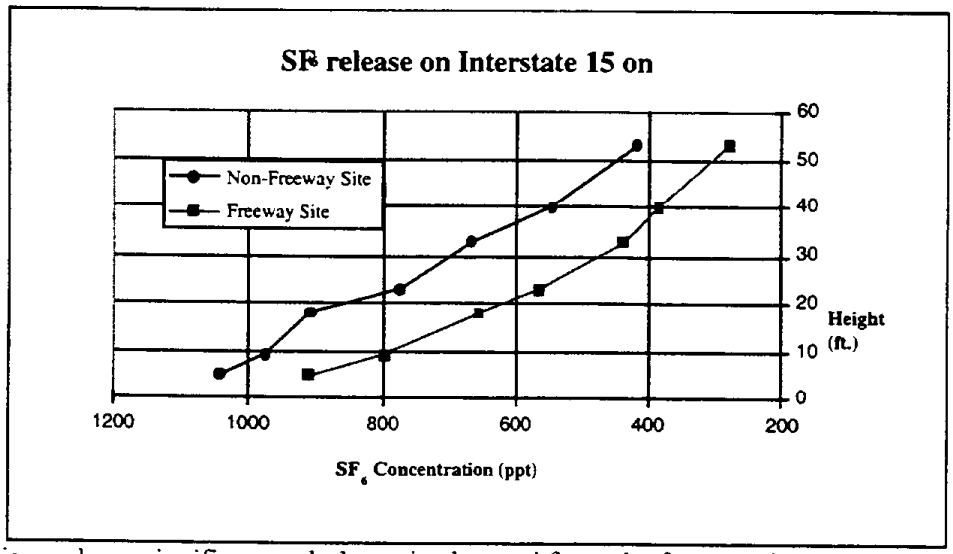

From this graph, no significant turbulence is observed from the freeway since both runs, freeway and non-freeway, have similar profiles.

4.5.6 Shoulder Resuspension

Two samples were taken from the dirt strip on Columbia Avenue, one before and after 100 vehicle passes. Each sample consisted of three sections with the vacuum at each end of the 82m length of dirt and at the middle, where each section is equivalent to two passes with the vacuum

head. The before and after samples are denoted by "A" and "B" respectively in Table 4-9. Passing 100 cars near the material did not make a difference in the amount of silt deposit on the shoulder.

Table 3-9. Silt Content from Columbia Avenue Samples.

Sample	Area	Total Mass Collected (g)	Silt Content (g/m^2)
A	3 sections (3.2' x 2.33' each)	1154.4	103.9
B	3 sections (3.2' x 2.33' each)	1339	107.6

4.6 Summary and Conclusions

The results of several monitoring episodes on Interstate 215/Highway 60 showed that the net change in PM mass concentration from the upwind to downwind locations was near the detection limit of the method (approximately 5 $\mu g/m^3$), although the downwind concentration was almost always higher. Approximately the same effect was observed on arterial roads studied in Riverside, which had nearly a tenfold lower traffic count. The emission factors for the freeway determined from the data using dispersion models averaged 0.25 gm/vehicle kilometer traveled (VKT), ranging from 0.03 to 0.56 gm/VKT. While this is similar to that predicted using the EPA AP-42 model with the default value of silt loading of 0.21 g/m^2, our measured silt loading values were a factor of four lower. Based on these results, the contribution of PM from roadways to the emission inventory should be reassessed.

Determining the chemical composition of the PM may be more useful than mass measurements in evaluating the contribution and significance of the PM from roadways, as much greater sensitivity would be possible for a chemical which originates primarily from road emissions unlike a bulk property such as mass for which the background is also high. The filters already collected have been archived and are suitable for analysis for elements by x-ray fluorescence (for atomic numbers higher than 10) and for elemental carbon by absorption. The filters are also suitable for morphological analysis by scanning electron microscopy to determine the contribution from tire, brake, and clutch wear.

5. References

Ashbaugh, L.; Chang, D.; Flocchini, R.G.; Carvacho, O.F.; James, T.A.; and Matsumara, R.T. (1996) *Traffic Generated PM_{10} "Hot Spots"*. Air Quality Group, Crocker Nuclear Laboratory, University of California, Davis, August 1996.

Barad, M. L., 1958: *Project Prairie Grass, a Filed Program in Diffusion.* Vol. 1, Geophysics Research Paper No. 59, Air Force Cambridge Research Center, Bedford, MA.

Cahill, T, D., Sperling, D., Chang, E., Gerhart, Covacho, O., and Ashbaugh, L.(1995) PM10 "Hot Spot" emissions from California Roads. Report submitted to the California Department of Transportation from Air Quality Group, University of California, Davis, CA 95616.

Claiborn, C.; Mitra, A. Adams, G.; Bamesberger, L.; Allwine, G.; Kantamaneni, R.; Lamb, B.; and Westberg, H.(1995) Evaluation of PM_{10} emission rates from paved and unpaved roads using tracer techniques. *Atmos. Env.* **29**:1075-1089.

Cowherd, C., Jr., and Englehart, P.J. (1984) Paved road particulate emissions. EPA-600/7-84-077.U.S.Environmental Protection Agency, Washington, D.C.

Csanady, G.T. (1973) *Turbulent Diffusion in the Environment.* Reidel, Dordrecht, Holland.

Du, S., and Venkatram, A.(1997) A parameterization of dispersion of ground-level releases. *Journal of Applied Meteorology*, 36, 1004-1015.

Dyck, R.I.J., and Stukel, J.J.(1976) Fugitive dust emissions from trucks on unpaved roads.*Environmental Science Technology* 10, 1046-1048.

EPA (1993) Emission factor documentation for AP-42. Section 13.2.1, Paved Roads. EPA contract No. 68-D0-0123, Work Assignment No. 44, MRI project No. 9712-44.

Gaffney, P.; Bode, R.; and Murchison, L. (1995) PM_{10} emission inventory improvement program for California. Report available from Patrick Gaffney, Air Resources Board, 2020 L Street, Sacramento, CA.95814.

Gryning, S., van Ulden, A.P. and Larsen, S.E., 1983: Dispersion from a continuous ground-level source investigated by a K model. Quart. *J. Roy. Met. Soc.* **109**. 357-366.

Harding Lawson Associates (1996) Final Report for the 1993-1994 ADEQ Paved Road Emissions Research Study. Maricopa Association of Governments.

Kantamaneni, R., Adams, G., Bamesberger, L., Allwine, E., Westberg, H., Lamb, B.and Claiborn, C.(1996) The measurement of Roadway PM10 emission rates using atmospheric tracer ratio techniques. *Atmospheric Environment* 24, 4209-4223.

McCaldin, R.O.(1978) Particulate emissions from vehicle travel over unpaved roads. Paper No.78-14.2, 71 st Annual Meeting of the Air Pollution Control Association, Houston, Texas, June 25-30.

Nieuwstadt, F.T.M., and van Ulden, A.P.(1978) A numerical study on the vertical dispersion of passive contaminants from a continuous source in the atmospheric surface layer.*Atmospheric Environment* 12, 2119-2124.

Panofsky, H.A., and Dutton, J.A.(1984) *Atmospheric Turbulence*, John Wiley & Sons, New York, 397pp.

Thomson, D. B. (1987) Criteria for the selection of stochastic models of particle trajectories in turbulent flows. J. Fluid Mech., 180, 529-556.

van Ulden, A. P., 1978: Simple estimates for vertical diffusion from sources near the ground. *Atmos. Environ.* **12**, 2125-2129.

Venkatram, A. (1996) An examination of the Pasquill-Gifford-Turner dispersion scheme. Atmospheric Environment, 30, 1283-1290.

Venkatram, A.(1982) A semi-empirical method to compute concentration associated with surface releases in the stable boundary layer.*Atmospheric Environment* 16, 245-248.

Venkatram, A. (1984) The inherent uncertainty in estimating dispersion in the convective boundary layer. *Atmos. Env.* **18**:307-310.

Venkatram, A. (1988) Inherent uncertainty in air quality modeling. *Atmospheric Environment* **22**:1221-1227.

Venkatram, A.(1992) The parameterization of the vertical dispersion of a scalar in the atmospheric boundary layer.*Atmospheric Environment* 26A, 1963-1966.

Venkatram, A.and Du, S.(1997) An analysis of the asymptotic behavior of cross-wind integrated ground-level concentrations using Lagrangian stochastic simulation.*Atmospheric Environment* 31, 1467-1476.

Wilson, J. D. (1982) Turbulent dispersion in the atmospheric surface layer. Boundary-layer Meteor., 102, 399-420.

Zimmer, R.A. , Reeser, W.K., and Cummins, P.(1992) Evaluation of PM_{10} emission factors for paved streets.In *PM_{10} Standards and Nontraditional Particulate Source Controls* (edited by Chow, J.C.and Ono, D.M.), pp311-323.

Appendix A
PM_{10} Sampling from Roadways Data Set

												Avg. Meteorlogical Data						
Date	Location	Type of Street	Car Count	Run Time	Avg. Upwind Conc.	St. Dev. of Upwind Conc.	Avg. Downwind Conc.	St. Dev. of Downwind Conc.	Avg. Downwind Conc.	St. Dev. of Downwind Conc.	Avg. Conc. Difference	Temp	Rel. Humidity	Wind Speed	Wind Direction	Sigma W	**Emission Rate**
			#/hr	hr	µg/m^3	µg/m^3	µg/m^3	µg/m^3	µg/m^3	µg/m^3	µg/m^3	° C	%	m/s	degrees	m/s	
1/8/96	Iowa Ave.	ART			65.4	6.9	81.2	11.3			15.8	17.6	36.8	1.75	263.7	0.21	238.9 - 699.8
1/9/96	Iowa Ave.	ART			70.6	4.2	81.1	1.7			10.5	17.6	36.8	1.15	232.5	0.21	104.4 - 334
1/18/96	Iowa Ave.	ART			38.5	2.8	46.4	4.3			7.9	17.6	36.8	1.6	255.4	0.21	108.8 - 328.5
4/26/96	Iowa Ave.	ART		10	102	11.3	96.5	13			-5.5	29.8	31.6	1.8	221	0.24	
5/2/96	Hwy 215 & 60	HWY		9.5	77.5	2.1	84.5	6.22			7.0	28.3	33.2	1.5	232	0.46	230 - 1175.5
5/6/96	Hwy 215 & 60	HWY			58.5	2.2	66.5	4.2			8.0	26.7	30.7	1.5	218	0.41	233.7 - 1252.2
5/9 - 5/10/96	Hwy 215 & 60	HWY		13	73	5	74.3	2.1	75.5	1.7	1.9	28	34	1.5	254.8	0.4	70.8 - 385.9
5/13 - 5/16/96	Hwy 215 & 60	HWY		31	66.4	10.1	61	3.4	64.7	2	-3.6	25.6	48.7	1.8	261.1	0.5	
5/20 - 5/23/96	Canyon Crest	ART		28	57	3	57	3			0.0	22.6	50	2.27	268.6	0.4	0
5/31 - 6/3/96	Hwy 215 & 60	HWY		32.3	57	1	56	1			-1.0	32.1	25.2	1.6	234	0.5	
6/4 - 6/7/96	Hwy 215 & 60	HWY		32	86	4	83				-3.0	29.5	43.6	1.5	250	0.36	
6/17 - 6/18/96	Riverside Dr.	ART	840	14	96.7	7.9	110.9	8.8			14.2	30.9	27.15	2.52	238.3	0.8	314.9 - 977.9
6/19 - 9/20/96	Riverside Dr.	ART	840	6.3	116	34.6	133.2	14.9			17.2	30.4	26.4	3.44	280.9	0.37	510.4 - 1418.6
6/25 - 6/26/96	Riverside Dr.	ART	840	14.8	77.4	2.7	79.58				2.2	21.7	47.8	3.7	216.9	0.38	170.8 - 412.8
7/9/96	Ag. Field	DIRT	101	1.5	156.73	17.4	528.9	174.5	334	22.4	274.7	29	36.1	2.5	254.5	0.37	5617 - 26693
7/9/96	Ag. Field	DIRT	187	2.5	88.1	14.8	504.9	346.3	328.6	80.1	328.7	29	36.1	2.5	254.5	0.37	9522 - 44141
8/6/96	Riverside Dr.	ART	50	5	76.78	2.4	83.46	6.1	80.37	4.1	5.1	17.4	80.2	0.65	160.2	0.1	
9/3/96	Riverside Dr.	ART	900	8	87.4	1.7	89.6	4.8	93.6	2.6	4.2	28.4	37.4	2.26	236	1.68	
9/5/96	Riverside Dr.	ART	900	9	77	2.3	107.6	33	88.4	3.8	21.0	28.8	39	2.5	232	0.28	
9/12/96	Ag. Field	DIRT	150	2.5	93.23	5.9	568.3	277.1	303.8	14.1	342.8	29	20.6	2.5	265.2	0.33	
9/12/96	Ag. Field	DIRT	150	2.5	107	86.61	447.5	292.6	311.3	65.9	272.4	29	20.6	2.5	265.2	0.33	
9/24/96	Riverside Dr.	ART	900	8	154.8	2.2	168.5	4.5	166.1	2.3	12.5	25	48.5	2.3	226	0.27	
10/2/96	Riverside Dr.	ART	822	6	126.8	4.2	133.63	2.25	136.81	0.59	8.4	21.1	58.1	1.24	195.44	0.21	
11/12/96	Canyon Crest	ART	1008	5	56.5	0.45	57.1	1.4	61.2	1.4	2.7	28.7	16.3	1.1	251	0.2	
11/13/96	Atlanta Ave.	COL	204	5.8	90.8	2.5	102.6	4.1	106.1	1.8	13.6	25.4	24.3	0.9	279.6	0.28	
11/19/96	Riverside Dr.	ART	900	6	162.8	3.13	179.8	0.35	177.5	1.6	15.9	20.2	52.33	2.1	216	0.23	
11/20/96	Canyon Crest	ART	1008	6.8	122.8	2.1	128.1	1.1	128.9	3.5	5.7	19.1	60.94	1.3	276.53	0.24	
3/17/97	Riverside Dr.	ART	1050	6	83.13	5.34	74.81	4.77	81.25	3.15	-5.1	20.4	41.6	1.8	186.9	0.3	
3/18/97	Canyon Crest	ART	1068	4	56.07	1.76	60.83	5.24	61.5	0.97	5.1	30.8	12.9	1.5	265.8	0.3	
3/19/97	Riverside Dr.	ART	1050	5	40.55	2.45	59.28	0.39	63.9	1.63	21.0	33.8	6.6	2.4	246.6	0.3	
3/21/97	Fogg St.	LOCAL	20	5	65.04	3.45	66.32	5.28	67.07	7.14	1.7	28.4	14.6	2.2	236.4	0.3	
3/26/97	Fogg St.	LOCAL	20	5.5	81.55	7.92	91.04	5.36	93.8	1.8	10.9	25.4	19.3	3.2	238	0.4	
3/27/97	Canyon Crest	ART	1068	5.5	83	5.34	74.81	4.77	81.25	3.15	-5.0	19.7	47	1.8	275.4	0.4	
5/27/97	Fogg St	LOCAL	18	7	59.70	2.18	63.08	2.35	63.72	3.71	3.7	33.9	16.0	2.5	234.6	0.4	
5/28/97	Canyon Crest	ART	960	7	64.11	11.27	56.81	1.74	63.33	2.76	-4.0	34.2	20	2.1	262.0	0.5	
5/29/97	Riverside Dr.	ART	780	6.25	67.24	3.51	69.51	1.35	74.22	2.51	4.6	33.9	21	2.55	225.8	0.37	
6/3/97	Fogg St.	LOCAL	47	7	85.60	1.9	85.2	3.2	90.2	1.7	2.1	25.6	46.8	2	264.6	0.33	
6/4/97	Riverside Dr.	ART	768	5.75	65.00	8.3	75.7	6.8	74.7	2.1	10.2	25.2	48.4	2.87	262.5	0.32	
6/5/97	Canyon Crest	ART	840	7	40.11	2.9	42.21	3.3	49.2	0.32	5.6	22.4	51.9	2.4	260.2	0.45	

Appendix B
Silt Sampling Data Set

Date	Location	Type of Street	Area Swept	Total Mass Collected	Silt Content	Comments
				g	g/m2	
5/28/96	Iowa (East lane)	ART	10' x 13' x 2	5.52	0.024	
5/28/96	Iowa (right lane)	ART	12' x 26'	1.11	0.003	
5/28/96	Iowa (shoulder)	ART	5.5' x 26'	19.73	0.107	
5/28/96	Canyon Crest (right lane)	ART	11' x 30'	0.64	0.0065	
5/28/96	Canyon Crest (left lane)	ART	11' x 30'	0.71	0.0013	
5/28/96	Canyon Crest (bike lane)	ART	4' x 30'	63.17	0.67	
5/28/96	Canyon Crest (Island)	ART	30' x 12' x 13'	251.94	0.26	
5/28/96	Canyon Crest (gutter)	ART	1' x 30'	207.87	5.96	
5/29/96	Columbia Ave. (right ln, 1st try)	COL	11' x 30'	112.39	0.107	
5/29/96	Columbia Ave. (right ln, 2nd pass)	COL	11' x 30'	56.01	0.063	
5/29/96	Columbia Ave. (duplicate)	COL	11' x 30'	144.22	0.112	
6/27/96	Riverside Dr. east side (active ln)	ART	30' x 13'	883.99	0.50	
6/27/96	Riverside Dr. east side (shoulder)	ART	8' x 30'	186.04	0.33	
6/27/96	Riverside Dr. east side (shoulder)	ART	4' x 30'	1551.2	6.60	
6/27/96	Riverside Dr. east side (curb)	ART	.5' x 5'	2795.72	556.65	
6/27/96	Riverside Dr. west side (shoulder)	ART	9' x 30'	665.3	3.80	
6/27/96	Riverside Dr. west side (curb)	ART	4' x 5'	2957.44	38.65	
8/13/96	Columbia Ave bag (A)	COL	6' x 50'	1685.45	2.285	Study to find the efficiency of
8/13/96	Columbia Ave bag (B)	COL	4' x 50'	1298.34		the vacuum Run 1 66%
8/13/96	Columbia Ave bag (C)	COL	10' x 50'	736.19	0.772	80%
8/13/96	Columbia Ave bag (D)	COL	10' x 50'	310.66	0.463	
8/13/96	Columbia Ave bag (E)	COL	6' x 50'	974.5	1.657	Run 2 78%
8/13/96	Columbia Ave bag (F)	COL	4' x 50'	992.63		
8/13/96	Columbia Ave bag (G)	COL	10' x 50'	428.57	0.37	41%
8/13/96	Columbia Ave bag (H)	COL	10' x 50'	146.67	0.217	
8/13/96	Columbia Ave bag (I)	COL	6' x 50'	691.17	1.494	Run 3 75%
8/13/96	Columbia Ave bag (J)	COL	4' x 50'	716.21		
8/13/96	Columbia Ave bag (K)	COL	10' x 50'	312.1	0.368	75%
8/13/96	Columbia Ave bag (L)	COL	10' x 50'	135.53	0.091	
8/27/96	Columbia Ave.	COL	3(3.2' x 2.33')	1154.38	103.931	Experiment to study the move-
8/27/96	Columbia Ave.	COL	3(3.2' x 2.33')	1338.95	107.596	ment of silt due from cars passing
9/3/96	Riverside Dr. east side (shoulder)	ART	6' x 12.5'	1395.83	7.694	
9/3/96	Riverside Dr. east side (small area near curb)	ART	1' x 12.5'	2159.82	46.204	
9/3/96	Riverside Dr. west side (shoulder)	ART	4' x 11'3"	3968.69	23.804	
9/3/96	Riverside Dr. west side (small area near curb)	ART	1' x 11'3"	1910.49	39.727	

9/19/96	Hwy 15, Corona (shoulder)	HWY	104.3' x 9'	366.08	0.61	
9/19/96	Hwy 15, Corona (small area near curb)	HWY	1' x 4'	1496.89	126.68	
9/19/96	Hwy 15, Corona (small area near curb)	HWY	1' x 4'	1643.49	142.64	
9/19/96	Hwy 15, Corona (active lane)	HWY	10' x 50'	57.46	0.13	
9/19/96	Hwy 15, Corona (shoulder)	HWY	104.3' x 9'	487.01	0.55	
9/19/96	Hwy 15, Corona (small area near curb)	HWY	1' x 4'	1822.21	132.94	
9/19/96	Hwy 15, Corona (small area near curb)	HWY	1' x 4'	1654.78	124.86	
9/23/96	Riverside Dr, east side	ART	7' x 25'	1545.72	9.54	after brush and vacuum sweeper
9/23/96	Riverside Dr, west side	ART	7' x 23.5'	1214.3	5.1	
10/2/96	Riverside Dr, east side	ART	21' x 7'	496.58	6.34	after vacuum sweeper
10/9/96	Hwy 91 Arlington Off-Ramp 3 passes near yellow line	HWY	3.25' x 100.83'	1569	2.07	
10/9/96	Hwy 91 Arlington Off-Ramp 3 passes farthest from yellow line	HWY	3.25' x 100.83'	1160.5	1.13	
10/10/96	Hwy 91 Arlington On-Ramp 3 passes near yellow line	HWY	3.25' x 100.83'	753.02	0.75	
10/10/96	Hwy 91 Arlington On-Ramp 3 passes farthest from yellow line	HWY	3.25' x 100.83'	197.78	0.04	
11/7/96	Hwy 18 (Crestline)	HWY	10' x 100	482.4	0.71	
11/12/96	Canyon Crest, west side (bike lane)	ART	5' x 10.5'	481.08	5.63	
11/12/96	Canyon Crest, east side (bike lane)	ART	20' x 4.5'	1373.53	7.45	
11/13/96	Atlanta Ave, west side (shoulder)	COL	5' x 10.5'	254.76	3.33	
11/13/96	Atlanta Ave, east side (shoulder)	COL	20' x 4.5'	1646.13	15.73	
11/13/96	Atlanta Ave, west side (act ln)	COL	20' x 9'	323.38	0.49	
11/19/96	Riverside Dr., west side	ART	9' x 40'	221.08	0.33	
11/19/96	Riverside Dr., east side	ART	9' x 40'	240.33	0.21	

11/20/96	Canyon Crest east side(bike lane)	ART	5' x 20'	148.75	3.16	
11/20/96	Canyon Crest east side (active lane)	ART	13.5' x 20'	19.29	0.16	
11/20/96	Canyon Crest west side (bike lane)	ART	5' x 20'	69.15	1.12	
11/20/96	Canyon Crest west side (active lane)	ART	13.5' x 20'	11.7	0.09	
12/3/96	Hwy 18 near 45 St.	HWY	10' x 100	143.88	0.08	
3/17/97	Riverside Dr. (active lane) east side	ART	40' x 10.5'	148.76	0.20	before sweeper
3/17/97	Riverside Dr. (curb) east side	ART	13.5' x 7'	433.52	3.13	before sweeper
3/17/97	Riverside Dr. (curb) west side	ART	6' x 5'	254.21	6.84	before sweeper
3/18/97	Canyon Crest (active lane) east side	ART	30' x 13.5'	18.52	0.07	before sweeper
3/18/97	Canyon Crest (bike lane & curb) east side	ART	6' x 5'	134.84	4.75	before sweeper
3/18/97	Canyon Crest (active lane) west side	ART	30' x 13.5'	17.64	0.06	before sweeper
3/18/97	Canyon Crest (bike lane & curb) west side	ART	6' x 5'	68.03	2.46	before sweeper
3/19/97	Riverside Dr. (active lane) east side	ART	40' x 10.5'	99.82	0.19	after sweeer
3/19/97	Riverside Dr. (curb) east side	ART	10' x 7'	681.18	12.14	after sweeer
3/19/97	Riverside Dr. (curb) west side	ART	11.25' x 6'	226.83	6.45	after sweeer
3/21/97	Fogg St. (active lane) east side	LOCAL	20' x 10'	379.49	0.55	before sweeper
3/21/97	Fogg St. (curb) east side	LOCAL	10.5' x 7'	99.83	2.16	before sweeper
3/21/97	Fogg St. (active lane) west side	LOCAL	20' x 9'	104.49	0.38	before sweeper
3/21/97	Fogg St. (curb) west side	LOCAL	10.5' x 7'	144.92	3.49	before sweeper
3/26/97	Fogg St. (active lane) east side	LOCAL	20' x 10'	39.44	0.15	after sweeper
3/26/97	Fogg St. (curb) east side	LOCAL	10.5' x 7'	46.54	1.16	after sweeper
3/26/97	Fogg St. (active lane) west side	LOCAL	20' x 9'	18.33	0.11	after sweeper
3/26/97	Fogg St. (curb) west side	LOCAL	10.5' x 7'	30.54	1.02	after sweeper
3/27/97	Canyon Crest (active lane) east side	ART	30' x 13.5'	11.12	0.06	after sweeper
3/27/97	Canyon Crest (bike lane & curb) east side	ART	6' x 5'	34.66	3.18	after sweeper
3/27/97	Canyon Crest (active lane) west side	ART	30' x 13.5'	7.03	0.03	after sweeper
3/27/97	Canyon Crest (bike lane & curb) west side	ART	6' x 5'	13.19	1.05	after sweeper

5/27/97	Fogg St. (active lane) east side	LOCAL	20' x 10'	69.56	0.62	before sweeper
5/27/97	Fogg St. (curb) east side	LOCAL	10.5' x 7'	112.39	1.26	before sweeper
5/27/97	Fogg St. (active lane) west side	LOCAL	20' x 9'	30.17	0.13	before sweeper
5/27/97	Fogg St.(curb) west side	LOCAL	10.5' x 7'	50.83	1.65	before sweeper
5/28/97	Canyon Crest (active lane) east side	ART	13.5' x 30'	15.4	0.06	before sweeper
5/28/97	Canyon Crest (curb) east side	ART	6' x 5'	121.54	2.14	before sweeper
5/28/97	Canyon Crest (active lane) west side	ART	30' x 13.5'	16.5	0.14	before sweeper
5/28/97	Canyon Crest (curb) west side	ART	6' x 5'	201.75	3.04	before sweeper
5/29/97	Riverside Dr. (active lane) east side	LOCAL	20' x 10'	26.63	0.16	before sweeper
5/29/97	Riverside Dr. (curb) east side	LOCAL	10.5' x 7'	378.42	4.31	before sweeper
5/29/97	Riverside Dr. (active lane) west side	LOCAL	20' x 9'	24.89	0.18	before sweeper
5/29/97	Riverside Dr. (curb) west side	LOCAL	10.5' x 7'	303.11	3.39	before sweeper
6/3/97	Fogg St. (curb) east side	LOCAL	10.5' x 7'	49.69	1.09	after sweeper
6/3/97	Fogg St. (active lane) east side	LOCAL	20' x 10'	33.84	0.12	after sweeper
6/3/97	Fogg St. (curb) west side	LOCAL	10.5' x 7'	18.13	0.97	after sweeper
6/3/97	Fogg St. (active lane) west side	LOCAL	20' x 9'	25.22	0.16	after sweeper
6/4/97	Riverside Dr. (active lane) east side	ART	40' x 13'	61.32	0.12	after sweeper
6/4/97	Riverside Dr. (curb) east side	ART	10' x 7'	144.84	3.66	after sweeper
6/4/97	Riverside Dr. (active lane) west side	ART	40' x 13'	14.25	0.05	after sweeper
6/4/97	Riverside Dr. (curb) west side	ART	11' x 6'	44.11	2.09	after sweeper
6/5/97	Canyon Crest (active lane) east side	ART	30' x 13.5	24.84	0.10	after sweeper
6/5/97	Canyon Crest (curb) east side	ART	6' x 5'	26.86	1.58	after sweeper
6/5/97	Canyon Crest (active lane) west side	ART	30' x 13.5'	13.41	0.07	after sweeper
6/5/97	Canyon Crest (curb) west side	ART	6' x 5'	20.19	1.44	after sweeper

Appendix C
SF_6 Tracer Gas Experiment Data Set

SF_6 Sampling										
					Avg. Meteorological Data					
Date	Location	Height/Distance of Samples Ft.	Conc.	Run Time Min	Wind Speed M/S	Wind Direction Degrees	Temperature °C	Relative Humidity %	Sigma W M/S	Comments
1/31/97	Hwy-15 (non-Freeway)	5' high, 300' from source 9' high, 300' from source 18' high, 300' from source 23' high, 300' from source 33' high, 300' from source 40' high, 300' from source 53' high, 300' from source	1043 ppt 973 ppt 908 ppt 777 ppt 668 ppt 545 ppt 420 ppt	30	2.5	219	24	23.3	0.3	SF_6 flow rate was 600 cc/min
1/31/97	Hwy-15 (freeway)	5' high, 300m from source 9' high, 300m from source 18' high, 300m from source 23' high, 300m from source 33' high, 300m from source 40' high, 300m from source 53' high, 300m from source	911 ppt 798 ppt 658 ppt 564 ppt 439 ppt 386 ppt 279 ppt	30	3.7	219	23.3	25.7	0.3	SF_6 flow rate was 600 cc/min
12/20/96	Hwy-15 (non-freeway)	5' high, 300' from source 9' high, 300' from source 19' high, 300' from source 23' high, 300' from source 33' high, 300' from source 40' high, 300' from source	2000 ppt 3811 ppt 1883 ppt 1476 ppt 1273 ppt 1333 ppt	45	2.8	225.5	20.3	14.7	0.286	SF_6 flow rate was 600 cc/min
12/20/96	Hwy-15 (freeway)	5' high, 300m from source 9' high, 300m from source 19' high, 300m from source 23' high, 300m from source 33' high, 300m from source 40' high, 300m from source	237 ppt 966 ppt 231 ppt 604 ppt 407 ppt 534 ppt	45	3.0	223.5	19.4	15.5	0.273	SF_6 flow rate was 600 cc/min
12/6/96 Run 1	Bourns' Parking Lot	40', 300' from source 33', 300' from source 23', 300' from source 19', 300' from source 9', 300' from source 5', 300' from source background @ 9', 416' from source	240 ppt 315 ppt 401 ppt 463 ppt 490 ppt 587 ppt 7 ppt	45	2.1	244	17.3	53.4	0.293	Changed flow rate from 100 cc/min to 300 cc/min after 5 min of run time.
12/6/96 Run 2	Bourns' Parking Lot	40', 300' from source 33', 300' from source 23', 300' from source 19', 300' from source 9', 300' from source 5', 300' from source background @ 9', 416' from source	391 ppt 564 ppt 700 ppt 849 ppt 968 ppt 1031ppt 10 ppt	45	1.9	234	17.4	52.5	0.338	Started with flow rate at 3-00 cc/min
4/26/96 Run 1	Iowa Ave.	6', next to curb 14.8', next to curb 31', next to curb 6', 91' from curb background @ 6',next to curb	48.89 ppb 39.19 ppb 27.66 ppb 13.83 ppb 9 ppb	60	1.88	220.97	28.70	31.63	0.24	SF_6 flow rate was 1000 cc/min
4/26/96 Run 2	Iowa Ave.	6', next to curb 14.8', next to curb 31', next to curb 6', 91' from curb background @ 6',next to curb	51.66 ppb 25.36 ppb 8.42 ppb 19.6 ppb 8 ppb	90	1.88	220.97	28.70	31.63	0.24	SF_6 flow rate was 1000 cc/min

SF_6 Sampling		Continued – page 2								
					Avg. Meteorological Data					
Date	Location	Height/Distance of Samples Ft.	Conc.	Run Time Min	Wind Speed M/S	Wind Direction Degrees	Temperature °C	Relative Humidity %	Sigma W M/S	Comments
4/26/96 Run 3	Iowa Ave.	6', next to curb 14.8', next to curb 31', next to curb 6', 91' from curb background @ 6',next to curb	40.93 ppb 19.6 ppb 0 ppb 13.83 ppb 9 ppb	60	1.88	220.97	28.70	31.63	0.24	SF_6 flow rate was 1000 cc/min
4/9/96 Run 1	Bourns' Parking Lot	3', 15' from source 6', 15' from source 14.8', 15' from source 30.4', 15' from source background @ 6'	24.84 ppb 15.12 ppb 7.56 ppb 1.08 ppb 0 ppb	25	2.73	268.4	20.34	43.26	0.32	SF_6 flow rate was 600 cc/min
4/9/96 Run 2	Bourns' Park ppb ing Lot	3', 15' from source 6', 15' from source 14.8', 15' from source 30.4', 15' from source background @ 6'	23.76 ppb 15.12 ppb 10.8ppb 3.24ppb 1.08ppb	30	2.73	268.4	20.34	43.26	0.32	SF_6 flow rate was 600 cc/min
4/9/96 Run 3	Bourns ppb Prking Lot	3', 15' from source 6', 15' from source 14.8', 15' from source 30.4', 15' from source background @ 6'	19.44 ppb 16.2 ppn 8.64 ppb 1.08 ppb 0 ppb	30	2.73	268.4	20.34	43.26	0.32	SF_6 flow rate was 600 cc/min
4/9/96 Run 4	Bourns' Parking Lot	3', 15' from source 6', 15' from source 14.8', 15' from source 30.4', 15' from source background @ 6'	27 ppb 19.44 ppb 7.56 ppb 0 ppb 0 ppb	30	2.73	268.4	20.34	43.26	0.32	SF_6 flow rate was 600 cc/min

SF_6 Sampling										
					Avg. Meteorological Data					
Date	Location	Height/Distance of Samples Ft.	Conc.	Run Time Min	Wind Speed M/S	Wind Direction Degrees	Temperature °C	Relative Humidity %	Sigma W M/S	Comments
4/8/96 Run 1	Iowa Ave.	3', 15' from source 6', 15' from source 14.8', 15' from source 30.4', 15' from source background @ 6'	23.32 ppb 19.61 ppb 12.72 ppb 4.24 ppb 1.06 ppb	30	1.92	257.81	25.99	23.49	0.26	SF_6 flow rate was 600 cc/min
4/8/96 Run 2	Iowa Ave.	3', 15' from source 6', 15' from source 14.8', 15' from source 30.4', 15' from source background @ 6'	22.26 ppb 16.96 ppb 12.72 ppb 6.36 ppb 1.06 ppb	30	1.92	257.81	25.99	23.49	0.26	SF_6 flow rate was 600 cc/min
4/8/96 Run 3	Iowa Ave.	3', 15' from source 6', 15' from source 14.8', 15' from source 30.4', 15' from source background @ 6'	34.98 ppb 27.56 ppb 18.02 ppb 5.3 ppb 1.06 ppb	30	1.92	257.81	25.99	23.49	0.26	SF_6 flow rate was 600 cc/min
4/8/96 Run 4	Iowa Ave.	3', 15' from source 6', 15' from source 14.8', 15' from source 30.4', 15' from source background @ 6'	25.44 ppb 19.08 ppb 11.66 ppb 2.12 ppb 0 ppb	30	1.92	257.81	25.99	23.49	0.26	SF_6 flow rate was 600 cc/min
12/18/95	Bourns' Parking Lot Grid	1.5', 15' from source 3', 15' from source 6', 15' from source	58.5 ppb 23.74 ppb 7.16 ppb	10	2.04	249.4	17.33	20.49	0.28	SF_6 flow rate was 300 cc/min
12/18/95	Bourns' Parking Lot Line	1.5', 15' from source 3', 15' from source 6', 15' from source	54.45 ppb 26 ppb 16.4 ppb	10	2.04	249.4	17.33	20.49	0.28	SF_6 flow rate was 300 cc/min
12/8/95	Bourns' Parking Lot Grid	1.5', 15' from source 3', 15' from source 6', 15' from source	51.6 ppb 37.9 ppb 19.31 ppb	10	1.02	221.55	21.94	35.17	0.22	Nozzles in vertical position scale is 50 ppb. SF_6 flow rate was 300 cc/min
12/1/95	Bourns' Parking Lot Grid	1.5', 15' from source 3', 15' from source 6', 15' from source	114.5 42.2 21.4	10	1.61	255.40	23.41	25.42	0.23	Nozzles in vertical position scale is 100 ppb. SF_6 flow rate was 600 cc/min
12/1/95	Bourns' Parking Lot Grid	1.5', 15' from source 3', 15' from source 6', 15' from source	130.0 49.0 17.0	10	1.61	255.40	23.41	25.42	0.23	Nozzles in vertical position scale is 500 ppb. SF_6 flow rate was 600 cc/min
12/1/95	Bourns' Parking Lot Grid	1.5', 15' from source 3', 15' from source 6', 15' from source	113.04 60.29 20.72	10	1.61	255.40	23.41	25.42	0.23	Nozzles in vertical position scale is 500 ppb. SF_6 flow rate was 600 cc/min

Appendix D
An Analysis of the Asymptotic Behavior of Cross-wind Integrated Ground-level Concentrations using Lagrangian Stochastic Simulation

Pergamon

PII: S1352-2310(96)00315-6

AN ANALYSIS OF THE ASYMPTOTIC BEHAVIOR OF CROSS-WIND-INTEGRATED GROUND-LEVEL CONCENTRATIONS USING LAGRANGIAN STOCHASTIC SIMULATION

AKULA VENKATRAM and SHUMING DU

College of Engineering, University of California, Riverside, CA 92521, U.S.A.

(*First received* 10 *April* 1996 *and in final form* 30 *September* 1996. *Published March* 1997)

Abstract—This paper examines the asymptotic behavior as a function of downwind distance of ground-level cross-wind-integrated concentration (CWIC) caused by a continuous ground-level source in the atmospheric surface layer. We first present asymptotic expressions obtained from an analysis of data from Project Prairie Grass (PPG, Barad, 1958), and then derive corresponding formulae from data generated using Lagrangian stochastic (LS) model simulations. Under stable and neutral stratification, the formulae derived from PPG data agree well with that from LS simulations. Assuming that the Lagrangian stochastic model represents current understanding of dispersion, this agreement suggests that the formulations for stable and neutral conditions are credible. On the other hand, for unstable stratification, we find that while the LS model yields a $\sigma_y \sim x^{0.72}$ law, the PPG data suggest a fall-off with distance that is closer to a $\sigma_y \sim x^{0.5}$ slope. At the present time, we cannot identify the reasons for this disagreement. © 1997 Elsevier Science Ltd. All rights reserved.

Key word index: Dispersion, surface layer, asymptotic behavior, Prairie Grass, ground-level concentration, Lagrangian stochastic modeling.

OBJECTIVE AND APPROACH

In this paper, we study the behavior of cross-wind-integrated concentrations (CWIC) associated with releases in the surface boundary layer. We are specifically interested in the relationship between concentrations and distance in the limits of very large or very small Monin–Obukhov lengths, which correspond to neutral, very unstable and very stable conditions. These relationships, which we refer to as asymptotic, not only provide insight into dispersion but also can be used to interpolate between the asymptotic limits to obtain expressions for the entire range of stability (see Venkatram, 1992).

We obtain understanding of asymptotic behavior through a process that builds evidence in favor of a postulated relationship between non-dimensional concentration and distance. We first derive tentative relationships through the analysis of observations made during the Prairie Grass experiment (Barad, 1958); these relationships have to be tentative because of the inevitable scatter between theory and observations. The formulation of the equations fitted to observations is guided by semi-empirical K-theory (Venkatram, 1992, for example). The next step in the evidence gathering process is to check the consistency between an equation derived from observations and that suggested by data generated by Lagrangian stochastic simulation, which represents our current understanding of dispersion. Consistency between the equations would argue for generality of the proposed equation.

BEHAVIOR OF GROUND-LEVEL CONCENTRATION OBSERVED IN PROJECT PRAIRIE GRASS DATA

Project Prairie Grass (PPG) (Barad, 1958) remains the most extensive and the most successful short-range field diffusion experiment, although it is about 40 years old. In the PPG experiment, SO_2 was released at a height of 0.5 m at a site covered with grass with roughness length of $z_0 = 0.006$ m. The concentrations associated with the release were sampled at 1.5 m along several cross-wind arcs at downstream distances ranging from 50 to 800 m. These samples were used to derive 10 min averaged concentrations. Vertical profiles of concentrations were measured on six towers on the 100 m arc.

In the analysis of the data, we use micrometeorological variables calculated by Horst *et al.* (1979) using the wind and temperature profiles measured in the Project Prairie Grass (PPG) experiment (Barad, 1958). In this study, we, following Briggs

(1982) and Venkatram (1992) employ surface layer similarity scaling. It may be argued that under unstable stratification mixed-layer scaling should be used, as in Nieuwstadt (1980), but we prefer to use surface layer scaling because in PPG, diffusion took place mainly in the surface layer.

We seek relationships between CWIC and downwind distance in the form

$$\frac{C^{y} u_* |L|}{Q} = \text{Function}\left(\frac{x}{|L|}\right) \qquad (1)$$

where C^{y} is the cross-wind-integrated concentration, u_* the surface friction velocity, L the Monin-Obukhov length, Q the emission rate, and x the downwind distance from the source. The asymptotes refer to the functional behavior at large $x_* = x/|L|$.

Figure 1 shows the dimensionless ground-level CWIC ($C^{y}_* = C^{y} u_* |L| / Q$) as a function of the dimensionless downstream distance ($x_* = x/|L|$). Under stable stratification, for $x_* > 10$, C^{y}_* varies as $x_*^{-2.3}$. One interesting aspect of the ground-level CWIC is that for small x_*, the ground-level CWIC exhibits an inverse linear law and appears *independent* of stratification stability. We will show this behavior holds for large downstream distances (x up to 1 km) under neutral stratification.

For unstable stratification, the asymptotic behavior of C^{y}_* is approximated by the power law, $C^{y}_* \sim x_*^{-n}$, $n \sim 2$. With mixed-layer scaling, Nieuwstadt (1980) should also have observed this relationship had he not considered Deardorff and Willis's (1975) water tank physical modeling data and Lamb's (1979) numerical modeling data — those modeling data are less reliable in deriving an empirical relationship relevant to the atmospheric surface layer. Similarly, the recent analysis of the CONDORS data by Briggs (1993) is inconclusive because the scatter of the data does not allow us to choose between x^{-2} and x^{-3}. Briggs prefers the "-3" exponent presumably because it is supported by Yaglom (1972). Note that the x_*^{-2} fall-off is incorporated into the empirical Pasquill - Gifford - Turner vertical dispersion curves used in most regulatory models (Venkatram, 1996).

In summary, the following formulae provide tentative descriptions of asymptotic downwind variation of ground-level CWIC:

$$C^{y}_* \sim x_*^{-2.3} \quad \text{(for stable stratification)} \qquad (2a)$$

$$C^{y}_* \sim x_*^{-1} \quad \text{(for neutral stratification)} \qquad (2b)$$

$$C^{y}_* \sim x_*^{-2} \quad \text{(for unstable stratification)} \qquad (2c)$$

Venkatram (1992) showed that these equations for the asymptotic behavior of concentration are supported by a simplified form of K-theory. van Ulden's (1978) predictions using an approximate form of K-theory also support these relationships; his predictions compared well with the Prairie Grass data. While the use of aspects of K-theory yields a "-2" fall-off in the CWIC during asymptotically unstable conditions, the

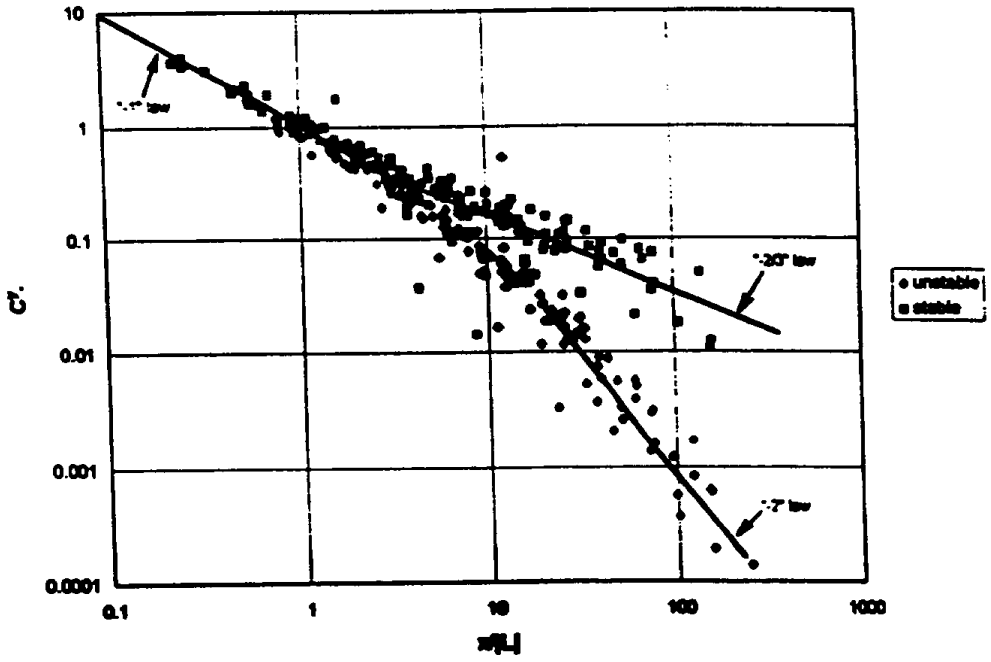

Fig. 1. The variation of dimensionless ground-level CWIC (cross-wind-integrated concentration) with dimensionless downstream distance, $x/|L|$, in the Project Prairie Grass experiment.

actual numerical solution of the eddy diffusivity equation appears to agree with the "-3.2" fall-off expected from free-convection theory (see Gryning *et al.*, 1983, Fig. 1). Wilson (1982) obtained the "-2" concentration using Lagrangian stochastic simulation (LSS). However, he obtained this result by using a length scale whose functional form was essentially derived by fitting model estimates to the corresponding vertical profile of concentrations observed at the 100 m arc in the Prairie Grass experiment. There is little *a priori* justification for his length scale formulation.

Survey of past work indicates that K-theory as well as early forms of LSS agree on equations (2a) and (2b) for stable and neutral conditions. There is less consensus on the prediction of CWIC vs distance for unstable conditions. The question we ask in this paper is whether the modern formulation of the Lagrangian stochastic simulation (LSS) model can provide better understanding of asymptotic behavior of CWIC in the surface boundary layer.

LAGRANGIAN STOCHASTIC MODELING OF VERTICAL DISPERSION

This section describes the application of LS simulation to derive data corresponding to the Prairie Grass experiment. These data will be used to examine the asymptotic relationships discussed earlier.

Lagrangian stochastic simulation (LSS) has emerged in the last 15 years to be a powerful tool to study turbulent diffusion (Wilson *et al.*, 1981; Sawford, 1985; Thomson, 1987). It is the most natural way to calculate trajectories of tracer particles drawn from the ensemble of flows constrained by similar external conditions, such as stratification stability, mean wind field, and boundary conditions. It is straightforward to calculate the mean concentration distribution from the modeled particle trajectories. LSS has been extensively used recently in studying diffusion in the convective boundary layer (Luhar and Britter, 1989; Weil, 1990; Du *et al.*, 1994; among others).

The LS model used in this study is one-dimensional in that random turbulent motion is confined to the vertical z direction:

$$dw = -\frac{C_0\varepsilon}{2\sigma_w^2}w\,dt + \frac{1}{2}\left(1+\frac{w^2}{\sigma_w^2}\right)\frac{\partial\sigma_w^2}{\partial z}dt + \sqrt{C_0\varepsilon}\,d\xi$$

$$dz = w\,dt$$

$$dx = U\,dt \tag{3}$$

where $d\xi$ is a random variable with zero mean and variance dt and C_0 an universal constant having value of 3.0 (Du *et al.*, 1995). Thomson (1987) proves that, in Gaussian turbulence, equation (3) is the uniquely correct one-dimensional model. We did not use a two-dimensional model because we wanted to avoid the so-called non-uniqueness problem of multi-dimensional models (Sawford and Guest, 1988), namely that for a given ensemble of turbulent flows constrained by the same external conditions, there are an infinite number of LS models satisfying Thomson's (1987) model design criteria. Equation (3) was originally derived by Wilson *et al.* (1983) using heuristic arguments.

In the atmospheric surface layer, the skewness factor of the turbulent vertical velocity, $S = \overline{w^3}/\sigma_w^3$, is less than 0.5, which allows us to assume that the distribution of mean concentration is close to Gaussian turbulence corresponding to $S = 0$ (Du, 1996).

To run the model, the standard deviation of vertical velocity σ_w and the mean rate of dissipation of turbulent kinetic energy, ε, are needed. We used the following formulae for these statistics in the surface layer (as well as the lower part of the mixed-layer under unstable stratification):

$$\sigma_w = 1.25u_*\left(1-3\frac{z}{L}\right)^{1/3}$$

(for unstable stratification)

$$\sigma_w = 1.25u_*$$

(for neutral and stable stratifications) (4)

$$\varepsilon = \frac{u_*^3}{\kappa z}\left(\varphi_m - \frac{z}{L}\right) \tag{5}$$

where φ_m is the non-dimensional gradient of mean wind. The σ_w profiles are suggested by Panofsky and Dutton (1984) from analyzing field experimental data, while equation (5) is simply the turbulent kinetic energy (TKE) budget equation stating that the dissipation of TKE is balanced by the mechanical and buoyant productions of TKE. We use the Businger-Dyer formulae for φ_m and Paulson's (1970) profiles for the mean wind speed:

$$\varphi_m = \left(1-16\frac{z}{L}\right)^{-1/4}$$

(for unstable stratification) (6a)

$$\varphi_m = 1 + 5\frac{z}{L}$$

(for stable stratification) (6b)

$$U = \frac{u_*}{\kappa}\left(\ln\frac{z}{z_0} - \psi_m\right) \tag{6c}$$

where

$$\psi_m = \ln\left[\left(\frac{1+\phi_m^{-2}}{2}\right)\left(\frac{1+\phi_m^{-1}}{2}\right)^2\right] - 2\arctan\phi_m^{-1} - \frac{\pi}{2}$$

(for unstable stratification)

$$\psi_m = -5\frac{z}{L}$$ (for stable stratification). (7)

We carried out model calculations for near ground-level releases (source height $h = 0.46$ m) up to a

downstream distance of $x = 8400$ m. We computed ground-level concentrations at $z = 1.5$ m corresponding to the observations at Prairie Grass. In the PPG experiment, the Monin-Obukhov length varied from ± 5 to ± 180 m; so we ran the model for different values of L: ± 5, ± 10, ± 20, ± 40, ± 80 and ± 160 m, respectively. In each simulation, we released 50,000 particles from the source and traced the two-dimensional particle trajectories to chosen receptors. At a receptor (x, z), the CWIC is

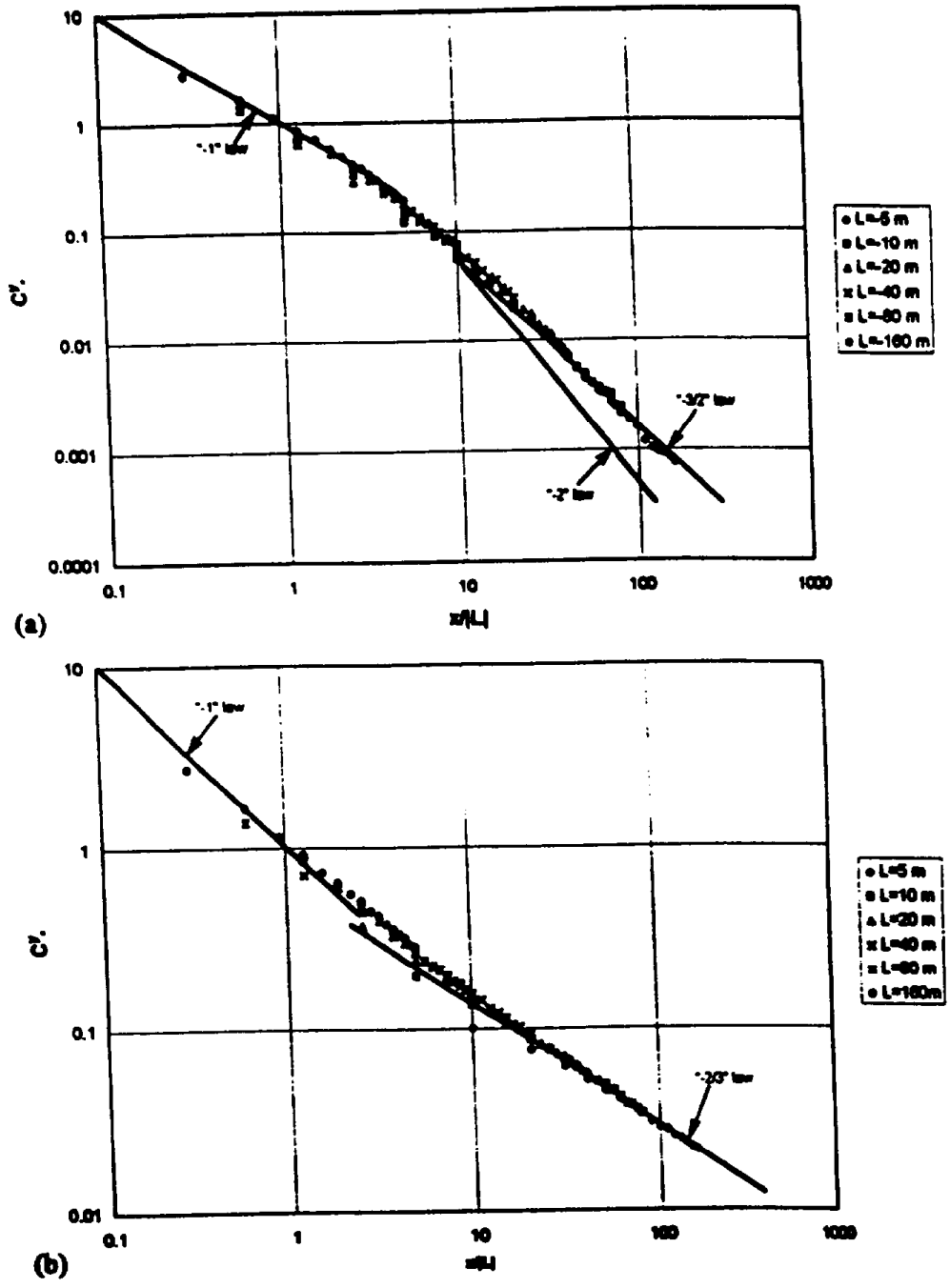

Fig. 2. Lagrangian stochastic (LS) simulation of the variation of dimensionless ground-level CWIC with dimensionless downstream distance, $(x/|L|)$.

calculated with

$$C'(x, z) = \frac{Qn(x, z, \Delta z)}{NU(z)\Delta z} \quad (8)$$

where Q is the point-source strength, Δz the size of the concentration sensor in the vertical direction, and $n(x, z, \Delta z)$ the number of particles passing through the sensor located at (x, z). Model results are not sensitive to the choice of Δz.

Figure 2 compares model results with the Prairie Grass data. The model results resemble the PPG data in the following ways: (1) near the source ($x_0 < 2$)

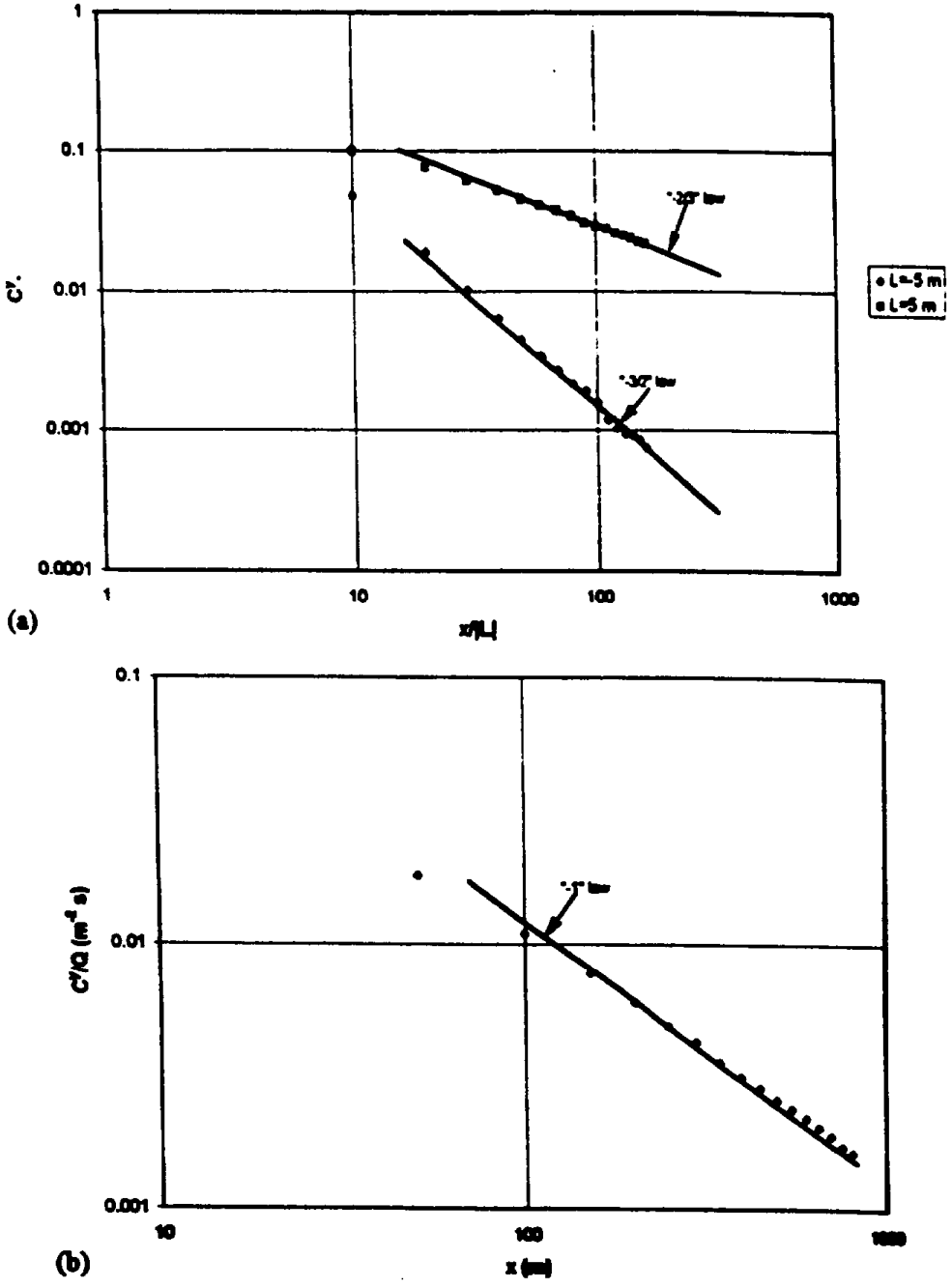

Fig. 3. LS simulation of the asymptotic behaviors for three extreme cases: (a) stable and unstable stratifications; and (b) neutral stratification.

C_*^2 decreases as x_*^{-1} and the relationship is independent of stratification stability; (2) under stable stratification, $C_*^2 \sim x_*^{-2/3}$ for large x_* (> 10), and (3) under unstable stratification, the model simulates the rapid decrease of C_*^2 with downstream distance but the predicted C_*^2 is larger than the measured at large x_* ($\sim$ 50–100) or under very unstable stratification.

To better understand the asymptotic behavior of the simulated CWIC, we plotted the simulated ground-level CWIC for three extreme conditions in Fig. 3: very stable ($L = 5$ m), neutral ($L = \pm\infty$) and very unstable ($L = -5$ m). For the stable and neutral cases, the LS model predictions follow the PPG asymptotes given by equations (2a) and (2b), but for extremely unstable stratification, the LS model result exhibits a "$-3/2$" power law, while the PPG data indicate a "-2" law. Although the difference between "$-3/2$" and "-2" laws is not large up to $x_* \sim 100$, it might be an indication that one-dimensional LSS is not capable of predicting vertical diffusion in the unstable surface layer.

DISCUSSION OF THE ASYMPTOTIC FORMULA UNDER UNSTABLE STRATIFICATION

Here we examine the possible reasons for the lack of agreement between the present LS model and the PPG data for strongly unstable stratification. One is that the deposition of the tracer material (SO_2) to the grass ground may lead to the observed decrease in concentration. To test this hypothesis we included deposition in the model with a probability that a tracer particle being absorbed by the ground is 0.5, which is equivalent to a deposition velocity up to $v_d \sim 0.3\sigma_w$, according to Wilson *et al.* (1989). Figure 4 indicates that the concentration is reduced but the "$-3/2$" law remains valid. This result is consistent with the Gryning *et al.* (1983) finding from K-theory modeling.

We next used a σ_w profile given by

$$\sigma_w^2 = 1.8 w_*^2 \left(\frac{z}{z_i}\right)^{2/3} \left(1 - 0.8\,\frac{z}{z_i}\right)^2 \qquad (9)$$

where w_* is the convective velocity scale, and z_i the mixed layer height. This formulation, which neglects shear-generated turbulence near the ground, was suggested by Lenschow *et al.* (1982) from an analysis of field data in the mixed layer.

Figure 5 shows that the use of equation (9) results in a "-2" power law for the ground-level CWIC, but the magnitude of the concentration for $x/|L| \sim 10$–100 is overestimated by at least a factor of 2. The reason for the "-2" fall-off of the concentration could be that the σ_w given by equation (9) provides the required rapid acceleration of the vertical velocity by neglecting the wind shear contribution. The actual concentration is overestimated because σ_w in the near ground region ($z \sim |L|$) is underestimated.

Yet another possible reason that may cause the discrepancy between LS prediction and PPG data is

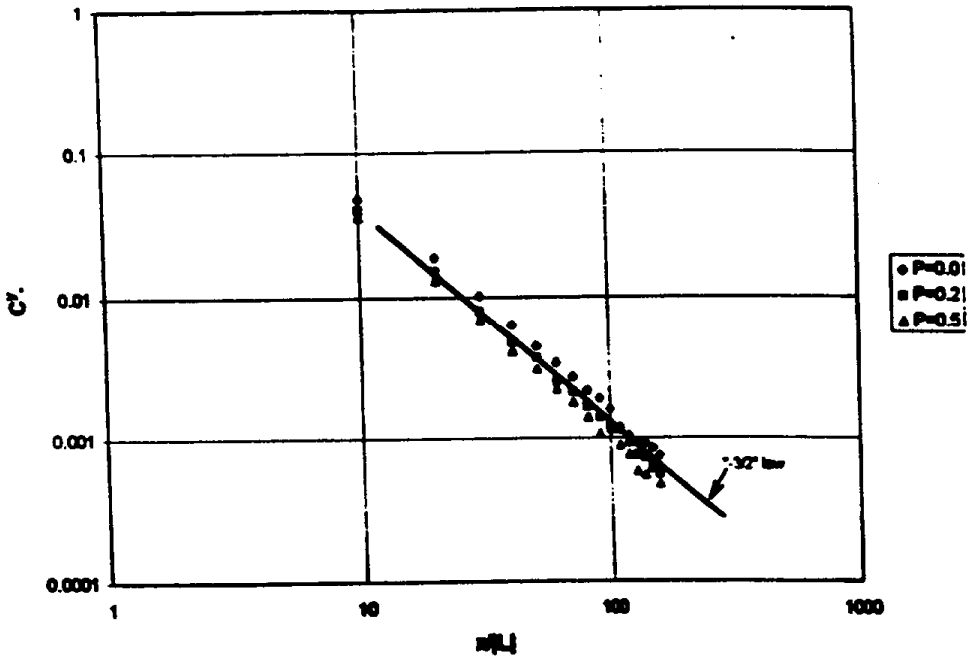

Fig. 4. The effect of surface deposition on the ground-level CWIC under unstable stratification.

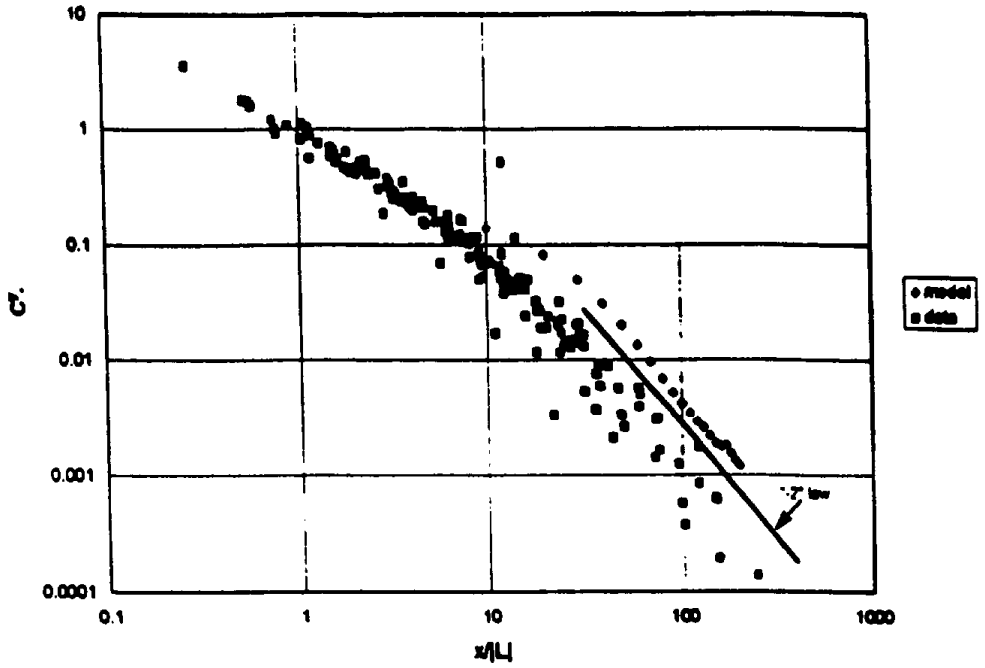

Fig. 5. Ground-level CWIC predicted by LS model with an alternative profile of σ_w.

the neglect of the skewness factor in the model. For large downstream distances, a substantial fraction of tracer particles is diffused into the mixed-layer where the effect of vertical velocity skewness may not be negligible. To test this hypothesis, we ran an LS model for skewed turbulence (Du *et al.*, 1994) with $S = 0.5$ but found the "$-3/2$" power law to remain valid in the range of $x_* \sim 10$–100 (see Fig. 6).

Briggs (personal communication) suggests that the "-2" behavior of ground CWIC is caused by the sweep of tracer material from the surface layer into the mixed layer ($z \gg |L|$). The LS model results show that with $L = -5$ m (very unstable) at downwind distance $x = 800$ m, $Z \approx \sigma_z \approx 300$ m (where Z and σ_z are the mean height and vertical spread of the plume, respectively), i.e., the majority of tracer material is in the mixed layer, but, as we have shown earlier, the ground-level CWIC still follows the "$-3/2$" law. This implies that Briggs' hypothesis is not supported by the LS simulation results.

It is possible that the disagreement between our LS simulation and the PPG data is due to experimental error: the concentration levels at large downstream distances are near the resolution limit of the experimental technique (Horst *et al.*, 1979). To address this issue, we plotted the data listed in Table 2 of van Ulden's (1978) paper in Fig. 7; this data set was screened for low concentrations. It is seen that both "-2" and "$-3/2$" slopes are acceptable in the range of $x/|L| = 10 \sim 100$. The "$-3/2$" decrease in CWIC is more strongly supported by data, shown in Fig. 8, collected at the National Reactor Test Station and reported by Horst *et al.* (1979). We also looked into the data gathered in the latest field diffusion experiment, CONDORS (see Briggs, 1993), but the scatter does not allow for a definite conclusion about the asymptotic behavior of CWIC.

SUMMARY

We studied the behavior of ground-level cross-wind integrated concentration using a one-dimensional Lagrangian stochastic model for Gaussian turbulence, which represents our current understanding of dispersion. The comparison between model predictions and Project Prairie Grass data for stable and neutral stratifications supports the validity of the following asymptotic expressions that were obtained earlier using a form of K-theory:

$$C_*^y \sim x_*^{-2} \quad \text{(for stable stratification)} \tag{10a}$$

$$C_*^y \sim x_*^{-3/2} \quad \text{(for neutral stratification)} \tag{10b}$$

The modeling also strongly suggests that for short travel distance of x_* less than 2,

$$C_*^y \sim x_*^{-1} \tag{11}$$

is valid no matter what the stratification is. However, under strongly unstable stratification for large x_*, the

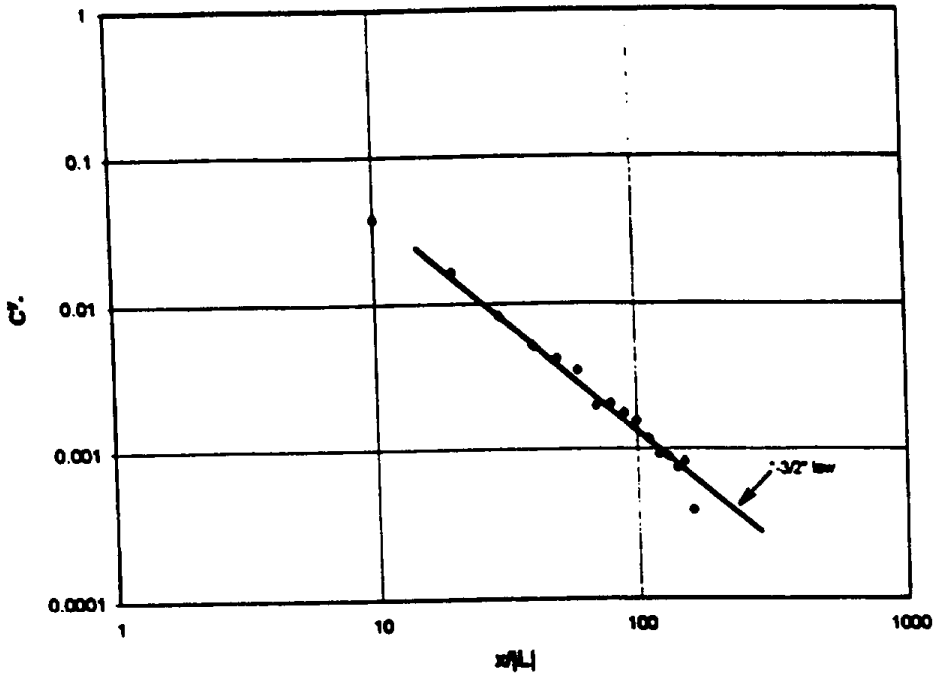

Fig. 6. The effect of vertical velocity skewness factor on the ground-level CWIC.

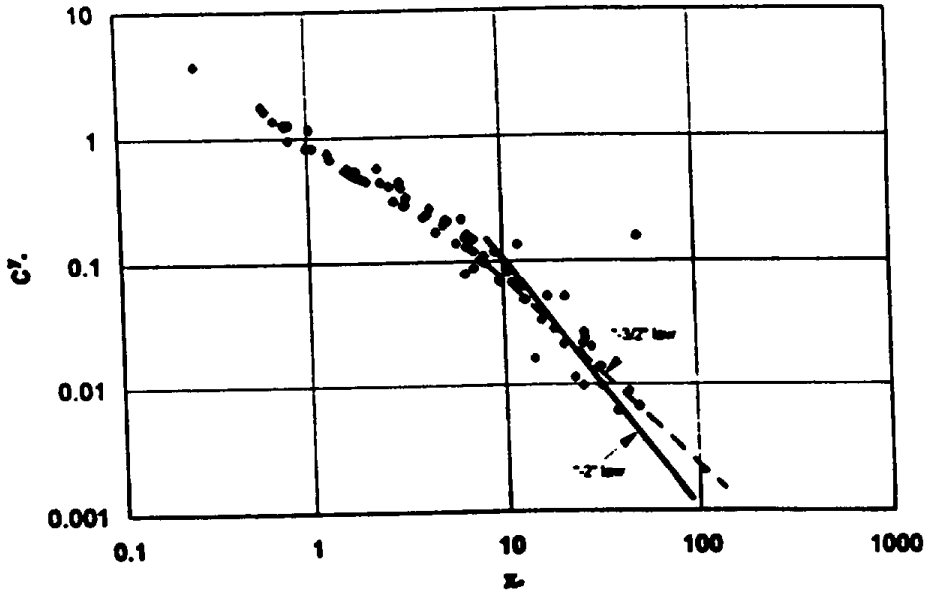

Fig. 7. The variation of ground-level CWIC with distance plotted with data from Table 2 of paper by van Ulden (1978).

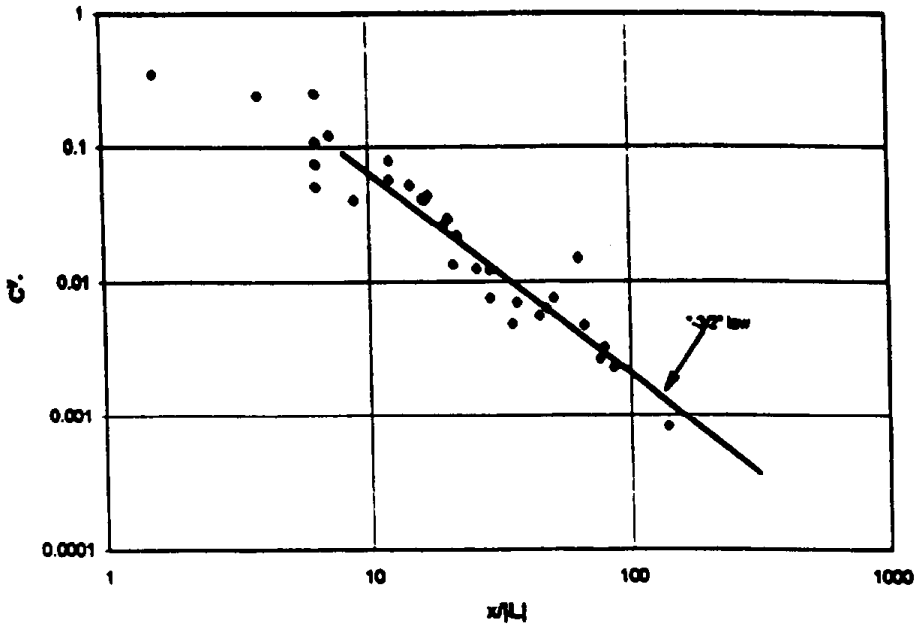

Fig. 8. The behavior of ground-level CWIC under unstable conditions. Data obtained from experiments conducted at the National Reactor Test Station, Idaho (Horst, 1979).

LS model yields

$$C_*^{\prime} \sim x_*^{-3/2} \tag{12}$$

which is not consistent with the more rapid fall-off observed in the PPG experiment. This disagreement may imply that the model we used is incapable of predicting vertical diffusion in the surface layer under very unstable stratification, or that the asymptotic behavior derived from the PPG experiment is not correct due to experimental errors. This problem can be resolved with data from a new field experiment. The new experiment will also allow us to examine the effects of a number of factors, such as velocity skewness, deposition of tracers to the ground, streamwise diffusion and the correlation between vertical velocity and streamwise velocity, on the distribution of mean concentration.

Acknowledgements—The work described in this paper was supported by a grant (Contract No. 94-366) from the California Air Resources Board. We are grateful to Dr Tony Van Curen, the ARB project manager, for encouraging research in small-scale dispersion.

REFERENCES

Barad M. L. (1958) Project Prairie Grass, a field program in diffusion. Vol. I. Geophysics Research Paper No. 59, Air Force Cambridge Research Center, Bedford, Massachusetts.

Briggs G. A. (1982) Similarity forms for ground-source surface-layer diffusion. *Boundary-Layer Met.* 23, 489–502.

Briggs G. A. (1993) Plume dispersion in the convective boundary layer. Part II: analyses of CONDORS field experiment data. *J. appl. Met.* 32, 1388–1425.

Deardorff J. W. and Willis G. E. (1975) A parameterization of diffusion into the mixed layer. *J. appl. Met.* 14, 1451–1458.

Du S. (1996) The effects of higher Eulerian velocity moments on the mean concentration distribution. *Boundary-Layer Met.* (in press).

Du S., Wilson J. D. and Yee E. (1994) Probability density function for velocity in the convective boundary layer, and implied trajectory models. *Atmospheric Environment* 28, 1211–1217.

Du S. *et al.* (1995) Estimation of the Kolmogorov constant (C_0) for the Lagrangian structure function, using a second-order Lagrangian model of grid turbulence. *Phys. Fluids* 7, 3083–3090.

Dyer A. J. and Bradley E. F. (1982) An alternative analysis of flux-gradient relationships at the 1976 ITCE. *Boundary-Layer Met.* 22, 1–19.

Gryning S., van Ulden A.P. and Larsen S. E. (1983) Dispersion from a continuous ground-level source investigated by a K model. *Q. Jl. R. Met. Soc.* 109, 357–366.

Horst T. W. (1979) Lagrangian similarity modeling of vertical diffusion from a ground source. *J. appl. Met.* 18, 333–340.

Horst T. W., Doran J. C. and Nickola P. W. (1979) Evaluation of empirical atmospheric diffusion data. Technical Final Report, Pacific Northwest Lab.

Lamb R. G. (1979) The effect of release height on material dispersion in the convective planetary boundary layer. Preprints 4th Symp. Turbulence, Diffusion and Air Pollution. AMS, pp. 27–33.

Luhar A. and Britter R. E. (1989) A random walk model for dispersion in inhomogeneous turbulence in a convective boundary layer. *Atmospheric Environment* 23, 1911–1924.

Nieuwstadt F. T. M. (1980) Application of mixed-layer similarity to the observed dispersion from a ground-level source. *J. appl. Met.* 19, 157–162.

Panofsky H. A. and Dutton J. A. (1984) *Atmospheric Turbulence*. 397 pp. Wiley, New York.

Paulson C. A. (1970) The mathematical representation of wind speed and temperature in the unstable atmospheric surface layer. *J. appl. Met.* 9, 857–861.

Sawford B. L. (1985) Lagrangian statistical simulation of concentration mean and fluctuation fields. *J. Clim. appl. Met.* 24, 1152–1166.

Sawford B. L. and Guest F. M. (1988) Uniqueness and universality of Lagrangian stochastic models of turbulent diffusion. *Proc. 8th Symp. Turb. Diff.* AMS, pp. 96–99.

Thomson D. J. (1987) Criteria for the selection of stochastic models of particle trajectories in turbulent flows. *J. Fluid Mech.* 180, 529–556.

van Ulden A. P. (1978) Simple estimates for vertical diffusion from sources near the ground. *Atmospheric Environment* 12, 2125–2129.

Venkatram A. (1982) A semi-empirical method to compute concentration associated with surface releases in the stable boundary layer. *Atmospheric Environment* 16, 245–248.

Venkatram A. (1992) Vertical dispersion of ground-level releases in the surface boundary layer. *Atmospheric Environment* 26A, 947–949.

Venkatram A. (1996) An examination of the Pasquill Gifford Turner dispersion scheme. *Atmospheric Environment* 30, 1283–1290.

Weil J. C. (1990) A diagnosis of the asymmetry in top-down and bottom-up diffusion using a Lagrangian stochastic model. *J. atmos. Sci.* 47, 501–515.

Wilson J. D. (1982) Turbulent dispersion in the atmospheric surface layer. *Boundary-Layer Met.* 22, 399–420.

Wilson J. D., Legg B. J. and Thomson D. J. (1983) Calculation of particle trajectories in the presence of a gradient in turbulent-velocity variance. *Boundary-Layer Met.* 27, 163–169.

Wilson J. D., Ferrndino E. J. and Thurtell G. W. (1989) A relationship between deposition velocity and trajectory reflection probability for use in stochastic Lagrangian dispersion models. *Agric. For. Met.* 47, 139–154.

Wilson J. D., Thurtell G. W. and Kidd G. E. (1981) Numerical simulation of particle trajectories in inhomogeneous turbulence II: Systems with variable turbulence velocity scale. *Boundary-Layer Met.* 21, 423–441.

Yaglom A. M. (1972) Turbulent diffusion in the surface layer of the atmosphere. *Izv. Akad. Nauk USSR Atmos. Ocean Phys.* 8, 333–340.

Appendix E
The Effect of Streamwise Diffusion on Ground-level Concentrations

The Effect of Streamwise Diffusion on Ground-Level Concentrations

by

Shuming Du and Akula Venkatram

College of Engineering, University of California, Riverside, CA

Abstract: This paper examines the effect of streamwise diffusion on the distribution of mean scalar concentrations associated with surface releases in the atmospheric surface layer. We use a two dimensional (streamwise-vertical) Lagrangian stochastic model to simulate dispersion. Before applying the model, we test its validity by comparing model results of mean concentration and streamwise mass flux density with wind tunnel data reported by Raupach and Legg (1983). The results from simulations conducted with the 2-D stochastic model indicated that: 1) inclusion of streamwise dispersion in a model provides a plausible explanation for the "-2" asymptote observed in Project Prairie Grass for the fall-off of ground-level concentrations under unstable conditions, and 2) streamwise diffusion plays a minor role in dispersion under stable conditions.

Key words: surface layer, dispersion, streamwise diffusion, Lagrangian stochastic model, Prairie Grass Experiment, atmospheric surface layer, convective conditions.

Introduction

Most studies to date have neglected the effect of streamwise diffusion on the mean cross-wind integrated concentration (CWIC), presumably because 1) the streamwise velocity fluctuation, u' is about one order of magnitude smaller than the average wind speed, U, through most of the depth of the boundary layer, and 2) vertical concentration gradients

are about ten times the horizontal concentration gradients. One dimensional models (Nieuwstadt and van Ulden, 1978; van Ulden, 1978; Gryning et al., 1983; Wilson et al., 1981; Weil, 1990; Venkatram and Du, 1997; among many others), which neglect streamwise diffusion, have been successful in describing most of the observed features of dispersion in the surface boundary layer. However, their results, as we will show later, are not consistent with the behavior of ground-level concentrations under unstable conditions observed in the Project Prairie Grass (PPG) experiment (Barad, 1958). Because the PPG experiment represents the best source of experimental data, we suspect that this inconsistency may imply that streamwise diffusion is important under unstable conditions.

The effect of streamwise velocity fluctuation on the distribution of mean concentration has been explored in a limited number of studies (Monin and Yaglom 1971, pp666-669; Brown et al. 1993 and references therein). These studies indicate that streamwise diffusion has a small effect relative to that caused by cross-wind diffusion and vertical diffuison. The results from the wind tunnel experiment conducted by Raupach and Legg (1983) are less definitive. They suggest that streamwise diffusion could be important close to the ground.

To examine the effect of streamwise diffusion, consider the budget for the mean cross-wind integrated concentration, C:

$$\frac{\partial}{\partial x}(UC) = -\frac{\partial}{\partial z}<\dot{w}\dot{c}> - \frac{\partial}{\partial x}<\dot{u}\dot{c}> \qquad (1)$$

We can gain some insight into the effects of streamwise diffusion by using simple mixing length arguments. A fluid parcel moving upwards carries a negative u' because it originates from slower moving fluid near the ground. On the other hand, it is associated with a positive c' because it originates from a higher concentration region. This means that $<\dot{u}\dot{c}>$ is negative for such parcels. It is easily seen that downward moving fluid parcels will also result in negative $<\dot{u}\dot{c}>$.

These mixing length arguments can be made more explicit as follows:

$$<u'c'> \sim -<u'l_z>\frac{\partial C}{\partial z} - <u'l_x>\frac{\partial C}{\partial x}, \qquad (2)$$

where l_z is a mixing length, whose value is positive when the parcel is moving upwards, and negative when moving downwards. Because an upward moving parcel is associated with a negative w', the effective eddy diffusivity, $K_{zz} = < w' l_z >$, is a negative quantity. On the other hand, $K_{zz} = < w' l_z >$ is a positive quantity. It is easy to show that the second term on the right hand side of the equation is of the order of σ_x / x times the first term, which implies that the first term dominates the second term at most distances from the source. So, we will confine our attention to the cross diffusion term $K_{zz} \partial C / \partial z$.

Because the gradient, $\partial C / \partial z$, achieves its minimum value (maximum absolute value) close to the source, $< u'c' >$ also attains its minimum close to a source and increases with distance: $-\partial < u'c' > / \partial x < 0$. This is confirmed by the data presented in Raupach and Legg (1983, Figure 7). This implies, as can be seen from Equation (1), that the ground-level concentration predicted by two-dimensional models will fall off faster than predictions from one-dimensional models. As discussed in the next section, this more rapid fall-off in concentration might explain the discrepancy between the observed behavior of concentrations in the PPG experiment and one-dimensional theory. This paper examines this possibility by simulating dispersion using a 2-D Lagrangian Stochastic model that includes streamwise diffusion. Before presenting results from the 2-D model, we will discuss the behavior of the concentrations in the PPG experiment, which motivated this study.

Concentration Variation in the Project Prairie Grass Experiment

Even though the Prairie Grass experiment was conducted as long ago as 1956 (Barad, 1958), the data from the experiment still represent the most complete available for the analysis of surface layer dispersion. The studies conducted with the data indicate consensus on the asymptotic behavior of ground-level concentrations under stable and neutral conditions (Venkatram and Du, 1997). However, there are still some questions on the far-field variation under convective conditions.

To illustrate the difficulty in interpreting the data we have plotted the data listed in Table 2 of van Ulden's (1978) paper. We seek relationships between CWIC and downwind distance in the form:

$$\frac{\overline{C}^{\prime} u_* |L|}{Q} = Function\left(\frac{x}{|L|}\right), \qquad (3)$$

where $\overline{C}^{\prime}$ is the cross-wind integrated concentration, u_* is the surface friction velocity, L is the Monin-Obukhov length, Q is the emission rate, and x is the downwind distance from the source.

The asymptotes refer to the functional behavior at large $x_* = x/|L|$. Specifically, we are looking for the exponent "n" when the right hand side of the equation is written as $(x/|L|)^n$; "n" is the slope when the relationship is plotted on a log-log graph. It is seen from Figure 1 that both "-2" and "-3/2" slopes are acceptable in the range of x/|L|=10~100, but the "-2" slope appears to provide a better fit to the data.

Because the method to scale data can cause artificial correlation between variables that might be un-correlated, we have re-plotted the PPG data to allow us to choose between the two possible models of asymptotic behavior:

$$\frac{\overline{C}^{\prime} u_*}{Q|L|} \sim \frac{1}{x^2} \qquad (4a)$$

and

$$\frac{\overline{C}^{\prime} u_*}{Q|L|^{1/2}} \sim \frac{1}{x^{3/2}} \cdot \qquad (4b)$$

corresponding to the -2 and -3/2 decrease in CWIC for unstable conditions. On a log-log plot, an adequate model would be indicated by the line of slope 1 passing through the middle of the data. Figure 2a shows that line of slope 1 passes through the data plotted in terms of the variables of Equation (4a). On the other hand, Figure 2b indicates that the unity slope line passes through the top of the data. Also, there is an unmistakable suggestion that the concentration falls off faster than -3/2. Thus, the "-2" power law

appears to be better than the "-3/2" law in describing the PPG data, and this choice is not an outcome of a particular scaling method.

The "-3/2" fall-off in concentration under convective conditions is supported by Lagrangian Similarity theory first formulated by Yaglom (1972). K-theory modeling based on surface-layer similarity (See Gryning et al., 1983) also yields a -3/2 decrease. Only an approximation of K-theory appears to produce the -2 law as shown in Venkatram (1992). The semi-empirical formula used by Venkatram (1992) to describe the PPG data is;

$$\bar{C}_*' = 1/(x_*(1+\alpha x_*^2)^{1/2}) \quad \alpha = 6.0\times 10^{-3}, \tag{5}$$

which embodies the "-2" fall-off in concentration, but is inconsistent with existing one-dimensional theory. As indicated earlier, we want to examine the possibility that this inconsistency is related to streamwise diffusion.

To obtain a preliminary estimate of the magnitude of streamwise diffusion relative to vertical diffusion, consider a concentration profile given by

$$C(x,z) = C_o \exp(-z^2/(2\sigma_z^2)). \tag{6}$$

Now, according to the mixing length arguments given earlier, the streamwise diffusion component is

$$\frac{\partial}{\partial x}\langle u'c'\rangle \sim \frac{\partial}{\partial x}\left(K_x \frac{\partial C}{\partial x}\right), \tag{7}$$

while the vertical component is

$$\frac{\partial}{\partial z}\langle w'c'\rangle \sim \frac{\partial}{\partial z}\left(K_z \frac{\partial C}{\partial z}\right). \tag{8}$$

If we assume that the diffusivities in Equations (7) and (8) are similar in magnitude, we can estimate the relative magnitude of the two terms as:

$$\frac{\partial}{\partial x}\langle u'c'\rangle / \frac{\partial}{\partial z}\langle w'c'\rangle \sim \frac{\partial}{\partial x}\left(\frac{\partial C}{\partial x}\right) / \frac{\partial^2 C}{\partial z^2} = \frac{nz}{x}, \tag{9}$$

if we write

$$\sigma_t = \alpha x^n. \qquad (10)$$

Because the magnitude of σ_t limits the vertical co-ordinate, z, in Equation (9), and n has its largest value under convective conditions, we expect streamwise diffusion to have its largest effect during convective conditions. The results from the numerical experiments, to be described later, examine this expectation.

A Two-dimensional LS Model

Lagrangian Stochastic simulation (LSS) has emerged in the last 15 years to be a powerful tool to study turbulent diffusion (Wilson et al. 1981a; Sawford 1985; Thomson 1987). It is the most natural way to calculate trajectories of tracer particles drawn from the ensemble of flows constrained by similar external conditions, such as stratification stability, mean wind field, and boundary conditions. It is straightforward to calculate the mean concentration distribution from the modeled particle trajectories. LSS has been extensively used recently in studying diffusion in the convective boundary layer (Luhar and Britter 1989; Weil 1990; Du et al. 1994; among others).

In this study, we use Thomson's (1987) simplest two-dimensional model given by:

$$\begin{aligned}
du &= \{-\frac{C_0\varepsilon}{2}[\lambda_{uu}(u-U)+\lambda_{uw}w]+\frac{\partial U}{\partial z}w\}dt+\sqrt{C_0\varepsilon}d\zeta_x(t),\\
dw &= \{-\frac{C_0\varepsilon}{2}[\lambda_{wu}(u-U)+\lambda_{ww}w]+\frac{1}{2}\frac{\partial \tau_{ww}}{\partial z}\}dt\\
&\quad+\frac{1}{2}\frac{\partial \tau_{ww}}{\partial z}[\lambda_{wu}(u-U)+\lambda_{ww}w]wdt+\sqrt{C_0\varepsilon}d\zeta_z(t), \qquad (11)\\
dx &= udt,\\
dz &= wdt,
\end{aligned}$$

where u and w are instantaneous velocity components in the downstream and vertical directions, U is the average wind speed, ε is the average rate of dissipation of turbulent kinetic energy, C_0 is an universal constant with a value of 3.0 (Du et al., 1995), $d\zeta_x$ and $d\zeta_z$ are two independent random numbers having zero mean and variance dt. The coefficients, λ_{ij}, that couple the velocities, are related to the Reynolds stress tensor, τ_{ij}, through

$$\lambda_w = (\tau_{ww} - \tau_{uw}^2 / \tau_{uu})^{-1},$$
$$\lambda_u = (\tau_{uu} - \tau_{uw}^2 / \tau_{ww})^{-1}, \qquad (12)$$
$$\lambda_{uw} = (\tau_{uw} - \tau_{uw}\tau_{ww} / \tau_{ww})^{-1}.$$

Notice that neglecting u' (as well as in τ_{ij}'s) in Equation (12) yields the commonly used one-dimensional model used by other investigators:

$$dw = -\frac{C_0\varepsilon}{2\sigma_w^2} w dt + \frac{1}{2}(1 + \frac{w^2}{\sigma_w^2})\frac{\partial \sigma_w^2}{\partial z} dt + \sqrt{C_0\varepsilon} d\zeta,$$
$$dz = w dt, \qquad (13)$$
$$dx = U dt,$$

where we have used σ_w^2 to denote τ_{ww}.

The model equations (11) assume Gaussian turbulence (i.e., the velocities u and w are jointly normal distributed), and are derived using the well-mixed criterion proposed by Thomson (1987) and Pope (1987). Note that for a given set of turbulence statistics, an infinite number of two-dimensional LS model equations can be derived from the well-mixed condition. At present, we cannot construct an unique equation (Sawford and Guest, 1988) from theoretical considerations. However, we can test the 2D model by comparing its predictions with measurements made in Raupach and Legg's wind tunnel(1983).

The model inputs are the standard deviations of vertical velocity (σ_w) and of streamwise velocity (σ_u), the mean rate of dissipation of turbulent kinetic energy (ε), and the mean wind speed (U). We used the following well-accepted formulae applicable in the surface layer for these variables (Panofsky and Dutton, 1984; Stull, 1988):

$$\sigma_w = \begin{cases} 1.25u_*(1 - 3\frac{z}{L})^{1/3} & (1/L < 0) \\ 1.25u_* & (1/L \geq 0) \end{cases} \qquad (14)$$

$$\sigma_u = 2.5u_* \qquad (15)$$

$$\varepsilon = \frac{u_*^3}{kz}(\varphi_m - \frac{z}{L}) \qquad (16)$$

where φ_m is the non-dimensional gradient of mean wind, and is related to z/L by

$$\phi_m = \begin{cases} (1 - 16z/L)^{-1/4} & (L < 0) \\ 1 + 5z/L & (L > 0) \end{cases}, \qquad (17)$$

and the mean wind speed

$$U = \frac{u_*}{\kappa}[\ln(\frac{z}{z_0}) - \Psi_m(\frac{z}{L})], \qquad (18)$$

and

$$\Psi_m = \begin{cases} \ln\left[\left(\frac{1+\phi_m^{-2}}{2}\right)\left(\frac{1+\phi_m^{-1}}{2}\right)^2\right] - 2\arctan\phi_m^{-1} + \frac{\pi}{2}, & (1/L \le 0) \\ -5\frac{z}{L}. & (1/L > 0) \end{cases} \qquad (19)$$

A Test of the Two-dimensional Model against Wind Tunnel Diffusion Measurements

We tested the model equations presented in the last section with measurements made by Raupach and Legg (1983) in a wind tunnel diffusion experiment. In the diffusion experiment, carried out in the Australian CSIRO Pye Laboratory wind tunnel, heat was used as tracer. Flow properties such as σ_u, σ_w, ε, $\langle u'w' \rangle$ and U were measured together with diffusion properties that included mean concentration, concentration variance, and mass flux density. For a detailed description of the experiment and the observational data, the reader is referred to Raupach and Legg (1983). One word needs stressing out here is that the flow statistics in the wind tunnel experiments are almost identical to that in the atmospheric surface layer under neutral stratification.

The data from the wind tunnel was used to evaluate model estimates of (1) the distribution of mean concentration, and (2) the distribution of streamwise mass flux density. The latter will tell us whether streamwise diffusion is responsible for a faster fall-off of ground-level concentration with downwind distance.

Figure 3 shows the vertical distribution of mean concentration predicted by our model at the downwind distances x/h = 7.5, where h is the source height (c_* is defined as

$Q/\rho c_p hu(h)$). This vertical profile is similar to that observed by Legg and Raupach (1983). The close agreement between the model predictions and the measurement supports the validity of the model Equations (11).

The vertical distributions of streamwise mass flux density at the downwind distances x/h = 7.5 is shown in Figure 4 which also compares the model prediction with the wind tunnel measurement from Raupach and Legg's Figure 7 (1983). Although the model estimates of the maximum and minimum differ from the corresponding observations by about 30%, the model predicts the correct qualitative behavior. In particular, the two-dimensional model prediction agrees with Raupach and Legg's findings that (1) streamwise mass flux density is driven by $\partial C/\partial z$ rather than $\partial C/\partial x$; (2) the eddy diffusivity K_{xz} is negative; and (3) in the upper part of the plume, $-\frac{\partial}{\partial x}<u'c'>$ <0 near the plume centerline. Note that the last observation implies that streamwise diffusion expedites the fall off of ground-level concentrations.

In summary, the comparison of the two-dimensional LS model predictions with wind tunnel observations supports the application of the model Equations (11) to the examination of the effects of streamwise diffusion in the atmospheric surface layer. The results are described in the next section. .

LS Simulation of Dispersion in the Atmospheric Surface Layer

We released 1,000,000 particles from a height of 0.46 m to simulate diffusion in the Prairie Grass experiment. Unstable cases were represented by Monin-Obukhov lengths of L= -5 m and L= -10 m. Figure 5 shows the results from these simulations. We see that in the range x/|L| = 50–200, the ground-level concentration falls off at a rate that is close to the "-2" power of the downwind distance. Data from the Prairie Grass experiment, while showing more scatter than the simulation data, are consistent with the "-2" asymptote predicted by the 2-D model.

The difference between the results from a 1-D model (Du and Venkatram, 1997) and the current 2-D model is shown more clearly in Figure 6. Notice that the concentrations from the 2-D model are higher the 1-D model close to the source, but then fall off more rapidly

than the 1-D model for $|x/L| > 30$. The higher concentrations are related to the effects of upwind diffusion, which are absent in the 1-D model. The figure also indicates that a curve that incorporates a "-2" asymptote fits the results from the 2D stochastic model. The solid line, corresponding to a fit to the 1-D model results (Du and Venkatram, 1997), does not show the "-2" fall-off at large distances.

Our earlier analysis indicated that the effects of streamwise diffusion are likely to be less important in stable conditions when the vertical plume growth rate is small compared to that under unstable conditions. Figure 7, showing results under stable conditions, bears out this expectation. The 2-D model results show little deviation from the "-2/3" distance fall-off predicted by the 1-D model. While the Prairie Grass data show considerable scatter, they are consistent with the predicted asymptote.

Conclusions

Most previous studies of turbulent diffusion in the atmospheric boundary layer have assumed that the effect of streamwise diffusion is negligible. To our knowledge this assumption has never been justified or seriously tested. This study examines the effects of streamwise diffusion by simulating dispersion with a 2-D Lagrangian stochastic model formulated using methods proposed by Thomson (1987). Because a 2-D model cannot be uniquely formulated, we tested our particular model with data reported by Raupach and Legg (1983). The distributions of mean concentration and streamwise mass flux density predicted by the model were consistent with observations at selected distances from the source. These results provided the support required to use the 2-D model to study the effects of streamwise diffusion.

Under unstable stratification, the 2-D model predicts a "-2" fall-off with distance at large $x/|L|$, which is consistent with observations from the Prairie Grass experiment. The 1-D model, which neglects streamwise diffusion, predicts a slower "-3/2" fall-off (Venkatram and Du, 1997). Under stable conditions, there is little difference between the asymptotic behaviors predicted by the 1-D and 2-D models; both of them predict a "-2/3" fall-off. The results from this study strongly suggest that the rapid "-2" concentration decrease with distance at large distances seen in Project Prairie is caused by streamwise diffusion

adding to the effects of vertical cross-stream diffusion, which by itself predicts a "-3/2" fall-off. This also implies that semi-empirical equations (for example, Venkatram 1992) that incorporate the "-2" asymptote should be used for practical dispersion calculations.

REFERENCES

Barad, M. L., 1958: *Project Prairie Grass, a Filed Program in Diffusion*. Vol. 1, Geophysics Research Paper No. 59, Air Force Cambridge Research Center, Bedford, MA.

Brown, M.J., Arya, A.P.S. and Snyder, W.R., 1993: Vertical dispersion from surface and elevated releases: an investigation of a non-Gaussian plume model. *J. Appl. Meteorol.* 32, 490-505.

Du, S., Sawford, B.L., Wilson, J.D. and Wilson, D.J., 1995: Estimation of the Kolmogorov constant (C_0) for the Lagrangian structure function, using a second-order Lagrangian model of grid turbulence. *Phys. Fluids* 7, 3083-3090.

Du, S. and Venkatram, A., 1997: A parameterization of vertical dispersion of ground-level releases. *J. Appl. Met.* 36, 1004-1015.

Du, S., Wilson, J. D. and Yee, E., 1994: Probability density functions for velocity in the convective boundary layer, and implied trajectory models. *Atmos. Envirion.* 28, 1211-1217.

Gryning, S., van Ulden, A.P. and Larsen, S.E., 1983: Dispersion from a continuous ground-level source investigated by a K model. Quart. *J. Roy. Met. Soc.* 109. 357-366

Luhar, A. and Britter, R.E., 1989: A random walk model for diffusion in inhomogeneous turbulence in a convective boundary layer. *Atmos. Environ.* 23, 1911-1924.

Monin, A.S. and Yaglom, A.M., 1971: *Statistical Fluid Mechanics*, Vol. 1, MIT Press, Cambridge, MA.

Nieuwstadt, F. T. M. and van Ulden, A.P., 1978: A numerical study on the vertical dispersion of passive contaminants from a continuous source in the atmospheric surface layer. *Atmos. Environ.* 12, 2119-2124.

Panofsky, H.A. and Dutton, J.A., 1984: *Atmospheric Turbulence*, Wiley, New York. 397pp.

Pope, S.B., 1987: Consistency conditions for random-walk models of turbulent diffusion. *Phys. Fluids*, 30, 2374-2379.

Raupach, M.R. and Legg, B.J., 1983: Turbulent diffusion from an elevated line source: measurements of wind-concentration moments and budgets. *J. Fluid Mech.*, 136, 111-137.

Sawford, B.L., 1985: Lagrangian statistical simulation of concentration mean and fluctuation fields. *J. Clim. Appl. Met.* 24, 1152-1161.

Sawford, B.L. and Guest, F.M, 1988: Uniqueness and universality of Lagrangian stochastic models of turbulent diffusion. *Proc. 8th Symp. Turb. Diff.*, Amer. Met. Soc., pp96-99.

Stull, R.B., 1988: *An Introduction to Boundary Layer Meteorology*, Kluwer Academic Publishers, Dordrecht, 666pp.

Thomson, D.J., 1987: Criteria for the selection of stochastic models of particle trajectories in turbulent flows. *J. Fluid Mech.* 180, 529-556.

van Ulden, A. P., 1978: Simple estimates for vertical diffusion from sources near the ground. *Atmos. Environ.* 12, 2125-2129.

Venkatram, A., 1992: Vertical dispersion of ground-level releases in the surface boundary layer. *Atmos. Environ.* 26A, 947-949.

Venkatram, A. and Du, S., 1997: An analysis of the asymptotic behavior of cross-wind-integrated ground-level concentrations using Lagrangian stochastic simualtion. *Atmos. Environ.* 31, 1467-1476.

Weil, J., 1990: A diagnosis of the asymmetry in top-down and bottom-up diffusion using a Lagrangian stochastic model. *J. Atmos. Sci.* 47, 501-515.

Wilson, J.D., Thurtell, G.W. and Kidd, G.E., 1981: Numerical simulation of particle trajectories in inhomogeneous turbulence II: Systems with variable turbulence velocity scale. *Boundary-Layer Met.* **21**, 421-423.

Yaglom, A. M., 1972: Turbulent diffusion in the surface layer of the atmosphere. *Izv. Atmos. Oceanic Phys.* **9**, 333-340.

Figure captions:

Figure 1. The variation of ground-level cross-wind integrated concentration (CWIC) with downstream distance. Data were obtained from van Ulden's (1978) Table 2.

Figure 2. PPG data displayed with different (from Figure 1) scaling methods. (a) $C^y u_*/Q|L| \sim 1/x^2$, also shown is Venkatram's (1992) formula; (b) $C^y u_*/Q|L|^{1/2} \sim 1/x^{3/2}$.

Figure 3. A comparison of the 2D model prediction of vertical profile of mean concentration with Raupach and Legg's measurement. The downwind distance x = 7.5h.

Figure 4. A comparison of the 2D model prediction of vertical profile of streamwise mass flux density with Raupach and Legg's measurement. The downwind distance x = 7.5h.

Figure 5. 2D LS model simulation of ground-level CWIC in a unstable surface layer. Also shown are the PPG observational data.

Figure 6. A comparison between 1D and 2D LS model predictions of ground-level CWIC. In calculation, L = -10m. Also shown are predictions obtained from empirical formulae of Du and Venkatram (1997) and of a revised form of Venkatram (1992). In the original Venkatram formula, $C^y{}_* = 1/x_*(1+\alpha x_*^2)^{1/2}$, where $x_* = x/|L|$ and $\alpha = 0.006$. In the revised form, we used $\alpha = 0.004$.

Figure 7. A comparison of 2D model prediction and PPG data under stable stratifications.

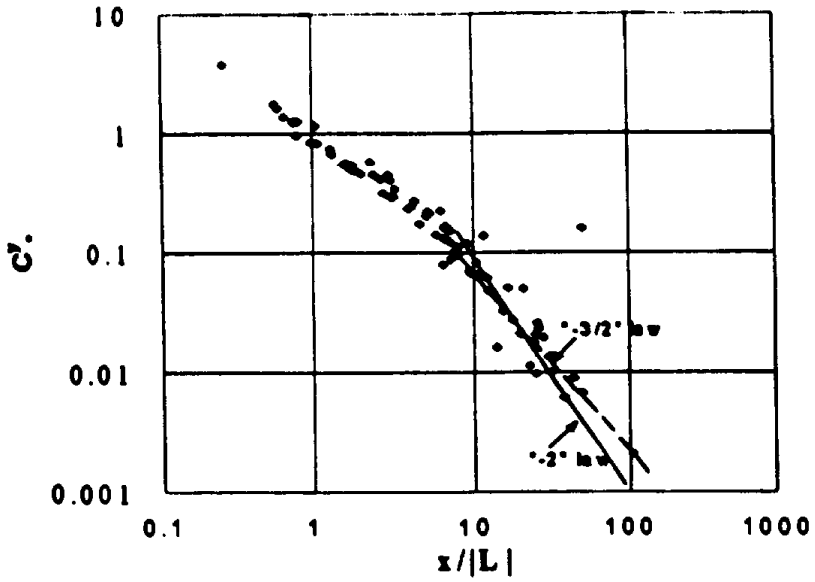

Figure 1. The variation of ground-level cross-wind integrated concentration (CWIC) with downstream distance. Data were obtained from van Ulden's (1978) Table 2.

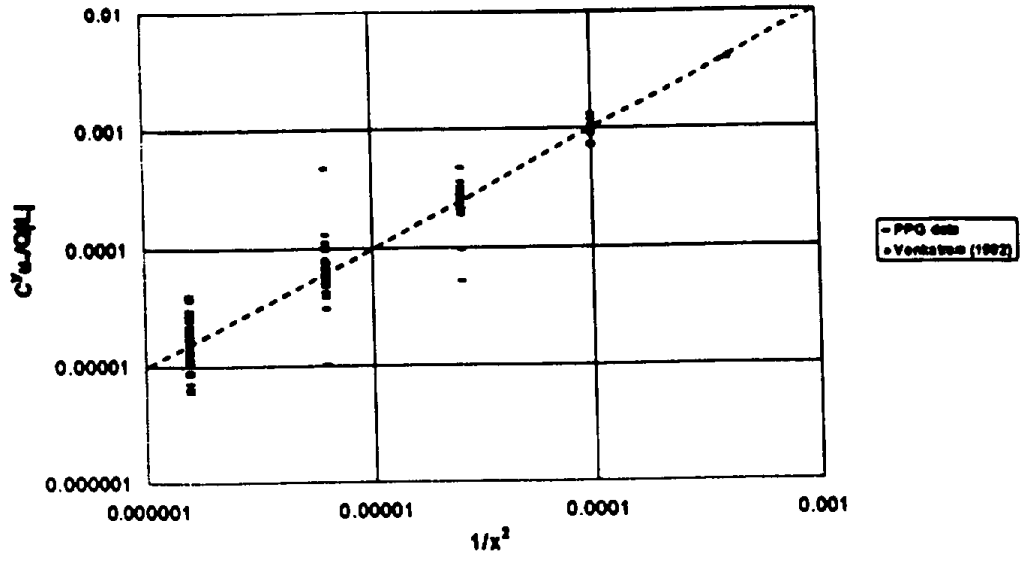

Figure 2. PPG data displayed with different (from Figure 1) scaling methods. (a) $C^y u_* / Q|L| \sim 1/x^2$, also shown is Venkatram's (1992) formula; (b) $C^y u_* / Q|L|^{1/2} \sim 1/x^{3/2}$.

Figure 2 (b). PPB data (z/L>10)

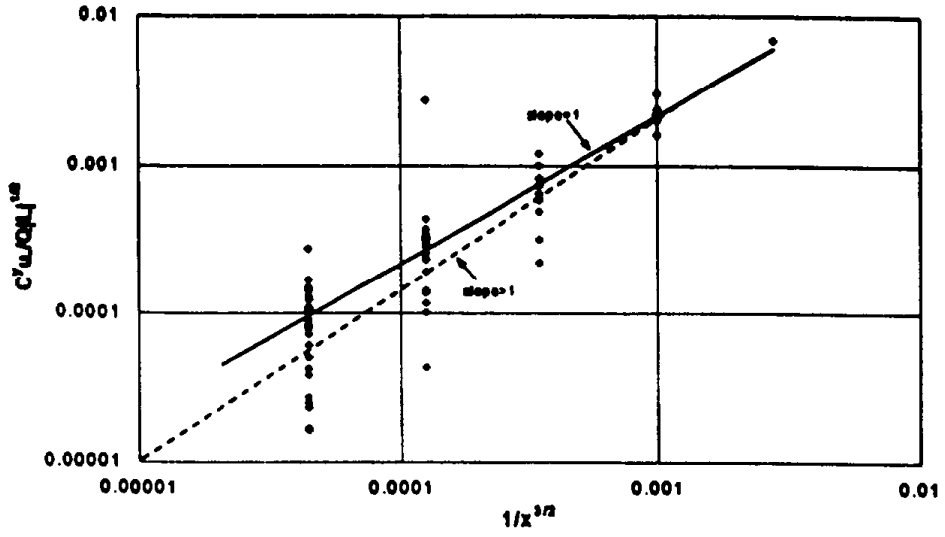

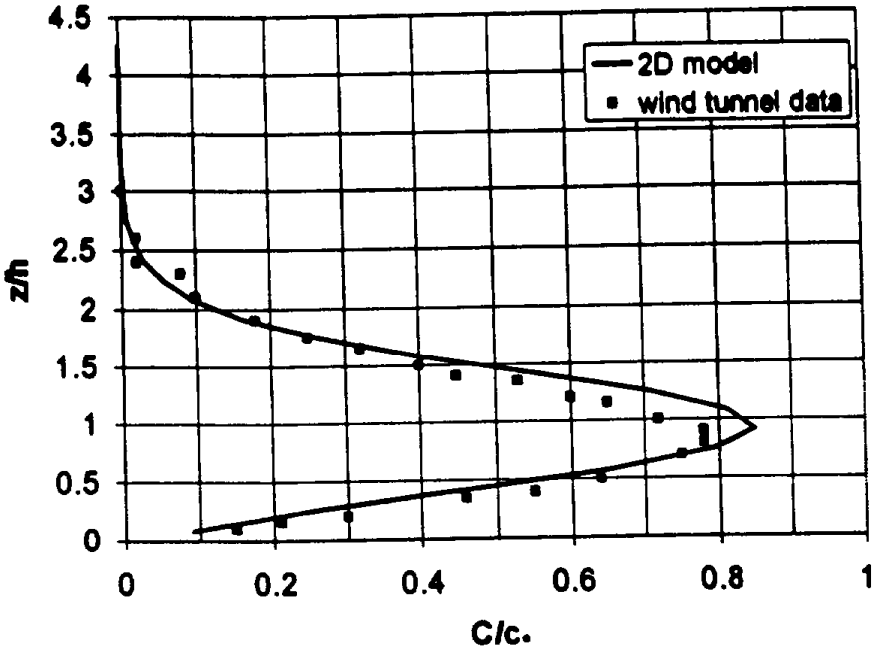

Figure 3. A comparison of the 2D model prediction of vertical profile of mean concentration with Raupach and Legg's measurement. The downwind distance x = 7.5h.

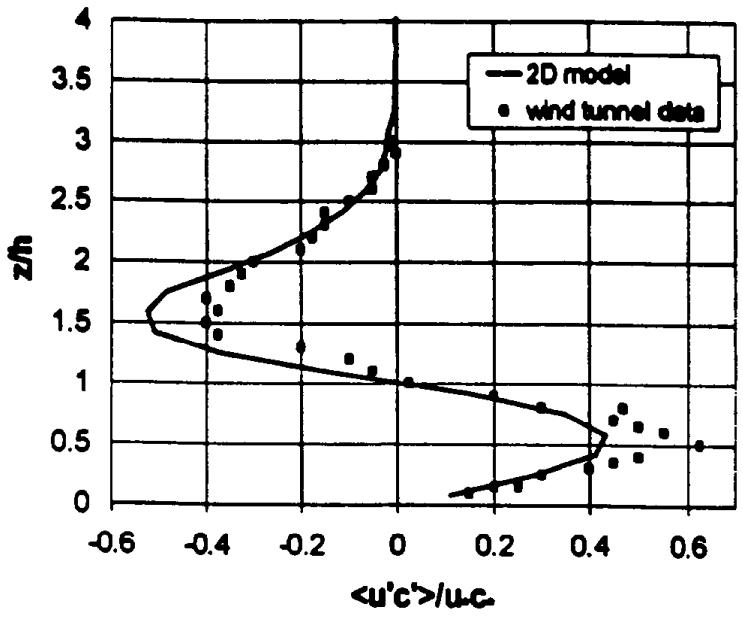

Figure 4. A comparison of the 2D model prediction of vertical profile of streamwise concentration flux with Raupach and Legg's measurement. The downwind distance x = 7.5h.

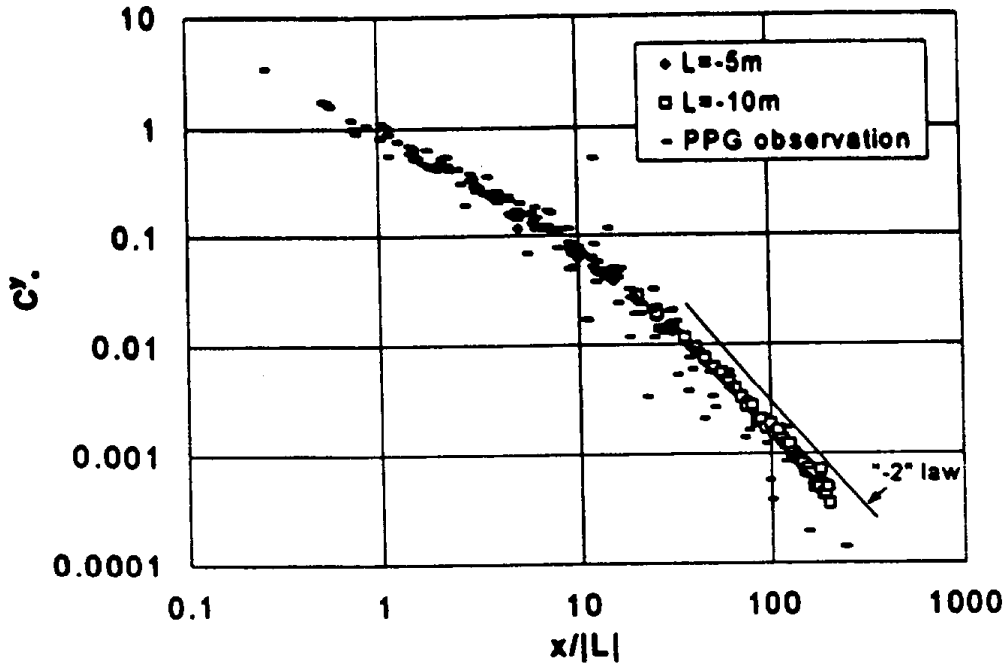

Figure 5. 2D LS model simulation of ground-level CWIC in a unstable surface layer. Also shown are the PPG observational data.

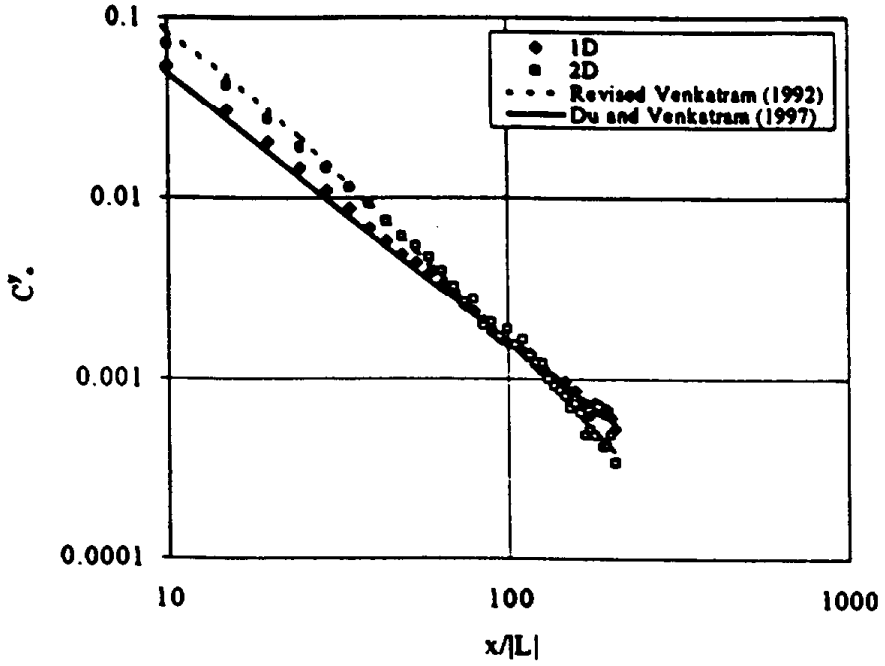

Figure 6. A comparison between 1D and 2D LS model predictions of ground-level CWIC. In calculation, L = -10m. Also shown are predictions obtained from empirical formulae of Du and Venkatram (1997) and of a revised form of Venkatram (1992). In the original Venkatram formula, $C^{y}_{*}=1/x_{*}(1+\alpha x_{*}^{2})^{1/2}$, where $x_{*}=x/|L|$ and $\alpha=0.006$. In the revised form, we used $\alpha=0.004$.

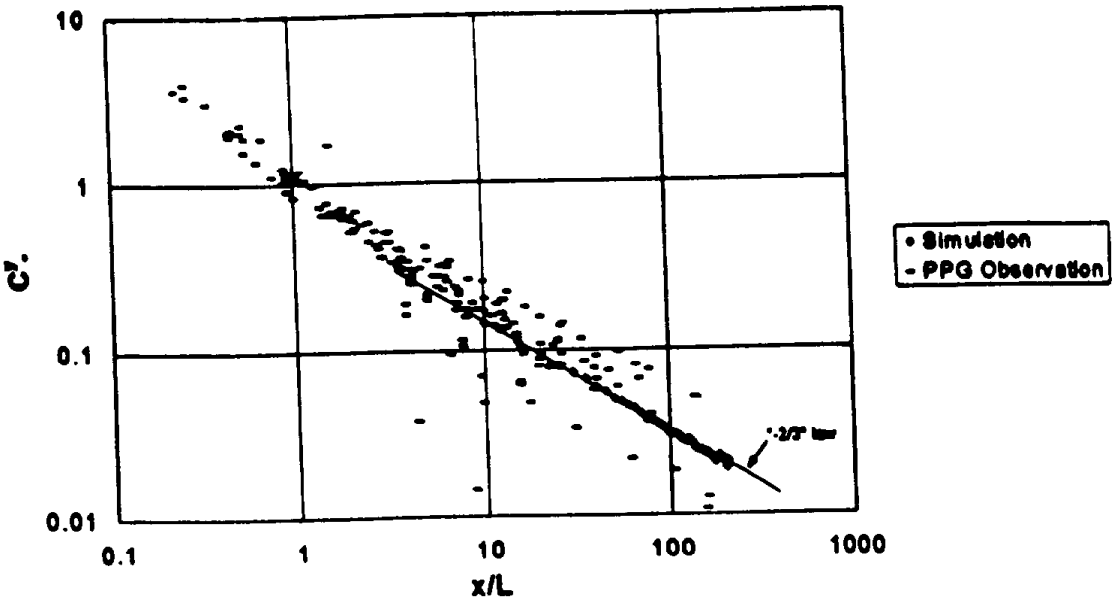

Figure 7. A comparison of 2D model prediction and PPG data under stable stratifications.

Appendix F
A Parameterization of Vertical Dispersion of Ground-level Releases

A Parameterization of Vertical Dispersion of Ground-Level Releases

SHUMING DU AND AKULA VENKATRAM

College of Engineering, University of California, Riverside, Riverside, California

(Manuscript received 2 August 1996, in final form 21 October 1996)

ABSTRACT

The authors propose a simple parameterization for estimating vertical dispersion in the surface boundary layer. It improves upon methods proposed earlier (e.g., by van Ulden, Briggs, and Pasquill and Smith) in that it is based on simulation results generated from a Lagrangian stochastic model, which represents the current understanding of dispersion; parameterizations proposed by other investigators have relied on semiempirical K theory or Lagrangian similarity theories. The new parameterization has been evaluated with data gathered from Project Prairie Grass and from the National Reactor Test Station in Idaho.

1. Introduction

This paper presents a parameterization of vertical dispersion in the surface layer. This scheme for estimating dispersion is meant to serve two purposes. One is to provide a compact description of the current understanding of dispersion in the surface layer. The second is to serve the same purpose as the widely used Pasquill–Gifford–Turner (PGT) scheme for vertical dispersion, which is to provide estimates of mean concentrations for practical industrial applications. An older version of this dispersion scheme has been incorporated into a model referred to as the American Meteorological Society–Environmental Protection Agency Regulatory Model (Cimorelli et al. 1996), which is designed to serve the functions of the Industrial Source Complex (ISC) model used in regulatory applications in the United States.

The PGT scheme represents one of the first parameterizations of dispersion in the surface layer. It was developed in 1961 by Pasquill (1961) and modified by Gifford (1961) and Turner (1970). It is largely an empirical scheme derived from observations made during a field experiment conducted in 1956 at Prairie Grass, Nebraska (Barad 1958). Since its introduction, our knowledge of micrometeorology and dispersion has improved substantially with the development of new laboratory techniques (Willis and Deardorff 1976), numerical simulation methods (Lamb 1982; Thomson 1987), and field experiments (Briggs 1993). Surface-layer dispersion has been investigated for at least the past 50 years (Sutton 1947, 1953; Eliott 1961; and Calder 1961 represent these studies). The results of the early work, which relied primarily on K theory applicable to neutral conditions, were incorporated into the PGT scheme.

In the 1970s, several investigators incorporated the then emerging understanding of micrometeorology (summarized in the Workshop on Micrometeorology; Haugen 1973) into two frameworks, K theory and Lagrangian similarity theory, to examine observations of dispersion in the surface boundary layer (e.g., Yaglom 1972; Chaudry and Meroney 1973; Horst 1979; Nieuwstadt and van Ulden 1978; Hunt and Weber 1979; Pasquill and Smith 1983). For the most part, these studies were remarkably successful in explaining most features of the Prairie Grass observations: ground-level concentrations and lateral dispersion were described adequately, but there was less success in explaining the vertical distribution of concentrations. Because the vertical distribution was measured only on towers at a single arc at 100 m in the Prairie Grass experiment and under unstable conditions, the towers were not high enough to capture the entire plume, and it was difficult to apply these theories to the vertical distribution with any confidence; thus, there are still gaps in our understanding in this regard.

Van Ulden (1978) was one of the first to translate this new understanding of dispersion into a simple model for practical applications. In his paper, he provided expressions for both the ground-level concentration and the vertical distribution. The vertical distribution was obtained by fitting an assumed functional form to observations made at the 100-m arc of the Prairie Grass experiment (Nieuwstadt and van Ulden 1978). Although van Ulden's model is relatively simple, the mean plume height that appeared in the expression for the concen-

Corresponding author address: Dr. Akula Venkatram, College of Engineering, University of California, Riverside, Riverside, CA 92521-0425.
E-mail: venky@engr.ucr.edu

tration requires the solution of an implicit equation. To get around this relatively minor problem, several others (Venkatram 1982; Briggs 1982) formulated explicit expressions for the ground-level concentration in terms of surface similarity variables. However, these expressions did not allow the estimation of concentrations above ground level; van Ulden's equations do provide the means once the implicit equation for the mean plume height is solved. The main problems with these simple schemes are 1) they are based on K theory or Lagrangian similarity theory, whose application can only be justified a posteriori by comparing model results to observations; 2) the vertical distribution is uncertain because it is based on a limited set of observations; and 3) the predicted behavior of ground-level concentrations under highly unstable conditions is not consistent with observations: the Prairie Grass observations indicate that the ground-level concentrations fall off as the "-2" power of the downwind distance, while the model estimates indicate a slower "$-3/2$" decrease.

Some of these uncertainties can be reduced by developing better theories for dispersion and obtaining more data with field experiments. While better field data are not likely to be available in the near future, we do have access to an improved dispersion theory in the form of random walk or Lagrangian stochastic (LS) models of particle motion in turbulent flows. The use of LS modeling became popular among dispersion modelers in the 1980s with the availability of inexpensive computer resources. It is conceptually more appealing than K theory because it is free of the flux-gradient closure assumptions and can be used in the near-source region (Sawford 1985; van Dop et al. 1985). The initial studies (Durbin and Hunt 1980; Wilson et al. 1981; Wilson 1982; Sawford 1985) used stochastic model equations whose form could only be justified by comparing results to observations of mean concentrations; they were used in the same manner as K theory. Lagrangian stochastic modeling became more acceptable after Thomson (1987), in a seminal paper, developed criteria to constrain the form of the trajectory equations. Currently, LS simulation represents our understanding of dispersion. In this paper, we develop our parameterization for dispersion in the surface layer using results generated with the LS model. The technical approach is described in the next section.

2. Technical approach

The parameterizations presented in this paper are developed with data generated with LS simulation, which represents our current understanding of dispersion. Lagrangian stochastic simulation, which has emerged in the last 15 years to be a powerful tool for studying turbulent diffusion (Wilson et al. 1981; Sawford 1985; Thomson 1987), is based on calculating trajectories of tracer particles drawn from an ensemble of flows constrained by similar external conditions, such as stability, mean wind field, and boundary conditions. It is straightforward to calculate the mean concentration distribution from the modeled particle trajectories. Before using results from LS simulation, we evaluated them with observations from experiments conducted at Prairie Grass and the National Test Reactor in Idaho. This evaluation then allowed us to treat LS simulation as the numerical laboratory for generating data to supplement observations.

The Lagrangian stochastic model used in this study is one-dimensional in that random turbulent motion is confined to the vertical z direction. The one-dimensional model neglects streamwise diffusion. We used a one-dimensional model to avoid the so-called nonuniqueness problem associated with multidimensional LS models (Sawford and Guest 1988). Our preliminary examination (with Thomson's two-dimensional model; Thomson 1987) of the effect of streamwise diffusion indicated that streamwise diffusion can alter the falloff rate of ground-level concentration with downwind distance, but the magnitude of the ground-level concentration differs by less than 30% from that of the one-dimensional model. We did not present results from these studies here because of the uncertainty in the form of the two-dimensional model equations.

The one-dimensional model equations used in this study read

$$dw = -\frac{C_0\varepsilon}{2\sigma_w^2}w\,dt + \frac{1}{2}\left(1 + \frac{w^2}{\sigma_w^2}\right)\frac{\partial\sigma_w^2}{\partial z}dt + (C_0\varepsilon)^{1/2}d\zeta,$$

$$dz = w\,dt,$$

and

$$dx = U\,dt, \tag{1}$$

where dw is the change in vertical velocity over a time interval dt, $d\zeta$ is a random variable with zero mean and variance dt, C_0 is a universal constant having a value of 3.0 (Du et al. 1995), ε is the mean rate of dissipation of turbulent kinetic energy, and σ_w is the standard deviation of vertical velocity. The fundamental assumption behind (1) is that the evolution of a tracer particle's state (w, z, t) is a Markovian process. The first and second terms on the right-hand side of the dw equation account for the contribution to the velocity increment over time difference dt due to a component correlated to the present state, while the last term, $(C_0\varepsilon)^{1/2}d\zeta$, accounts for random forcing that is not correlated to the tracer particle's present state. In high–Reynolds number flows, like those in the atmospheric boundary layer, the Markovian assumption is plausible provided the time increment Δt satisfies $t_\eta \ll \Delta t \ll T_L$, where t_η is the Kolmogorov time microscale and T_L the Lagrangian integral timescale. In the atmospheric boundary layer, a time increment satisfying this constraint is easy to choose.

To evaluate the model with observations, we need

vertical profiles of σ_w and ε. This information was estimated from surface-layer parameterizations (Paulson 1970; Panofsky and Dutton 1984).

We evaluate the LS model against data obtained in the Project Prairie Grass (PPG). PPG was an extensive short-range diffusion experiment carried out near O'Neill, Nebraska, in 1956 (Barad 1958). During the experiment, ground-level lateral distribution of concentration was measured along arcs of downwind distances of 50, 100, 200, 400, and 800 m, and the vertical distribution of concentration was measured on six towers along the arc of downwind distance of 100 m. We carried out model calculations for near-ground-level releases (source height $h = 0.46$ m) up to a downstream distance of $x = 800$ m, the farthest arc distance at PPG. We computed ground-level concentrations at $z_r = 1.5$ m corresponding to the observations at PPG. In the PPG experiment, the Monin–Obukhov length varied from ± 5 to ± 180 m, so we ran the model for different values of L: ± 5, ± 10, ± 20, ± 40, ± 80, and ± 160 m. In each simulation, we released 50 000 particles from the source and traced the two-dimensional particle trajectories to chosen receptors. At a receptor (x, z), the crosswind-integrated concentration (CWIC) is calculated from

$$C'(x, z) = \frac{Qn(x, z, \Delta z)}{NU(z)\Delta z}, \tag{2}$$

where Q is the point-source strength, Δz the size of the concentration sensor in the vertical direction, and $n(x, z, \Delta z)$ the number of particles passing through the sensor located at (x, z).

In a previous study (Venkatram and Du 1997), we evaluated results from LS simulation against observations from the Prairie Grass experiment. The results from the study indicate that the LS model provides a satisfactory description of the behavior of the ground-level concentration under both stable and unstable conditions. Figure 1 shows the comparison between the results of the LS model and the Prairie Grass data. The results are presented in terms of the variables

$$C'_* = \frac{C'_y u_* |L|}{Q} \quad \text{and} \quad x_* = \frac{x}{|L|}, \tag{3}$$

where C'_y is the crosswind-integrated ground-level concentration, u_* the surface friction velocity, and L the Monin–Obukhov length.

Note that under unstable conditions, the observed concentrations appear to fall off as a -2 power law of x_* at large x_* while the LS model indicates a $-3/2$ falloff. Because the scatter in the observed data does accommodate a $-3/2$ decrease in concentrations, we will tentatively assume that the LS model is an adequate representation of reality. The scatter in LS simulation results at larger distances is related to the decrease with distances in the sample size used in calculating averages.

This evaluation then allows us to treat the LS model as a numerical laboratory that can be used to generate a database to supplement an observational database. For example, the LS model can provide vertical profile information that is not available from PPG. Furthermore, results from the LS model can be averaged to obtain stable statistics that are difficult to obtain in the field, such as concentration fluxes. We next present results from the LS model that form the basis of the equations for estimating dispersion in the surface boundary layer.

3. Characteristics of results from the LS model

In this paper, "ground-level" concentration is defined as concentration at a height of 1.5 m, consistent with the PPG experiment. Lagrangian stochastic model simulation results suggest that for a short travel distance, $C_* \sim x_*^{-1}$, no matter what the stratification is, and that for large x_*, $C_* \sim x_*^{-3/2}$ under stable stratification and $C_* \sim x_*^{-1/2}$ under unstable stratification. These characteristics are shown in Fig. 1.

Figure 2 shows the predicted variation with distance of the standard deviation of vertical spread σ_z, defined by

$$\sigma_z = \left(\frac{\int_0^z (z - h)^2 C'(z)\, dz}{\int_0^z C'(z)\, dz} \right)^{1/2}, \tag{4}$$

where h is the source height. We see that under unstable stratification, σ_z initially increases linearly with downwind distance and then as the 3/2 power of the distance at large x_*; this is consistent with Yaglom's (1972) "free-convection" theory. For stable stratification, σ_z grows with x_* initially and then as $x_*^{1/2}$ for large x_*.

Also shown in Fig. 2 is the LS model predicted variation of mean plume height

$$\bar{z} = \frac{\int_0^z zC'(z)\, dz}{\int_0^z C'(z)\, dz}. \tag{5}$$

The behavior of $\bar{z}$ is similar to that of σ_z. Note that the $x^{1/2}$ asymptote for stable conditions and $x^{3/2}$ for unstable conditions agree with the predictions of van Ulden (1978).

Figure 3 gives vertical profiles of concentration obtained from LS simulation ($L = \pm 5$ m, $L = \pm 20$ m, $L = \pm 80$ m, and $L = \pm\infty$ m). Following Nieuwstadt and van Ulden (1978) (hereafter NvU), we fit these curves with

$$\frac{C'}{C'_0} = \exp\left[-b\left(\frac{z}{\bar{z}}\right)^s\right] \tag{6}$$

and

$$b = \left[\frac{\Gamma(2/s)}{\Gamma(1/s)}\right]^s.$$

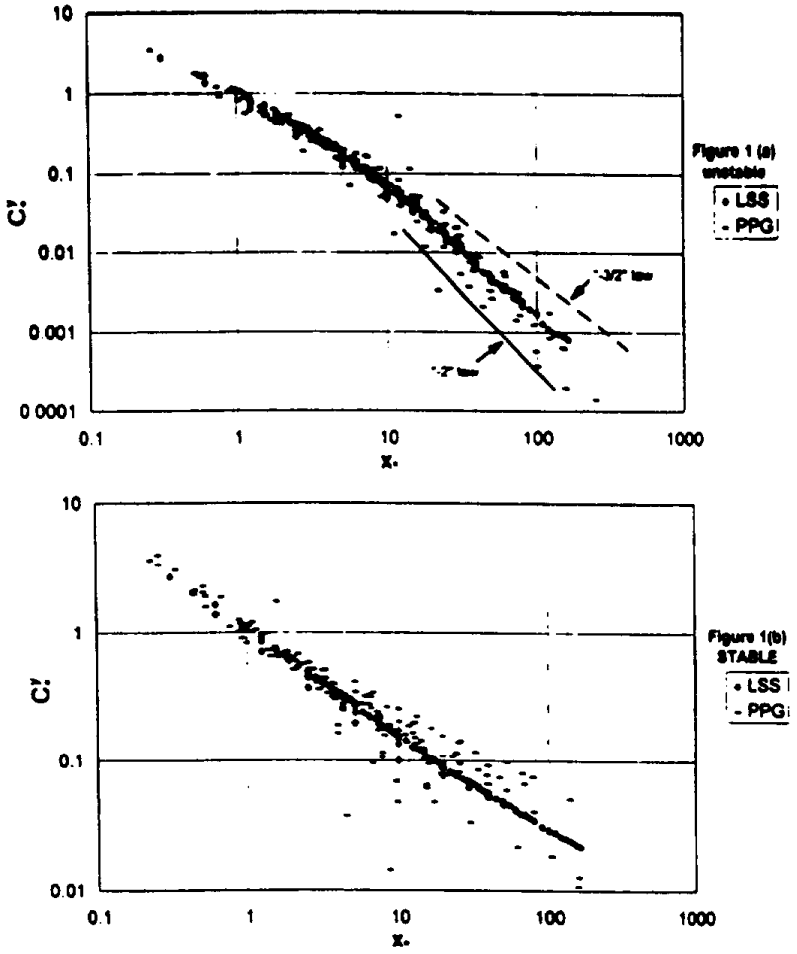

FIG. 1. Comparison of ground-level CWIC obtained from LS simulation (LSS) with PPG data. (a) Unstable stratification and (b) stable stratification.

where $\Gamma(x)$ is a Gamma function defined as $\Gamma(x) = \int_0^\infty e^{-t}t^{x-1}\,dt$. The expression for b is derived by imposing consistency between (5) and (6).

We find that the best fit [fitted by eye; we compared the vertical profiles obtained from LS simulation and those obtained from (6) with different values of s] between (6) and simulation results is obtained with s = 1.3 for unstable stratification, s = 1.5 for neutral stratification, and s = 2.0 for stable stratification.

The analysis of PPG data by NvU indicates that s = 1.0, 1.3, and 2.0 for unstable, neutral, and stable cases, respectively. For stable stratification, the present result is identical to that of NvU, but under unstable and neutral stratification, the present values of s differ from those of NvU. This difference could be related to the difficulty in obtaining crosswind integrated vertical distributions from the relatively coarse network of the Prairie Grass experiment. This does not affect our results because we can generate as much data as needed using the LS model.

4. A simple parameterization for vertical diffusion

The analyses of results from LS numerical simulation allow us to propose a simple parameterization for vertical dispersion in the surface layer. We write the vertical variation of the crosswind-integrated concentration as

$$\frac{C^y(z)}{C^y(0)} = \exp\left[-b\left(\frac{z}{\bar{z}}\right)^s\right],$$

where the values of parameters s and b are shown in Fig. 4. The ground-level concentration C_0 can be expressed in terms of mean plume height $\bar{z}$ and an effective transport velocity $u_e(x)$:

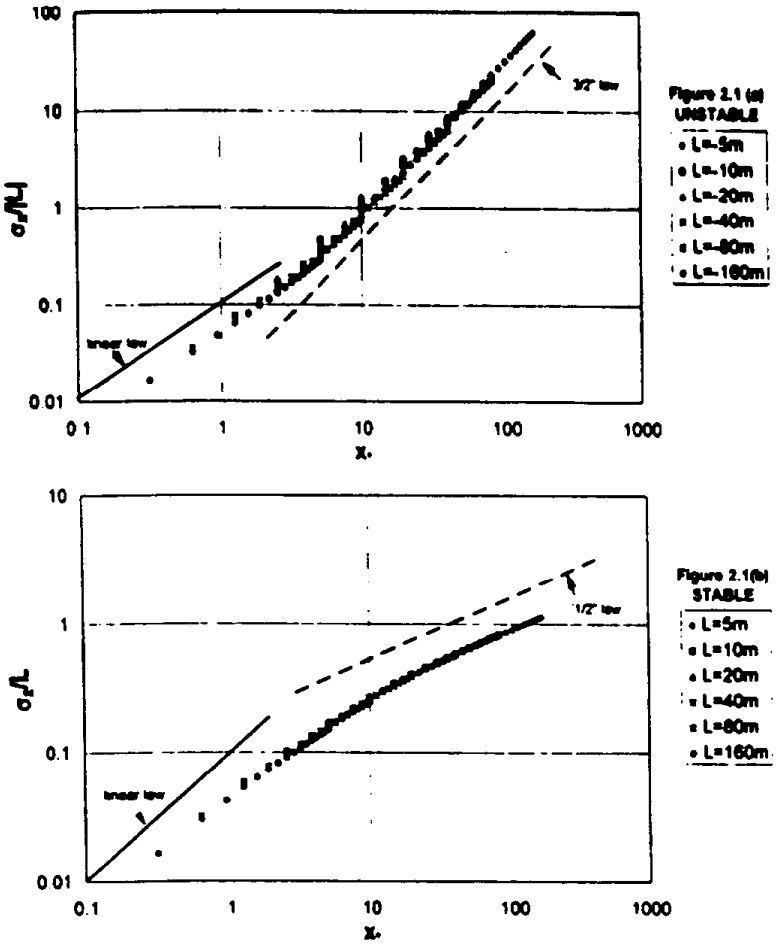

FIG. 2. Bulk property of plumes predicted by the Lagrangian stochastic model: 1) plume spread in the vertical direction (a) under unstable stratification and (b) under stable stratification, and 2) mean plume height (a) under unstable stratification and (b) under stable stratification.

$$C'(0) = \frac{Q}{u_r \bar{z}}. \tag{7}$$

The plume height $\bar{z}$, according to LS simulation, is parameterized as

$$\bar{z} = 0.04 x g(x_*), \tag{8}$$

where $x_* = x/|L|$, and the Monin–Obukhov length L is defined by

$$L = -\frac{T_a}{g} \frac{u_*^3}{kQ_*}, \tag{9}$$

where Q_* is the surface kinematic heat flux and T_a is the near-surface temperature. The function $g(x_*)$ is given by

$$g(x_*) = \begin{cases} (1 + 0.35x_*)^{1/2}, & L < 0 \\ (1 + 0.24x_*)^{-1/2}, & L > 0. \end{cases} \tag{10}$$

The effective transport velocity [defined in this study by (7)] u_r is a function of distance from the release x, the plume height $\bar{z}$ and the friction velocity u_*:

$$u_r = \frac{m(x_*) u_* x}{\bar{z}}, \tag{11}$$

where the function $m(x_*)$ is given by

$$m(x_*) = \begin{cases} (1 + 0.15x_*^{1/2})^{1/4}, & L < 0 \\ (1 + 0.26x_*)^{1/4}, & L > 0. \end{cases} \tag{12}$$

As mentioned in the previous section, the LS modeling data indicate that $s = 1.3$ for unstable stratification and $s = 2.0$ for stable stratification. For near-neutral conditions [in the narrow range $1/L = (-0.01, 0.01)$ m^{-1}], we propose linear interpolations for s and the corresponding value of b:

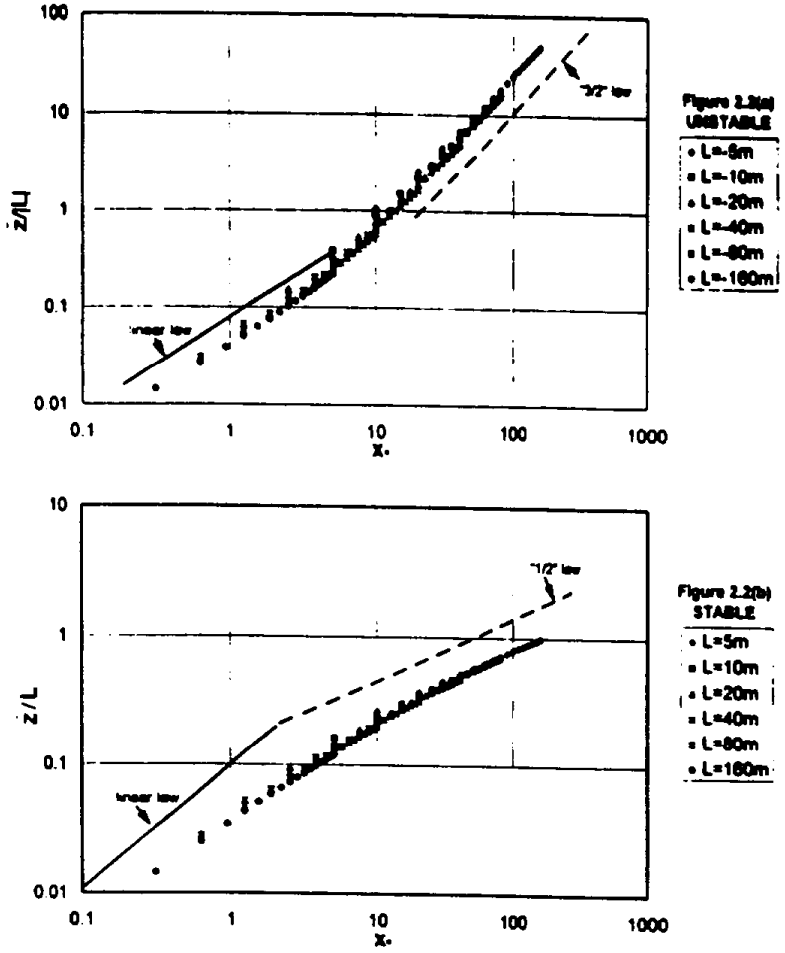

FIG. 2. (*Continued*)

$$s = 1.3 + 70(x_L + 0.01)$$

$$(-0.01\ \mathrm{m}^{-1} < x_L < 0.01\ \mathrm{m}^{-1})$$

and

$$b = 0.68 - 18(x_L + 0.01), \tag{13}$$

where $x_L = 1/L$.

Figure 4 depicts the variation of s and b used in our parameterization.

The next section evaluates the performance of this dispersion parameterization with selected observations.

5. Comparison of estimates from parameterization with observations

Figure 5 compares the ground-level CWIC predicted by the simple scheme with the simulation results from LS simulation. The parameterization differs from the LS simulation results by less than 10%. We next test our estimates by comparing them against data from Project Prairie Grass (Barad 1958) and the National Reactor Test Station (NRTS) experiment (Islitzer and Dumbauld 1963). The field experiment at NRTS was carried out in southeast Idaho. Sixty-minute-averaged ground-level concentrations were measured along arcs of downstream distances of 100, 200, 400, 800, and 3200 m over a flat terrain due to a continuous point source located at a height of 1 m. Vertical distributions of mean concentration were also measured from a row of towers with downwind distances of 200–400 m. Here, we only used ground-level concentrations measured along the 800- and 3200-m arcs.

Figure 6 compares estimates from the parameterization with observations of ground-level concentrations from Prairie Grass. Although there is scatter, the estimates pass through the middle of the observations. This is to be expected in view of the agreement between results from LS simulation and Prairie Grass observa-

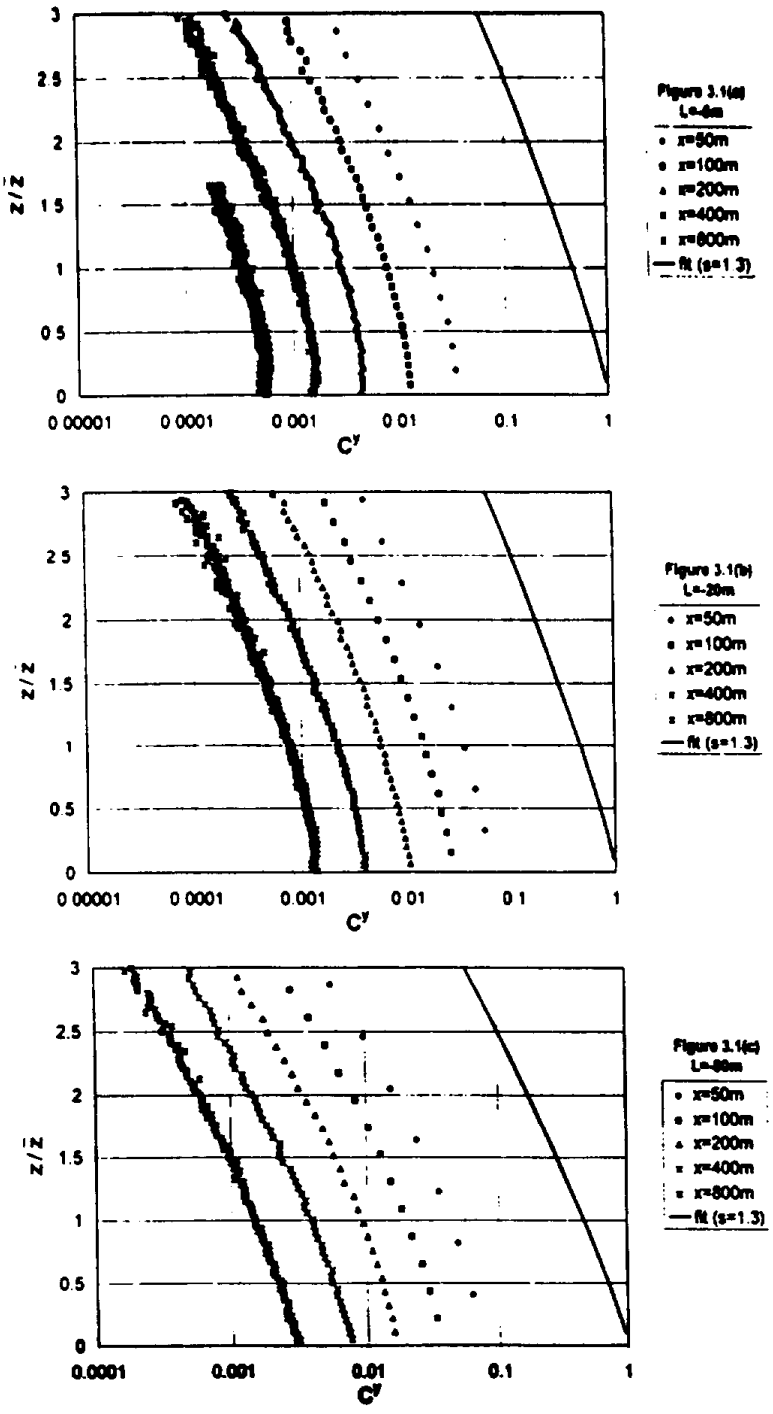

FIG. 3. Vertical profiles of CWIC computed from LS simulation. The solid line is the proposed vertical distribution $\exp(-|kz|^s)$: 1) unstable stratification (a) $L = -5$ m, (b) $L = -20$ m, and (c) $L = -80$ m; 2) stable stratification (a) $L = 5$ m, (b) $L = 20$ m, and (c) $L = 80$ m; and 3) neutral stratification.

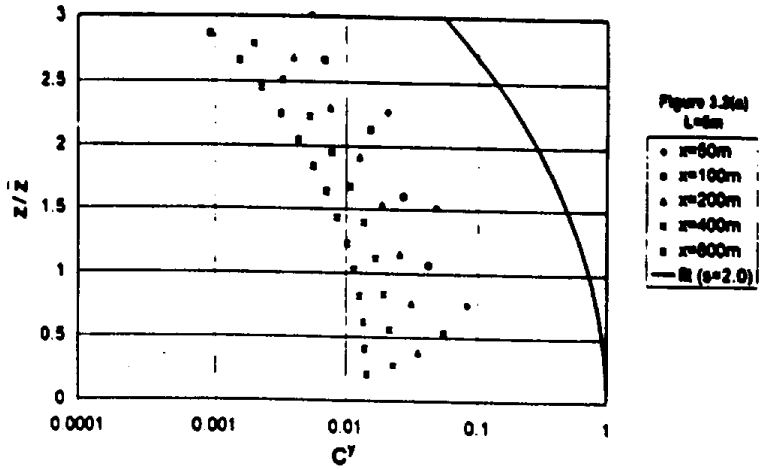

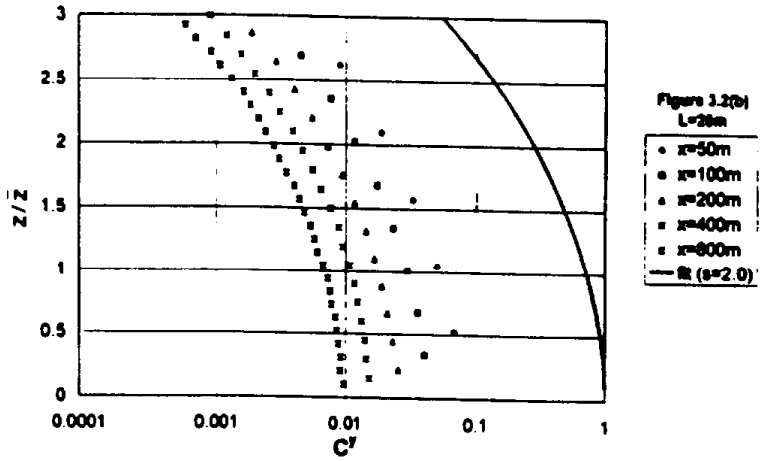

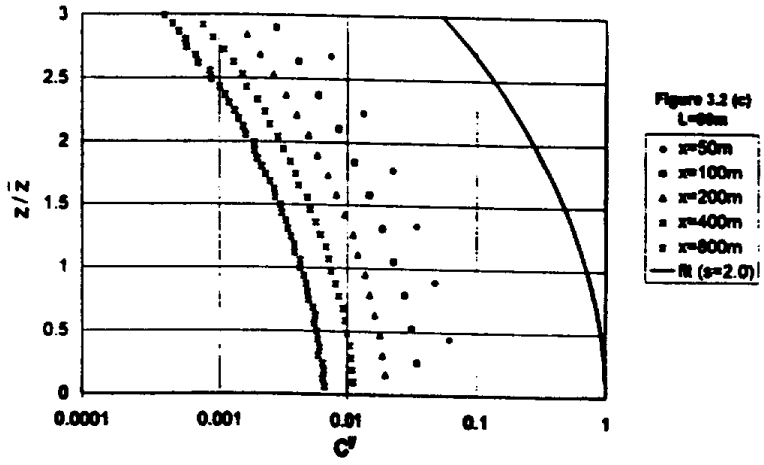

FIG. 3. (*Continued*)

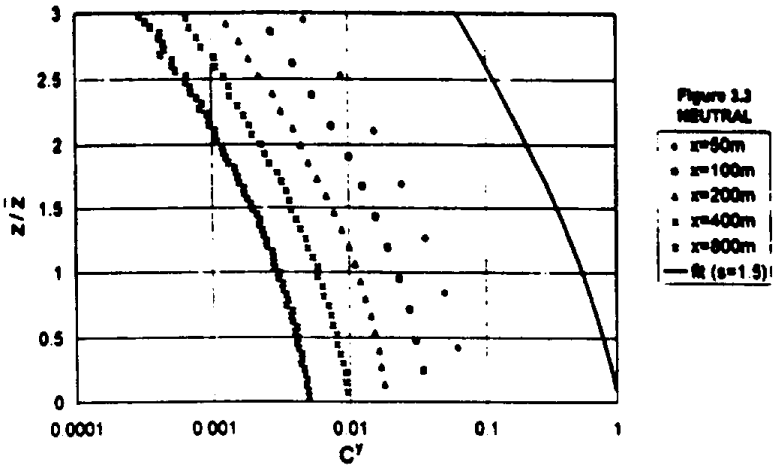

FIG. 3. (*Continued*)

tions. Notice, as pointed out earlier, that the observed concentrations under unstable conditions appear to fall off faster than our parameterization indicates; however, the scatter in the data does accommodate the theoretically justified $-3/2$ decrease. The $-3/2$ falloff incorporated in the parameterization is supported by ground-level concentration data obtained in the NRTS experiment, as shown in Fig. 7.

The only vertical concentration data that are available to us are the vertical concentration profiles measured in PPG experiment. In PPG, vertical profiles of mean concentration were measured at nine levels (0.5, 1.0, 1.5, 2.5, 4.5, 7.5, 10.5, 13.5, and 17.5 m) on six towers on

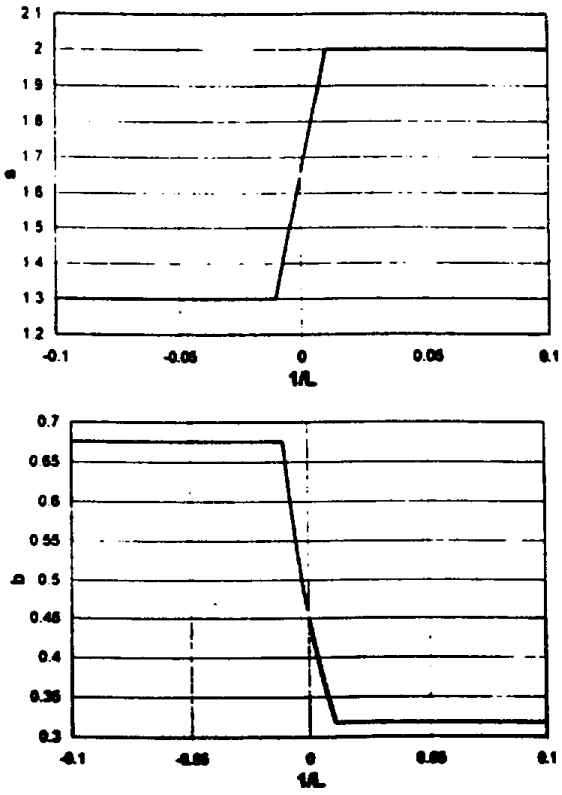

FIG. 4. Values of s and b to be used in the simple scheme.

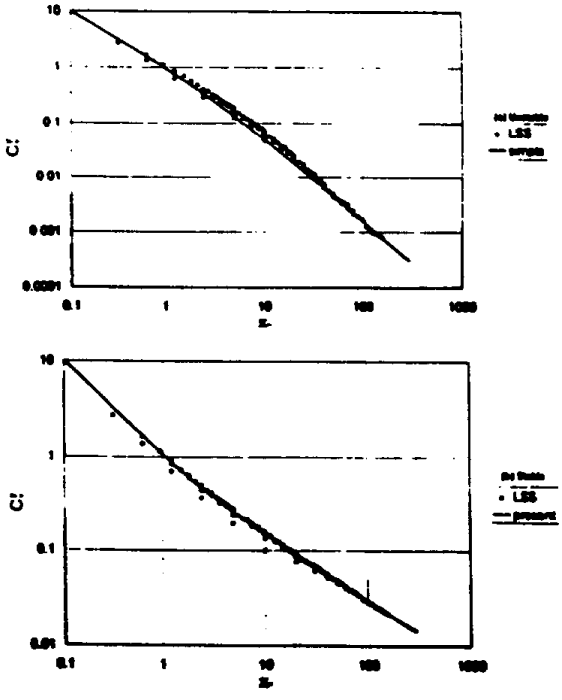

FIG. 5. A comparison of the simple scheme against LS simulation data: ground-level concentrations.

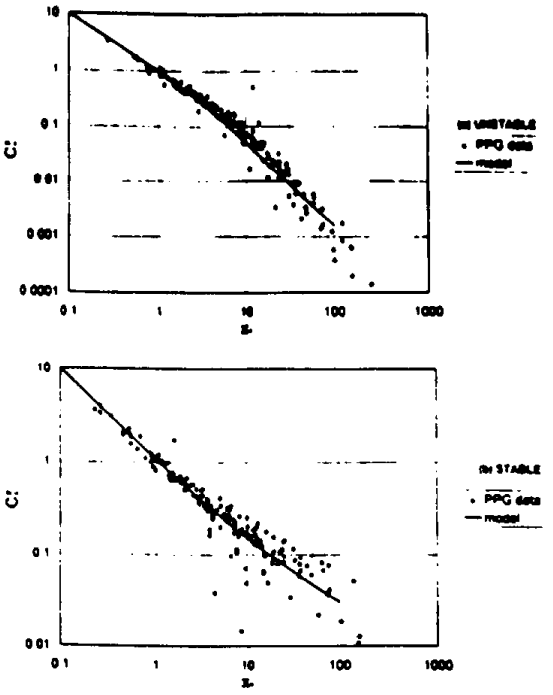

FIG. 6. Comparison of estimates of ground-level CWIC from the parameterization against PPG data. (a) Unstable case and (b) stable case.

an arc of downstream distance $x = 100$ m from the source. We initially used the following criterion to choose data for comparison: at least four of the six towers should record concentrations (in order that the towers can laterally capture the whole plume). Because only one stable experiment met this criterion, we relaxed our criterion for stable cases by using data when two or more towers were in the plume. This resulted in 19 runs out of a total of 52 runs for model comparison.

Figure 8 compares estimates of the vertical distribution of mean concentration with observational data. We see that under stable and moderately unstable stratification ($|L| > 10$ m), estimates from the scheme are within 25% of the observations. It is only under highly unstable conditions ($|L| < 10$ m) that the deviation between the model estimate and observations is significant; the maximum difference between the prediction and measurement can be as high as a factor of 2. These errors could be related to the relatively short release time of 10 min, which might not be long enough to yield stable concentration values in the unstable boundary layer.

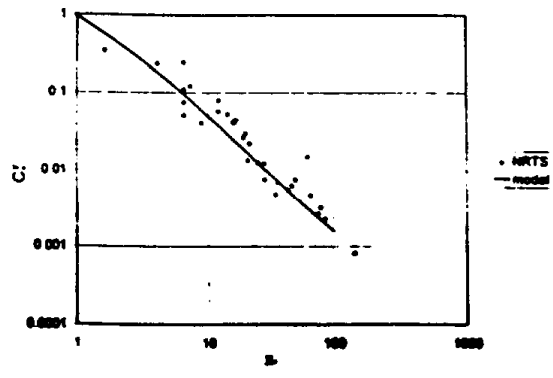

FIG. 7. Comparison of parameterization estimates with National Reactor Test Station data: ground-level CWIC.

Equations (6)–(12) represent the proposed parameterization for dispersion in the surface layer. The next section discusses its application to practical situations.

6. Discussion

The proposed scheme is meant to be applied in the same manner as the widely used Pasquill–Gifford–Turner dispersion scheme. To be as useful as the PGT scheme, it should provide concentration estimates using commonly available meteorological information as inputs. The formulation of the scheme is simple enough for practical applications once we have estimated the model inputs, which are the surface friction velocity u_* and the Monin–Obukhov length L. We can always use Golder's (1972) empirical correlation between L and the stability class. However, this represents a step backward because the Monin–Obukhov length merely becomes a link between the old stability class and the dispersion calculation. The use of dispersion models based on current understanding requires thinking about dispersion in terms of the surface friction velocity u_* and the Monin–Obukhov length L instead of stability classes.

To take full advantage of the concepts underlying the current understanding of dispersion, we should estimate the governing variables u_* and L (or the surface heat flux) directly. Methods for estimating these variables from readily available meteorological observations are described in Van Ulden and Holtslag (1985). Alternatively, we can use a simple correlation between L and the 10-m wind speed and solar insolation, or net radiation, as suggested by Briggs (1982).

We can always estimate the friction velocity from the neutral profile equation if the height of measurement is close to the ground. Then, u_* can be estimated from

$$u_* = \frac{ku(z_r)}{\ln(z_r/z_o)}, \tag{14}$$

where z_r is the height at which the wind speed is measured and z_o is the roughness length. The surface heat flux Q_o required in the computation of L is bounded by the incoming solar radiation during the day and net radiation during the night. As Weil (1985) has suggested, Q_o during the day can be taken to about 0.3 times the incoming the solar radiation.

If accurate concentration estimates are required, we

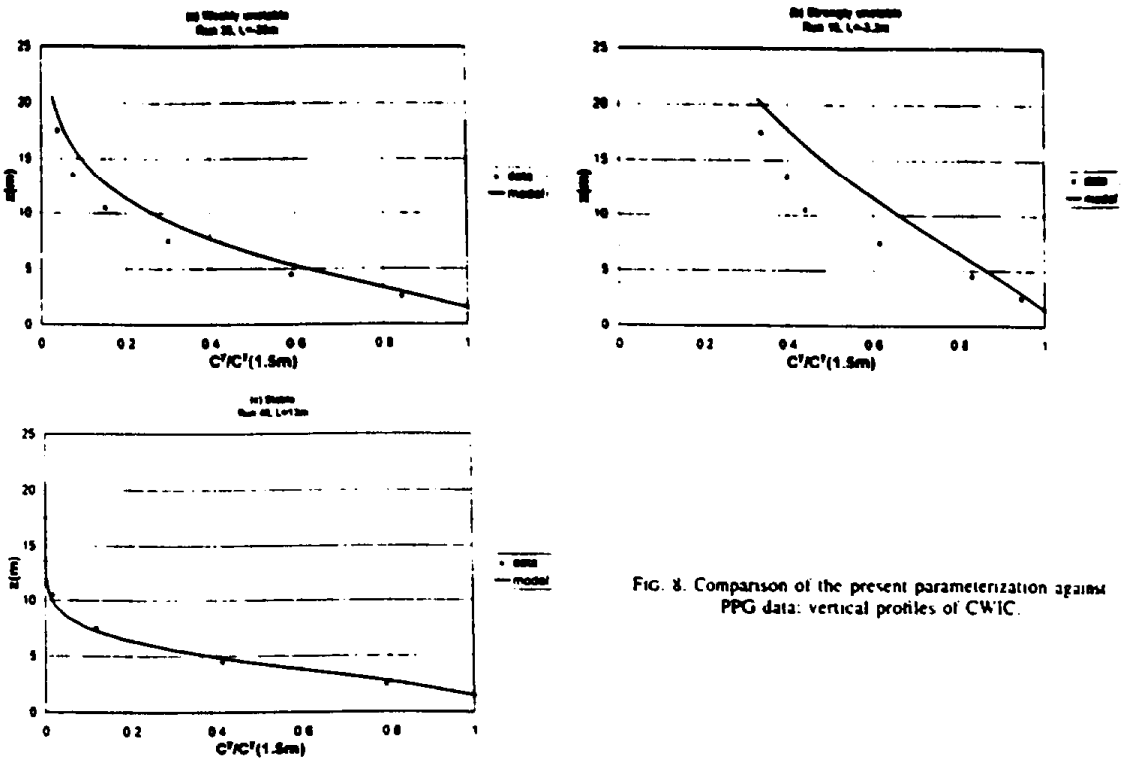

FIG. 8. Comparison of the present parameterization against PPG data: vertical profiles of CWIC.

have to make the micrometeorological measurements to compute u_* and L. However, before making such measurements, we can use the parameterization presented in this paper to examine the sensitivity of the concentration to inputs. For example, during the night, the concentration at, say, a height of 1 m is insensitive to the estimate of Q_* because it depends on two variables, the surface concentration and the mean plume height, whose changes with L compensate for each other. The surface concentration increases with decrease in L, but its effect at a height above ground decreases with L because ξ decreases with L.

We point out that this surface-layer parameterization cannot be readily extended to elevated releases. For such releases, we need to use other schemes, such as those suggested by Hanna and Paine (1989) and Weil (1985).

Acknowledgments. The work described in this paper was supported by Grant 94-366 from the California Air Resources Board (ARB). We are grateful to Dr. Tony van Curen, the ARB project manager, for encouraging research in small-scale dispersion.

REFERENCES

Barad, M. L., 1959: *Project Prairie Grass, a Field Program in Diffusion.* Vol. 1., Air Force Cambridge Research Center.

Briggs, G. A., 1982: Similarity forms for ground-source surface layer diffusion. *Bound.-Layer Meteor.*, 23, 489–502.

——, 1993: Plume dispersion in the convective boundary layer. Part II: Analyses of CONDORS field experiment data. *J. Appl. Meteor.*, 32, 1388–1425.

Calder, K. L., 1961: Atmospheric diffusion of particulate material considered as a boundary value problem. *J. Meteor.*, 18, 413.

Chaudhry, F. H., and R. N. Meroney, 1973: Similarity theory of diffusion and the observed vertical spread in the diabatic surface layer. *Bound.-Layer Meteor.*, 3, 405–415.

Cimorelli, A. J., A. Venkatram, S. G. Perry, R. F. Lee, J. C. Weil, R. J. Paine, and R. B. Wilson, 1996: Current progress in the AERMIC model development program. *89th Annual Meeting and Exhibition*, Air and Waste Manage. Assoc., 1–27.

Du, S., B. L. Sawford, J. D. Wilson, and D. J. Wilson, 1995: Estimation of the Kolmogorov constant (C_0) for the Lagrangian structure function, using a second-order Lagrangian model of grid turbulence. *Phys. Fluids*, 7, 3083–3090.

Durbin, P. A., and J. C. R. Hunt, 1980: Dispersion from elevated sources in turbulent boundary layers. *J. Mech.*, 19, 679–695.

Elliott, W. P., 1961: The vertical diffusion of gas from a continuous source. *Int. J. Air Water Pollut.*, 4, 33.

Gifford, F. A., 1961: Uses of routine meteorological observations for estimating atmospheric dispersion. *Nucl. Saf.*, 2, 47–51.

Golder, D., 1972: Relations among stability parameters in the surface layer. *Bound.-Layer Meteor.*, 3, 47–58.

Hanna, S. R., and R. J. Paine, 1989: Hybrid plume dispersion model (HPDM): Development and application. *J. Appl. Meteor.*, 28, 206–224.

Haugen, D. A., 1973: *Workshop on Micrometeorology*. Amer. Meteor. Soc., 392 pp.

Horst, T. W., 1979: Lagrangian similarity modeling of vertical dif-

fusion from a ground-level source. *J. Appl. Meteor.*, **18**, 733–740.

Hunt, J. C. R., and A. H. Weber, 1979: A Lagrangian statistical analysis of diffusion from a ground-level source in a turbulent boundary layer. *Quart. J. Roy. Meteor. Soc.*, **105**, 423–443.

Islitzer, N. F., and R. K. Dumbauld, 1963: Atmospheric diffusion-deposition studies over flat terrain. *Int. J. Air Water Pollut.*, **7**, 999–1022.

Lamb, R. G., 1982: Diffusion in the convective boundary layer. *Atmospheric Turbulence and Air Pollution Modelling*, F. T. M. Nieuwstadt and H. van Dop, Eds., D. Reidel Publishing, 159–320.

Nieuwstadt, F. T. M., and A. P. van Ulden, 1978: A numerical study on the vertical dispersion of passive contaminants from a continuous source in the atmospheric surface layer. *Atmos. Environ.*, **12**, 2119–2124.

Panofsky, H. A., and J. A. Dutton, 1984: *Atmospheric Turbulence*. John Wiley & Sons, 397 pp.

Pasquill, F., 1961: The estimation of the dispersion of windborne material. *Meteor. Mag.*, **90**, 33–49.

——, and F. B. Smith, 1983: *Atmospheric Diffusion*. 3d ed. Ellis Horwood, 437 pp.

Paulson, C. A., 1970: The mathematical representation of wind speed and temperature in the unstable atmospheric surface layer. *J. Appl. Meteor.*, **9**, 857–861.

Sawford, B. L., 1985: Lagrangian statistical simulation of concentration mean and fluctuation fields. *J. Climate Appl. Meteor.*, **24**, 1152–1166.

——, and G. M. Guest, 1988: Uniqueness and universality of Lagrangian stochastic models of turbulent dispersion. Preprints, *Eighth Symp. on Turbulence and Diffusion*, San Diego, CA, Amer. Meteor. Soc., 96–99.

Sutton, O. G., 1947: The problem of diffusion in the lower atmosphere. *Quart. J. Roy. Meteor. Soc.*, **73**, 257.

——, 1953: *Micrometeorology*. McGraw-Hill, 333 pp.

Thomson, D. J., 1987: Criteria for the selection of stochastic models of particle trajectories in turbulent flows. *J. Fluid Mech.*, **180**, 529–556.

Turner, D. B., 1970: *Workbook of Atmospheric Dispersion Estimates*. USEPA Office of Air Programs, 84 pp.

van Dop, H., F. T. M. Nieuwstadt, and J. C. R. Hunt, 1985: Random walk models for particle displacements in inhomogeneous unsteady turbulent flows. *Phys. Fluids*, **28**, 1639–1653.

van Ulden, A. P., 1978: Simple estimates for vertical diffusion from sources near the ground. *Atmos. Environ.*, **12**, 2125–2129.

Venkatram, A., 1982: A semi-empirical method to compute concentration associated with surface releases in the stable boundary layer. *Atmos. Environ.*, **16**, 245–248.

——, and S. Du, 1997: An analysis of the asymptotic behavior of cross-wind integrated concentration using Lagrangian stochastic simulation. *Atmos. Environ.*, in press.

Weil, J. C., 1985: Updating applied diffusion models. *J. Climate Appl. Meteor.*, **24**, 1111–1130.

Willis, G. E., and J. W. Deardorff, 1976: A laboratory model of diffusion into the convective planetary boundary layer. *Quart. J. Roy. Meteor. Soc.*, **102**, 427–446.

Wilson, J. D., 1982: Turbulent dispersion in the atmospheric surface layer. *Bound.-Layer Meteor.*, **22**, 399–420.

——, G. W. Turtell, and G. E. Kidd, 1981: Numerical simulation of particle trajectories in inhomogeneous turbulence. II: Systems with variable turbulence velocity scale. *Bound.-Layer Meteor.*, **21**, 423–441.

Yaglom, A. M., 1972: Turbulent diffusion in the surface layer of the atmosphere. *Izv. Akad. Nauk USSR, Atmos. Oceanic Phys.*, **8**, 333–340.